Regulation of human sex-linked homologs *DDX3X* and *DDX3Y* and phenotypic consequences

by
Shruthi Rengarajan

B.A., Biochemistry & Molecular Biology
Boston University, 2016
M.A., Biotechnology
Boston University, 2016

Submitted to the Department of Biology
in Partial Fulfillment of the Requirements for the Degree of

Doctor of Philosophy in Biology

at the

MASSACHUSETTS INSTITUTE OF TECHNOLOGY

June 2024

Author . . . . . Shruthi Rengarajan
Department of Biology
March 28, 2024

Certified by. . . . . David C. Page
Professor of Biology
Member, Whitehead Institute
Investigator, Howard Hughes Medical Institute
Thesis Supervisor

Accepted by . . . . . .Mary Gehring
Associate Professor of Biology
Member, Whitehead Institute
Director, Biology Graduate Committee

Regulation of human sex-linked homologs *DDX3X* and *DDX3Y* and phenotypic consequences

by
Shruthi Rengarajan

Submitted to the Department of Biology on March 28th, 2024 in partial fulfillment of the requirements for the Degree of Doctor of Philosophy in Biology

ABSTRACT

The X-linked gene *DDX3X* and its Y-linked homolog *DDX3Y* comprise one of 17 gene pairs retained on the human X and Y chromosomes during their evolution from ordinary autosomes; both genes are widely expressed in human tissues. Mutations of *DDX3X* and *DDX3Y* result in a wide range of sex-dependent phenotypes, necessitating the study of their regulation.

In this thesis, we show that *DDX3X* is extraordinarily dosage-sensitive, and that perturbation of either *DDX3X* or *DDX3Y* expression is buffered -- by negative cross-regulation of *DDX3X* and *DDX3Y* in 46,XY cells, and by negative auto-regulation of *DDX3X* in 46,XX cells. In 46,XY cells, knockdown of either *DDX3X* or *DDX3Y* by CRISPRi causes transcript levels of the homologous gene to rise. In 46,XX cells, chemical inhibition of DDX3X protein activity elicits an increase in *DDX3X* transcript levels. This regulation is mediated through mRNA stability and buffers total levels of *DDX3X* and *DDX3Y* protein in human cells. Our findings indicate that gene regulatory mechanisms present on ancestral autosomes were retained and modified during the 200-million-year evolution of the human sex chromosomes.

This regulation has key consequences for human diseases. We re-analyzed data from the Cancer Dependency Map to identify genetic dependencies on the broadly expressed regulators on the Y chromosome. We find that *DDX3Y* is required for the survival of a set of cancer cell lines that present with loss-of-function mutations in *DDX3X*, uncovering a novel dependency in male tumors. Altogether, this work identifies a regulatory mechanism on the human sex chromosomes that has important consequences for human disease.

Thesis Supervisor: David C. Page
Title: Professor of Biology

Acknowledgements

This thesis would not have been possible without contributions from many people. Firstly, I would like to thank my advisor David Page, for his endless optimism and insights into scientific presentation and writing. Thank you to Winston, Jason, Nikolai and Erik for your contributions to this thesis, particularly the Slavov lab for being excellent collaborators and their patience in teaching me proteomics. Thank you to members of the Page lab for their advice and support over the years. I could not have asked for a more collaborative and thoughtful group of colleagues and I am grateful to each and every one of you. I would like to acknowledge Adrianna San Roman and Jennifer Hughes for their rigorous feedback and knowledge, Susan Tocio and Jorge Adarme for keeping the lab running and Hannah Harris for being a constant source of humor and support.

Thank you to my committee members Dave Bartel and Matt Vander Heiden for their useful suggestions and for keeping me on track, as well as all the members of the Bartel lab who have shared reagents and advice. I would also like to thank Kathy Liu for her time and expertise as my external committee member. Thank you to my former advisors Miguel Rivera and John Celenza for their scientific mentorship of many years.

Thank you to so many friends for keeping me sane and being the best support system: Amrita, Charmi, Ellen, Farah, Laurel, Talya, Teresa. Thank you to Dia and Elizabeth for being the only roommates I could have spent these years with and for listening to me vent and practice presentations. Thank you to all my family scattered throughout the globe for their well wishes. Thank you to Vijay for being my confidante, advocate and proofreader; this would not be possible without you. And finally, thank you to my parents for 29 years of faith and support; I'm forever grateful.

TABLE OF CONTENTS:

List of Figures

List of Tables

Chapter 1:
Introduction

In mammals, sex determination is achieved by sex chromosome constitution: Typical females have two X chromosomes and typical males have one X and one Y chromosome in their cells. Specifically, it is a gene on the Y chromosome that determines gonadal sex (Koopman et al., 1991). The expression of Y-linked transcription factor *Sry* activates a signaling cascade in the early embryo leading to testis development in males (Sekido & Lovell-Badge, 2009). In females, the X chromosomes are present in two distinct epigenetic configurations, the 'active' X (Xa) and the 'inactive' X (Xi). Xa is transcriptionally active and expresses most of its genetic content, approximately 800 genes. Conversely, Xi is marked by closed chromatin and limited gene expression; only 25% of X-encoded genes are expressed from Xi (Lyon, 1962; San Roman et al., 2023). The X and Y chromosomes are largely non-recombining except for a small pseudoautosomal region (Skaletsky et al., 2003) and the difference in X and Y content represents the largest source of genetic variation in the human population.

X and Y differentiation is the result of Y-chromosome gene loss over the course of sex chromosome evolution. While the present-day X chromosome retains 98% of its ancestral gene content, the Y has only retained about 3% (Skaletsky et al., 2003). These surviving genes are essential for male viability or fertility. This includes a class of genes known as 'X-Y pairs', homologous genes on the sex chromosomes that are highly dosage-sensitive and haploinsufficient (Bellott et al., 2014). These critical homologs are broadly expressed throughout the human body and encode key

regulators of cellular function, and potential differences in their function and regulation represent an exciting avenue to study sex differences that are chromosomal in origin. What are the mechanisms by which these genes give rise to sex differences in health and disease? How can we understand their regulation in XX and XY individuals? These are the questions this thesis aims to answer by focusing on *DDX3X* and *DDX3Y,* a highly conserved, essential X-Y homologous pair.

In this introduction, I will first describe the evolutionary history of the X and Y chromosomes to explain the origin and significance of the X-Y gene pairs. I will then describe *DDX3X* and *DDX3Y* in detail, highlighting their protein function and deep conservation, including the breadth of DDX3 homologs. This will also include a summary of the current studies on the similarities and differences between DDX3X and DDX3Y. Moreover, I will highlight several phenotypes associated with mutation and overexpression of *DDX3X* and *DDX3Y* and how they present in a sex-dependent manner, providing insight into their critical roles across the human body. Currently, there are no studies on the regulation of these genes, which could be critical to understand the sex differential phenotypes caused by changes in *DDX3X* and *DDX3Y* gene dosage. My study of regulatory mechanisms governing *DDX3X* and *DDX3Y,* as well as their contribution to human phenotypes, will be the subjects of Chapters 2 and 3.

EVOLUTION OF THE MAMMALIAN SEX CHROMOSOMES

Evolution from autosomes

The mammalian sex chromosomes evolved from an ordinary pair of autosomes over the past 200 million years. This began with the acquisition of a sex-determining gene on one of the chromosomes (Ohno, 1967). In mammals, this is *Sry* on the Y chromosome. Recombination was then suppressed between the two chromosomes resulting in differentiation of the homologous chromosomes. This was caused by a series of at least four inversions on the Y chromosome, leading to loss of recombination outside the pseudoautosomal ends. There are four evolutionary strata corresponding to these events, where gene order of the X chromosome genes is unperturbed (Lahn & Page, 1999). The resulting present-day Y chromosome only recombines with the X in the pseudoautosomal region, identical sequences on the tip of the sex chromosomes. These regions are crucial for proper alignment of the X and Y chromosomes during male meiosis (Burgoyne et al., 1992). Outside of these regions, gene content on the X (Non-pseudoautosomal X: NPX) and the Y (Non-pseudoautosomal Y: NPY) are diverged. The X chromosome has retained 98% of its ancestral genes while the Y has retained only 3%, as inferred from comparison to avian genomes where ancestral genes are autosomal (Bellott et al., 2010; Ross et al., 2005; Skaletsky et al., 2003).

While the X chromosome is able to recombine in mammalian females, the absence of a recombination partner led to the genetic decay of the Y chromosome. The Y chromosome behaves as one recombination unit, and this mode of inheritance reduces selection efficiency. There are several hypotheses to explain gene decay on

the Y. One of them is genetic ‘hitchhiking,’ where deleterious mutations that lead to erosion are brought along with beneficial mutations at other loci (Rice, 1987). Conversely, beneficial mutations could be lost due to their association with deleterious alleles, termed ‘background selection’ (Charlesworth et al., 1993). As the Y chromosome has a small effective population size (there are three X chromosomes for every Y in the population), it is also susceptible to the ‘Muller’s Ratchet’ hypothesis (Muller, 1964). As the Y chromosome gains deleterious mutations, genetic drift and the absence of recombination leads to the loss of the least mutated Y chromosome, and the constant accumulation of mutations (Engelstädter, 2008). Previous work has argued that complete Y decay will lead to the extinction of the chromosome (Graves, 2006). However, genomic sequencing of multiple mammalian Y chromosomes demonstrates that the gene content on the mammalian Y has reached relative stability. Human Y chromosomes have lost very few genes since diverging from other primate lineages as well as more distant lineages, such as bull and mouse (Hughes et al., 2012, 2020).

HOMOLOGOUS GENES ON THE X and Y CHROMOSOMES

Gene content on the Y chromosome

The relative stability of the Y chromosome suggests that the remaining Y-linked genes have been preserved by selection for male fertility and viability. Indeed, the majority of 45, X embryos (missing a second sex chromosome) are inviable, and the presence of a Y chromosome is sufficient to confer viability (Hook & Warburton, 1983). What are the

genes that are preserved on the Y? Sequencing of the NPY region revealed that the gene content on the Y is broadly split into three categories: 1. Genes that reside in large amplicons that are comprised of palindromes and tandem repeats ('Ampliconic'), 2. Genes that reside in a region nearly identical to the X chromosome resulting from an evolutionarily recent transposition event in the human lineage ('X-transposed) and 3. Genes that are homologous to the X-chromosome but not identical, marking them as ancestral ('X-degenerate') (Skaletsky et al., 2003).

The X-transposed region is largely depleted for functional genes, and the genes in the ampliconic region differ greatly from the X-degenerate genes. Ampliconic genes are expressed exclusively in the testis and many are involved in spermatogenesis, demonstrating their role in male fertility. In contrast, the X-degenerate genes (henceforth referred to as 'X-Y pairs') are expressed throughout the human body in males and have broad regulatory functions, making them candidates for conferring male viability. Indeed, it is argued that dosage-sensitivity is key to the survival of these genes: they are critical regulators of cellular processes like transcription, translation and signaling (Bellott et al., 2014). Effectively, two copies of such genes are expressed in XY males, resulting in maintenance of ancestral dosage (assuming functional equivalence between the X-Y pairs). But how is this dosage maintained in XX females?

Dosage compensation on the X chromosome

All species with chromosomal sex determination have a homogametic (e.g. XX or ZZ) and heterogametic (e.g. XY or ZW) sex, thus necessitating the development of strategies for dosage compensation between the sexes. Different dosage compensation strategies have developed independently. These strategies include upregulating X-linked genes in XY males, as in *D. melanogaster,* and downregulating the X chromosomes in XX females, as in *C. elegans* (Disteche, 2012). In mammals, dosage compensation occurs through random X-inactivation, a cell-autonomous process where a single X chromosome is epigenetically inactivated in each cell of an XX female. The X-inactivation hypothesis was first put forth by Ohno who observed the presence of the highly heterochromatinized X in female cells (Barr & Bertram, 1949; Ohno, 1967). Mary Lyon further hypothesized that this condensation corresponded to the suppression of expression, equalizing the dosage of X chromosome genes in males and females (Lyon, 1962). This process involves the expression of *Xist*, a long non-coding RNA that coats the Xi, as well as the recruitment of repressive chromatin factors (Brown et al., 1991).

But what happens to the expression of genes with widely expressed and functionally coherent Y homologs? The X homologs of X-Y pair genes, along with a handful of other genes, are expressed from Xi, despite the widespread epigenetic silencing of the chromosome (Lahn & Page, 1997). This process varies among species, while only 3% of X chromosome genes are expressed from the mouse Xi, approximately 25% of human X genes are expressed from Xi (Berletch et al., 2011; San

Roman et al., 2023). Sometimes referred to as 'escape' from X-inactivation, the precise mechanism of this gene-by-gene dosage compensation strategy is as yet not defined. Regardless, it enables both alleles of dosage-sensitive regulators to be expressed in XX females, ensuring female viability and matching the expression from X-Y pair genes in XY males.

However, there could be differences in 1) the function of the X vs Y encoded protein, 2) the regulation of the X vs Y homolog or 3) the regulation of the X homolog in XX cells vs the X-Y gene pair in XY cells. Any of these scenarios would result in a sex difference between XX females and XY males. The dosage sensitivity and broad function of these homologs also implies that even subtle differences in expression or function could result in genome-wide changes to the transcriptome/translatome, resulting in phenotypic changes. In this thesis, I elucidate one example of such a phenomenon, resulting from the study of *DDX3X* and *DDX3Y* regulation.

DDX3X and *DDX3Y*: FUNCTION, CONSERVATION and PHENOTYPES

DDX3X function

DDX3X and DDX3Y belong to a class of RNA-binding proteins known as DEAD or DEAH box helicases. While members of the family perform diverse cellular functions, most of the proteins can hydrolyze ATP to bind and remodel RNA. As a result, they all contain an RNA binding and ATPase domain as well as a highly conserved helicase

core including the Asp-Glu-Ala-Asp/His catalytic center from which they derive their name (Rosner & Rinkevich, 2007). The proteins largely have unstructured N and C-termini, often associated with their localization and/or oligomerization.

DDX3X works as a cooperative dimer to unwind double-stranded RNA duplexes. It binds to the sugar-phosphate backbone of double-stranded RNAs that have single-stranded regions 3' of the duplex. It is then able to unwind such duplexes in an ATP-dependent manner (Song & Ji, 2019). The duplex is first locally destabilized upon ATP binding; dissociation and enzyme recycling occur upon ATP hydrolysis. DDX3X is particularly effective at unwinding long, complex RNA structures using iterative cycles of binding and dissociation. This function is primarily studied in translation initiation; DDX3X is a key part of the pre-initiation scanning complex (Soto-Rifo & Ohlmann, 2013). It is responsible for unwinding 5' UTR RNA structure prior to the start codon, promoting the translation of genes with structurally complex UTRs. Indeed, knockdown of *DDX3X* abrogates the translational efficiency of hundreds of mRNAs with long and GC-rich 5' UTRs (Calviello et al., 2021). DDX3X directly binds these UTRs as well as thousands of other mRNAs. While the role of DDX3X binding at genes with non-complex UTRs is not yet fully characterized, recent work suggests that this binding might lead to mRNA destabilization (Jowhar et al., 2023). DDX3X has also been associated with stress granule assembly, spliceosome activity, nuclear export and viral response. I discuss these secondary functions below.

DDX3X has been affinity purified with components of the spliceosome as well as spliced mRNPs in vivo. It is strongly associated with many core proteins of the exon-junction complex, such as Y1F and Magoh. It appears to be dispensable for global mRNA splicing and knockdown of *DDX3X* does not interfere with proper splicing in reporter assays (Soto-Rifo & Ohlmann, 2013). *DDX3X* knockdown does change the ratio of *KLF4* splicing isoforms in breast cancer cells, suggesting a limited role in the splicing of select genes (Cannizzaro et al., 2018). DDX3X also strongly associates with mRNA and protein nuclear export factors such as NXF1 and CRM1 (Fröhlich et al., 2016). As DDX3X is mostly cytoplasmic and has a critical role in translation, this could suggest a role for DDX3X in post-transcriptional mRNA export. However, knockdowns of *DDX3X* show that it does not affect the global nuclear to cytoplasmic ratios of mRNAs; it is not essential for the vast majority of nuclear export (Lai et al., 2008).

DDX3X is a core component of stress granules, which sequester specific mRNPs to achieve a stress-induced translational activation and repression program. Genetic or chemical inhibition of DDX3X disrupts the assembly and disassembly of these granules suggesting that the enzymatic activity of this protein is key for proper cellular stress response (Cui et al., 2020). The relatively unstructured N-and C-termini of DDX3X undergo the liquid-liquid phase separation that allow for this sequestration (Valentin-Vega et al., 2016). In macrophages, sequestered vs free DDX3X levels serve as a 'live-or-die' checkpoint by balancing the stress response vs the cell-death response (Samir et al., 2019). DDX3X is also essential to activate the Interferon signaling pathway

through *Infb* transcription. It is an essential co-factor of the TBK1/IKK transcription factor complex in promoting *Infb* transcription and is associated with the *Infb* promoter. DDX3X can also repress the activity of the E-cadherin promoter, though the mechanism of this process is not well-understood (Soulat et al., 2008; Wu et al., 2014).

Similarities and differences with *DDX3Y*

While the majority of functional work on these proteins focuses on DDX3X, there have been few insights into the molecular functions of DDX3Y. I summarize this work here and compare and contrast DDX3X and DDX3Y function. The X- and Y-encoded proteins are 91% identical at the amino acid level (Lahn & Page, 1997). While they have significantly diverged in their N- and C-terminal regions, the RNA binding, ATPase and helicase domains are largely conserved.

Early experiments showed that DDX3Y is functionally interchangeable with DDX3X *in vitro* in ensuring cell viability (Sekiguchi et al., 2004). More recent work has shown that the proteins have partially overlapping functions. They bind similar mRNAs in vivo and have similar effects on translation initiation in exogenous expression experiments, lending further evidence to their interchangeability (Venkataramanan et al., 2021). However, the proteins have different in-vitro affinities for double-stranded RNA. DDX3Y binds RNA less tightly than DDX3X and displays slower duplex unwinding (Owens et al., 2022). While these subtle differences may be overcome by exogenous

overexpression experiments, they may have consequences at cellular concentrations. The two proteins also have differing capacities for stress granule formation and translational repression; the unstructured regions of DDX3Y are able to form more rigid liquid condensates, potentially leading to differences in how the two homologs activate the stress response (Shen et al., 2022).

Conservation and orthologs

DDX3X is highly conserved, with orthologs in mammals, flies, worms, and yeast. *DDX3X* and *DDX3Y* are maintained as an X-Y pair across all lineages of eutherian mammals for which we have high quality sequence, confirming their haploinsufficiency. In other lineages, *DDX3* orthologs are autosomal and have similarly essential functions in RNA metabolism. The C. elegans ortholog *Laf*-1 is essential for germ-line development. LAF-1 is expressed most highly in embryos, where it promotes P-granule formation, but is expressed at all developmental stages (Elbaum-Garfinkle et al., 2015). In *D. melanogaster*, the *DDX3* ortholog *Belle* is an essential translation factor. Complete loss-of-function (LOF) mutations of *Belle* result in embryonic lethality while hypomorphs are sterile, consistent with high dosage-sensitivity across lineages (Johnstone et al., 2005). Indeed, even the yeast ortholog *Ded1* is essential and is a key translation initiation factor. In contrast with human DDX3X, Ded1 regulates the translation of most mRNAs, while DDX3X aids in the translation of hundreds of complex mRNAs (Sharma et al., 2017).

There are also *DDX3Y*-specific paralogs in rodent lineages, as a result of retrotransposition from the Y chromosome. While many of these genes are pseudogenes and do not show protein activity, some, like rat *PL10*, have developed testis-specific expression and may play a role in the male reproductive tract (Chang & Liu, 2010).

Phenotypic consequences of perturbation

The deep conservation of *DDX3X* and its essentiality/haploinsufficiency in many lineages suggests that perturbations to *DDX3X* and/or *DDX3Y* might be deleterious in humans. Indeed, human *DDX3X* and *DDX3Y* mutations are associated with several disorders.

Germline mutations in *DDX3X* vs *DDX3Y* cause starkly different phenotypes in males. Rare germline mutations of *DDX3X* cause a neurodevelopmental disorder ('DDX3X syndrome') in males; only 5 such males have been identified (Kellaris et al., 2018; Nicola et al., 2019). Meanwhile, germline deletions of *DDX3Y*, encompassing what is termed the 'Azoospermia Factor a (AZFa)' region, have only been reported in cases of male infertility; these men present with azoospermia, or complete spermatogenic failure (Sun et al., 2000). This difference is also seen with somatic LOF mutations. *DDX3X* mutations drive many male-biased lymphomas, melanomas, medulloblastomas and leukemias (Brandimarte et al., 2014; Gong et al., 2021; Patmore et al., 2020; Phung et al., 2019). However, *DDX3Y* somatic mutations have not been

identified as drivers in human cancers. There are conflicting reports that several cancers might be marked by *DDX3X* or *DDX3Y* over-expression (He et al., 2018).

DDX3X mutations present differently in males vs females. Females with *DDX3X* syndrome have de novo mutations that completely ablate *DDX3X* helicase function (Snijders Blok et al., 2015). No males with these mutations have been reported, suggesting embryonic lethality in XY individuals. The aforementioned males with this syndrome inherit a hypomorphic allele from an unaffected mother. This suggests that all mutations result in better outcomes in females, which have a second copy of *DDX3X*.

Why do *DDX3X* mutations manifest phenotypically differently in females vs males? Why are there such stark differences in the phenotypic consequences of *DDX3X* and *DDX3Y* mutations in males? These questions have been difficult to answer due to the lack of scholarship about the relationship between the homologs. While *DDX3Y* is expressed throughout the human body in males, it has primarily been studied for its role in spermatogenesis. This is a result of early work that suggested that DDX3Y protein expression was restricted to the testis. However, recent studies have contradicted that theory and demonstrated robust DDX3Y protein expression in non-reproductive tissues (Godfrey et al., 2020). Still, there have been few studies of DDX3Y function and no studies of *DDX3X* and *DDX3Y* regulation.

This introduction highlights the importance of studying an evolutionary unique class of genes and summarizes the multi-functional roles of DDX3X and DDX3Y in the

cell. In Chapter 2, I describe my studies of *DDX3X* and *DDX3Y* regulation and uncover post-transcriptional auto- and cross-regulation that buffers changes to their expression. This regulation may underpin the sex differences in phenotypes I have described above. In Chapter 3, I ask if this regulatory phenomenon gives rise to previously unidentified gene dependencies in XY cancer cell lines. I find that cells with damaging *DDX3X* mutations become reliant on *DDX3Y* to survive, highlighting *DDX3Y* as a candidate druggable target in XY cancers. Finally, I suggest that studying the X-Y pair genes may serve in both identifying deeply conserved gene regulatory schemes and provide insight into the mechanisms behind sex-specific and sex-biased human phenotypes.

References

Bellott, D. W., Hughes, J. F., Skaletsky, H., Brown, L. G., Pyntikova, T., Cho, T.-J., Koutseva, N., Zaghlul, S., Graves, T., Rock, S., Kremitzki, C., Fulton, R. S., Dugan, S., Ding, Y., Morton, D., Khan, Z., Lewis, L., Buhay, C., Wang, Q., … Page, D. C. (2014). Mammalian Y chromosomes retain widely expressed dosage-sensitive regulators. *Nature*, *508*(7497), 494–499. https://doi.org/10.1038/nature13206

Bellott, D. W., Skaletsky, H., Pyntikova, T., Mardis, E. R., Graves, T., Kremitzki, C., Brown, L. G., Rozen, S., Warren, W. C., Wilson, R. K., & Page, D. C. (2010). Convergent evolution of chicken Z and human X chromosomes by expansion and gene acquisition. *Nature*, *466*(7306), 612–616. https://doi.org/10.1038/nature09172

Berletch, J. B., Yang, F., Xu, J., Carrel, L., & Disteche, C. M. (2011). Genes that escape from X inactivation. *Human Genetics*, *130*(2), 237–245. https://doi.org/10.1007/s00439-011-1011-z

Brandimarte, L., La Starza, R., Gianfelici, V., Barba, G., Pierini, V., Di Giacomo, D., Cools, J., Elia, L., Vitale, A., Luciano, L., Bardi, A., Chiaretti, S., Matteucci, C., Specchia, G., & Mecucci, C. (2014). DDX3X-MLLT10 fusion in adults with NOTCH1 positive T-cell acute lymphoblastic leukemia. *Haematologica*, *99*(5), 64–66. https://doi.org/10.3324/haematol.2013.101725

Brown, C. J., Ballabio, A., Rupert, J. L., Lafreniere, R. G., Grompe, M., Tonlorenzi, R., & Willard, H. F. (1991). A gene from the region of the human X inactivation centre is expressed exclusively from the inactive X chromosome. *Nature*, *349*(6304), 38–44. https://doi.org/10.1038/349038a0

Burgoyne, P. S., Mahadevaiah, S. K., Sutcliffe, M. J., & Palmer, S. J. (1992). Fertility in mice requires X-Y pairing and a Y-chromosomal “spermiogenesis” gene mapping to the long arm. *Cell*, *71*(3), 391–398. https://doi.org/10.1016/0092-8674(92)90509-b

Calviello, L., Venkataramanan, S., Rogowski, K. J., Wyler, E., Wilkins, K., Tejura, M., Thai, B., Krol, J., Filipowicz, W., Landthaler, M., & Floor, S. N. (2021). DDX3 depletion represses translation of mRNAs with complex 5’ UTRs. *Nucleic Acids Research*, *49*(9), 5336–5350. https://doi.org/10.1093/nar/gkab287

Cannizzaro, E., Bannister, A. J., Han, N., Alendar, A., & Kouzarides, T. (2018). DDX3X RNA helicase affects breast cancer cell cycle progression by regulating expression of KLF4. *FEBS Letters*, *592*(13), 2308–2322. https://doi.org/10.1002/1873-3468.13106

Chang, T.-C., & Liu, W.-S. (2010). The molecular evolution of PL10 homologs. *BMC Evolutionary Biology*, *10*, 127. https://doi.org/10.1186/1471-2148-10-127

Charlesworth, B., Morgan, M. T., & Charlesworth, D. (1993). The effect of deleterious mutations on neutral molecular variation. *Genetics*, *134*(4), 1289–1303. https://doi.org/10.1093/genetics/134.4.1289

Cui, B. C., Sikirzhytski, V., Aksenova, M., Lucius, M. D., Levon, G. H., Mack, Z. T., Pollack, C., Odhiambo, D., Broude, E., Lizarraga, S. B., Wyatt, M. D., & Shtutman, M. (2020). Pharmacological inhibition of DEAD-Box RNA Helicase 3 attenuates stress granule assembly. *Biochemical Pharmacology*, *182*, 114280. https://doi.org/10.1016/j.bcp.2020.114280

Disteche, C. M. (2012). Dosage Compensation of the Sex Chromosomes. *Annual Review of Genetics*, *46*, 537–560. https://doi.org/10.1146/annurev-genet-110711-155454

Elbaum-Garfinkle, S., Kim, Y., Szczepaniak, K., Chen, C. C.-H., Eckmann, C. R., Myong, S., & Brangwynne, C. P. (2015). The disordered P granule protein LAF-1 drives phase separation into droplets with tunable viscosity and dynamics. *Proceedings of the*

National Academy of Sciences of the United States of America, *112*(23), 7189–7194. https://doi.org/10.1073/pnas.1504822112

Engelstädter, J. (2008). Muller's Ratchet and the Degeneration of Y Chromosomes: A Simulation Study. *Genetics*, *180*(2), 957–967. https://doi.org/10.1534/genetics.108.092379

Fröhlich, A., Rojas-Araya, B., Pereira-Montecinos, C., Dellarossa, A., Toro-Ascuy, D., Prades-Pérez, Y., García-de-Gracia, F., Garcés-Alday, A., Rubilar, P. S., Valiente-Echeverría, F., Ohlmann, T., & Soto-Rifo, R. (2016). DEAD-box RNA helicase DDX3 connects CRM1-dependent nuclear export and translation of the HIV-1 unspliced mRNA through its N-terminal domain. *Biochimica Et Biophysica Acta*, *1859*(5), 719–730. https://doi.org/10.1016/j.bbagrm.2016.03.009

Godfrey, A. K., Naqvi, S., Chmátal, L., Chick, J. M., Mitchell, R. N., Gygi, S. P., Skaletsky, H., & Page, D. C. (2020). Quantitative analysis of Y-Chromosome gene expression across 36 human tissues. *Genome Research*, *30*(6), 860–873. https://doi.org/10.1101/gr.261248.120

Gong, C., Krupka, J. A., Gao, J., Grigoropoulos, N. F., Giotopoulos, G., Asby, R., Screen, M., Usheva, Z., Cucco, F., Barrans, S., Painter, D., Zaini, N. B. M., Haupl, B., Bornelöv, S., Ruiz De Los Mozos, I., Meng, W., Zhou, P., Blain, A. E., Forde, S., … Hodson, D. J. (2021). Sequential inverse dysregulation of the RNA helicases DDX3X and DDX3Y facilitates MYC-driven lymphomagenesis. *Molecular Cell*, *81*(19), 4059-4075.e11. https://doi.org/10.1016/j.molcel.2021.07.041

Graves, J. A. M. (2006). Sex chromosome specialization and degeneration in mammals. *Cell*, *124*(5), 901–914. https://doi.org/10.1016/j.cell.2006.02.024

He, Y., Zhang, D., Yang, Y., Wang, X., Zhao, X., Zhang, P., Zhu, H., Xu, N., & Liang, S. (2018). A double-edged function of DDX3, as an oncogene or tumor suppressor, in cancer progression (Review). *Oncology Reports*, *39*(3), 883–892. https://doi.org/10.3892/or.2018.6203

Hook, E. B., & Warburton, D. (1983). The distribution of chromosomal genotypes associated with Turner's syndrome: Livebirth prevalence rates and evidence for diminished fetal mortality and severity in genotypes associated with structural X abnormalities or mosaicism. *Human Genetics*, *64*(1), 24–27. https://doi.org/10.1007/BF00289473

Hughes, J. F., Skaletsky, H., Brown, L. G., Pyntikova, T., Graves, T., Fulton, R. S., Dugan, S., Ding, Y., Buhay, C. J., Kremitzki, C., Wang, Q., Shen, H., Holder, M., Villasana, D., Nazareth, L. V., Cree, A., Courtney, L., Veizer, J., Kotkiewicz, H., … Page, D. C. (2012). Strict evolutionary conservation followed rapid gene loss on human and rhesus Y chromosomes. *Nature*, *483*(7387), 82–86. https://doi.org/10.1038/nature10843

Hughes, J. F., Skaletsky, H., Pyntikova, T., Koutseva, N., Raudsepp, T., Brown, L. G., Bellott, D. W., Cho, T.-J., Dugan-Rocha, S., Khan, Z., Kremitzki, C., Fronick, C., Graves-Lindsay, T. A., Fulton, L., Warren, W. C., Wilson, R. K., Owens, E., Womack, J. E., Murphy, W. J., … Page, D. C. (2020). Sequence analysis in Bos taurus reveals pervasiveness of X-Y arms races in mammalian lineages. *Genome Research*, *30*(12), 1716–1726. https://doi.org/10.1101/gr.269902.120

Johnstone, O., Deuring, R., Bock, R., Linder, P., Fuller, M. T., & Lasko, P. (2005). Belle is a *Drosophila* DEAD-box protein required for viability and in the germ line. *Developmental Biology*, *277*(1), 92–101. https://doi.org/10.1016/j.ydbio.2004.09.009

Jowhar, Z., Xu, A., Venkataramanan, S., Dossena, F., Hoye, M. L., Silver, D. L., Floor, S. N., & Calviello, L. (2023). A ubiquitous GC content signature underlies multimodal mRNA regulation by DDX3X. *bioRxiv*, 2023.05.11.540322. https://doi.org/10.1101/2023.05.11.540322

Kellaris, G., Khan, K., Baig, S. M., Tsai, I.-C., Zamora, F. M., Ruggieri, P., Natowicz, M. R., & Katsanis, N. (2018). A hypomorphic inherited pathogenic variant in DDX3X causes male intellectual disability with additional neurodevelopmental and neurodegenerative features. *Human Genomics*, *12*(1), 11. https://doi.org/10.1186/s40246-018-0141-y

Koopman, P., Gubbay, J., Vivian, N., Goodfellow, P., & Lovell-Badge, R. (1991). Male development of chromosomally female mice transgenic for Sry. *Nature*, *351*(6322), 117–121. https://doi.org/10.1038/351117a0

Lahn, B. T., & Page, D. C. (1997). Functional coherence of the human Y chromosome. *Science (New York, N.Y.)*, *278*(5338), 675–680. https://doi.org/10.1126/science.278.5338.675

Lahn, B. T., & Page, D. C. (1999). Four evolutionary strata on the human X chromosome. *Science (New York, N.Y.)*, *286*(5441), 964–967. https://doi.org/10.1126/science.286.5441.964

Lai, M.-C., Lee, Y.-H. W., & Tarn, W.-Y. (2008). The DEAD-Box RNA Helicase DDX3 Associates with Export Messenger Ribonucleoproteins as well asTip-associated Protein and Participates in Translational Control. *Molecular Biology of the Cell*, *19*(9), 3847–3858. https://doi.org/10.1091/mbc.E07-12-1264

Lyon, M. F. (1962). Sex Chromatin and Gene Action in the Mammalian X-Chromosome. *American Journal of Human Genetics*, *14*(2), 135–148.

Muller, H. J. (1964). THE RELATION OF RECOMBINATION TO MUTATIONAL ADVANCE. *Mutation Research*, *106*, 2–9. https://doi.org/10.1016/0027-5107(64)90047-8

Nicola, P., Blackburn, P. R., Rasmussen, K. J., Bertsch, N. L., Klee, E. W., Hasadsri, L., Pichurin, P. N., Rankin, J., Raymond, F. L., DDD Study, & Clayton-Smith, J. (2019). De novo DDX3X missense variants in males appear viable and contribute to syndromic intellectual disability. *American Journal of Medical Genetics. Part A*, *179*(4), 570–578. https://doi.org/10.1002/ajmg.a.61061

Ohno, S. (1967). *Sex Chromosomes and Sex-Linked Genes* (Vol. 1). Springer. https://doi.org/10.1007/978-3-642-88178-7

Owens, M. C., Yanas, A., Shen, H., Zhang, C., & Liu, K. F. (2022). Biochemical Characterization of the Sexually Dimorphic Helicases DDX3X and DDX3Y. *The FASEB Journal*, *36*(S1). https://doi.org/10.1096/fasebj.2022.36.S1.R3383

Patmore, D. M., Jassim, A., Nathan, E., Gilbertson, R. J., Tahan, D., Hoffmann, N., Tong, Y., Smith, K. S., Kanneganti, T.-D., Suzuki, H., Taylor, M. D., Northcott, P., & Gilbertson, R. J. (2020). DDX3X Suppresses the Susceptibility of Hindbrain Lineages to Medulloblastoma. *Developmental Cell*, *54*(4), 455-470.e5. https://doi.org/10.1016/j.devcel.2020.05.027

Phung, B., Cieśla, M., Sanna, A., Guzzi, N., Beneventi, G., Cao Thi Ngoc, P., Lauss, M., Cabrita, R., Cordero, E., Bosch, A., Rosengren, F., Häkkinen, J., Griewank, K., Paschen, A., Harbst, K., Olsson, H., Ingvar, C., Carneiro, A., Tsao, H., … Jönsson, G. (2019). The X-Linked DDX3X RNA Helicase Dictates Translation Reprogramming and Metastasis in Melanoma. *Cell Reports*, *27*(12), 3573-3586.e7. https://doi.org/10.1016/j.celrep.2019.05.069

Rice, W. R. (1987). Genetic hitchhiking and the evolution of reduced genetic activity of the Y sex chromosome. *Genetics*, *116*(1), 161–167. https://doi.org/10.1093/genetics/116.1.161

Rosner, A., & Rinkevich, B. (2007). The DDX3 subfamily of the DEAD box helicases: Divergent roles as unveiled by studying different organisms and in vitro assays. *Current Medicinal Chemistry*, *14*(23), 2517–2525. https://doi.org/10.2174/092986707782023677

Ross, M. T., Grafham, D. V., Coffey, A. J., Scherer, S., McLay, K., Muzny, D., Platzer, M., Howell, G. R., Burrows, C., Bird, C. P., Frankish, A., Lovell, F. L., Howe, K. L., Ashurst, J. L., Fulton, R. S., Sudbrak, R., Wen, G., Jones, M. C., Hurles, M. E., … Bentley, D. R.

(2005). The DNA sequence of the human X chromosome. *Nature*, *434*(7031), 325–337. https://doi.org/10.1038/nature03440

Samir, P., Kesavardhana, S., Patmore, D. M., Gingras, S., Malireddi, R. K. S., Karki, R., Guy, C. S., Briard, B., Place, D. E., Bhattacharya, A., Sharma, B. R., Nourse, A., King, S. V., Pitre, A., Burton, A. R., Pelletier, S., Gilbertson, R. J., & Kanneganti, T.-D. (2019). DDX3X acts as a live-or-die checkpoint in stressed cells by regulating NLRP3 inflammasome. *Nature*, *573*(7775), 590–594. https://doi.org/10.1038/s41586-019-1551-2

San Roman, A. K., Godfrey, A. K., Skaletsky, H., Bellott, D. W., Groff, A. F., Harris, H. L., Blanton, L. V., Hughes, J. F., Brown, L., Phou, S., Buscetta, A., Kruszka, P., Banks, N., Dutra, A., Pak, E., Lasutschinkow, P. C., Keen, C., Davis, S. M., Tartaglia, N. R., … Page, D. C. (2023). The human inactive X chromosome modulates expression of the active X chromosome. *Cell Genomics*, *3*(2), 100259. https://doi.org/10.1016/j.xgen.2023.100259

Sekido, R., & Lovell-Badge, R. (2009). Sex determination and SRY: Down to a wink and a nudge? *Trends in Genetics: TIG*, *25*(1), 19–29. https://doi.org/10.1016/j.tig.2008.10.008

Sekiguchi, T., Iida, H., Fukumura, J., & Nishimoto, T. (2004). Human DDX3Y, the Y-encoded isoform of RNA helicase DDX3, rescues a hamster temperature-sensitive ET24 mutant cell line with a DDX3X mutation. *Experimental Cell Research*, *300*(1), 213–222. https://doi.org/10.1016/j.yexcr.2004.07.005

Sharma, D., Putnam, A. A., & Jankowsky, E. (2017). Biochemical Differences and Similarities between the DEAD-Box Helicase Orthologs DDX3X and Ded1p. *Journal of Molecular Biology*, *429*(23), 3730–3742. https://doi.org/10.1016/j.jmb.2017.10.008

Shen, H., Yanas, A., Owens, M. C., Zhang, C., Fritsch, C., Fare, C. M., Copley, K. E., Shorter, J., Goldman, Y. E., & Liu, K. F. (2022). Sexually dimorphic RNA helicases DDX3X and DDX3Y differentially regulate RNA metabolism through phase separation. *Molecular Cell*, *82*(14), 2588-2603.e9. https://doi.org/10.1016/j.molcel.2022.04.022

Skaletsky, H., Kuroda-Kawaguchi, T., Minx, P. J., Cordum, H. S., Hillier, L., Brown, L. G., Repping, S., Pyntikova, T., Ali, J., Bieri, T., Chinwalla, A., Delehaunty, A., Delehaunty, K., Du, H., Fewell, G., Fulton, L., Fulton, R., Graves, T., Hou, S.-F., … Page, D. C. (2003). The male-specific region of the human Y chromosome is a mosaic of discrete sequence classes. *Nature*, *423*(6942), 825–837. https://doi.org/10.1038/nature01722

Snijders Blok, L., Madsen, E., Juusola, J., Gilissen, C., Baralle, D., Reijnders, M. R. F., Venselaar, H., Helsmoortel, C., Cho, M. T., Hoischen, A., Vissers, L. E. L. M., Koemans, T. S., Wissink-Lindhout, W., Eichler, E. E., Romano, C., Van Esch, H., Stumpel, C., Vreeburg, M., Smeets, E., … Kleefstra, T. (2015). Mutations in DDX3X Are a Common Cause of Unexplained Intellectual Disability with Gender-Specific Effects on Wnt Signaling. *American Journal of Human Genetics*, *97*(2), 343–352. https://doi.org/10.1016/j.ajhg.2015.07.004

Song, H., & Ji, X. (2019). The mechanism of RNA duplex recognition and unwinding by DEAD-box helicase DDX3X. *Nature Communications*, *10*, 3085. https://doi.org/10.1038/s41467-019-11083-2

Soto-Rifo, R., & Ohlmann, T. (2013). The role of the DEAD-box RNA helicase DDX3 in mRNA metabolism. *Wiley Interdisciplinary Reviews. RNA*, *4*(4), 369–385. https://doi.org/10.1002/wrna.1165

Soulat, D., Bürckstümmer, T., Westermayer, S., Goncalves, A., Bauch, A., Stefanovic, A., Hantschel, O., Bennett, K. L., Decker, T., & Superti-Furga, G. (2008). The DEAD-box helicase DDX3X is a critical component of the TANK-binding kinase 1-dependent innate immune response. *The EMBO Journal*, *27*(15), 2135–2146. https://doi.org/10.1038/emboj.2008.126

Sun, C., Skaletsky, H., Rozen, S., Gromoll, J., Nieschlag, E., Oates, R., & Page, D. C. (2000). Deletion of azoospermia factor a (AZFa) region of human Y chromosome caused by recombination between HERV15 proviruses. *Human Molecular Genetics*, *9*(15), 2291–2296. https://doi.org/10.1093/oxfordjournals.hmg.a018920

Valentin-Vega, Y. A., Wang, Y.-D., Parker, M., Patmore, D. M., Kanagaraj, A., Moore, J., Rusch, M., Finkelstein, D., Ellison, D. W., Gilbertson, R. J., Zhang, J., Kim, H. J., & Taylor, J. P. (2016). Cancer-associated DDX3X mutations drive stress granule assembly and impair global translation. *Scientific Reports*, *6*, 25996. https://doi.org/10.1038/srep25996

Venkataramanan, S., Gadek, M., Calviello, L., Wilkins, K., & Floor, S. N. (2021). DDX3X and DDX3Y are redundant in protein synthesis. *RNA (New York, N.Y.)*, *27*(12), 1577–1588. https://doi.org/10.1261/rna.078926.121

Wu, D.-W., Lee, M.-C., Wang, J., Chen, C.-Y., Cheng, Y.-W., & Lee, H. (2014). DDX3 loss by p53 inactivation promotes tumor malignancy via the MDM2/Slug/E-cadherin pathway and poor patient outcome in non-small-cell lung cancer. *Oncogene*, *33*(12), 1515–1526. https://doi.org/10.1038/onc.2013.107

Chapter 2
Post-transcriptional cross- and auto-regulation buffer expression of the human RNA helicases *DDX3X* and *DDX3Y*

Shruthi Rengarajan[1,2], Jason Derks[3], Daniel W. Bellott[1], Nikolai Slavov[3], David C. Page[1,2,4]

Affiliations:

1. Whitehead Institute, Cambridge, MA 02142, USA
2. Department of Biology, Massachusetts Institute of Technology, Cambridge, MA 02139, USA
3. Departments of Bioengineering, Biology, Chemistry and Chemical Biology, Single Cell Proteomics Center, and Barnett Institute, Northeastern University, Boston, MA, USA
4. Howard Hughes Medical Institute, Whitehead Institute, Cambridge, MA 02142, USA

Author contributions:

S.R., N.S and D.C.P designed the experiments. S.R. and J.D. performed the experiments. S.R, D.W.B., and J.D., performed computational analyses. S.R. and D.C.P. wrote the manuscript with edits from N.S. and J.D.

Abstract

The Y-linked gene *DDX3Y* and its X-linked homolog *DDX3X* survived the evolution of the human sex chromosomes from ordinary autosomes. *DDX3X* encodes a multi-functional RNA helicase, with mutations causing developmental disorders and cancers. We find that *DDX3X* is extraordinarily dosage-sensitive and that perturbation of either *DDX3X* or *DDX3Y* expression is buffered -- by negative cross-regulation of *DDX3X* and *DDX3Y* in 46,XY cells, and by negative auto-regulation of *DDX3X* in 46,XX cells. Studying cells of individuals with sex chromosome aneuploidy, we find that when the number of Y chromosomes increases, *DDX3X* transcript levels fall; conversely, when the number of X chromosomes increases, *DDX3Y* transcript levels fall. In 46,XY cells, CRISPRi knockdown of either *DDX3X* or *DDX3Y* causes transcript levels of the homologous gene to rise. In 46,XX cells, chemical inhibition of DDX3X protein activity elicits an increase in *DDX3X* transcript levels. *DDX3X-DDX3Y* cross-regulation is mediated through mRNA destabilization – as shown by metabolic labeling of newly transcribed RNA -- and buffers total levels of *DDX3X* and *DDX3Y* protein in human cells. We infer that posttranscriptional auto-regulation of the ancestral (autosomal) *DDX3* gene transmuted into auto- and cross-regulation of *DDX3X* and *DDX3Y* as these sex-linked genes evolved from ordinary alleles of their autosomal precursor.

Introduction

DDX3X and *DDX3Y* are homologous but non-identical genes on the human X and Y chromosomes (Lahn & Page, 1997). They encode pleiotropic RNA helicases implicated in multiple aspects of RNA metabolism, including stability, splicing, export, translation, and stress response (Soto-Rifo & Ohlmann, 2013). *DDX3X* is highly conserved, with orthologs in mammals, flies, worms, and yeast (Elbaum-Garfinkle et al., 2015; Johnstone et al., 2005; Sharma et al., 2017). Human *DDX3X* mutations are associated with several neurodevelopmental disorders and cancers (Snijders Blok et al., 2015; Valentin-Vega et al., 2016). *DDX3X* is expressed throughout the body from the "inactive" X chromosome (Xi) in females as well as from the "active" X chromosome (Xa) in males and females (Lahn & Page, 1997; Tukiainen et al., 2017). While *DDX3Y* is also ubiquitously expressed (from the Y chromosome) in males (Godfrey et al., 2020), it has primarily been studied for its role in spermatogenesis (Ramathal et al., 2015). The X-and Y-encoded proteins are 91% identical at the amino acid level (Lahn & Page, 1997). While they have significantly diverged in their N- and C-terminal regions, the RNA binding and helicase domains are largely conserved (Rosner & Rinkevich, 2007). Early experiments showed that DDX3Y was functionally interchangeable with DDX3X *in vitro* (Sekiguchi et al., 2004). More recent work has shown that the proteins have partially overlapping functions, with similar effects on protein synthesis (Venkataramanan et al., 2021) but differing capacities for stress granule formation and translational repression (Shen et al., 2022; Venkataramanan et al., 2021).

DDX3X and *DDX3Y* constitute one of 17 gene pairs on the human X and Y chromosomes that survived the chromosomes' evolution from two ordinary pairs of autosomes during the past 200 million years. A series of inversions suppressed crossing over between the X and Y chromosomes outside of a diminishing pseudoautosomal region (PAR), exposing the non-pseudoautosomal bulk of the Y chromosome to genetic decay (Lahn & Page, 1999). While the human X chromosome retains 98% of the genes present on the ancestral autosomes, only 3% remain on the human Y chromosome (Bellott et al., 2014). The surviving Y chromosome genes were preserved by selection to maintain the ancestral dosage of regulators of key cellular processes. As a group, these gene pairs are broadly expressed and highly dosage-sensitive. Among this select group of X-Y gene pairs, *DDX3X* and *DDX3Y* are the only pair with starkly different developmental phenotypes reported with loss of function mutations. Males with *DDX3X* mutations are extremely rare and present with a disorder that causes neurodevelopmental, behavioral and cardiac phenotypes (Kellaris et al., 2018). Conversely, males with germline deletions of *DDX3Y* suffer from spermatogenic failure but are otherwise healthy (Sun et al., 2000). We reasoned that control of *DDX3X* and *DDX3Y* dosage might be especially crucial to understand this difference and sought to identify mechanisms that regulate *DDX3X* and *DDX3Y* levels.

Here we report that *DDX3X* and *DDX3Y* are extraordinarily dosage sensitive, even when compared with other human X-Y gene pairs. Their dosage is buffered by post-transcriptional cross-regulation in 46,XY cells, while *DDX3X* is post-

transcriptionally auto-regulated in 46,XX cells, consistent with this regulatory mechanism having been present on and preserved from the ancestral autosomes that evolved to become the human sex chromosomes.

Results

DDX3X and *DDX3Y* are especially dosage-sensitive compared to genes with a similar evolutionary trajectory

We first asked if *DDX3X* and *DDX3Y* are more dosage-sensitive than other human X-Y gene pairs. For each of the 17 gene pairs, we tallied whether dosage sensitivity had necessitated 1) expression from Xi in human females and 2) maintenance of a Y-homolog across males of diverse species -- both features of highly dosage-sensitive genes (Bellott et al., 2014). We addressed the first point by re-analyzing Xi expression data recently generated from cultured human cells (San Roman et al., 2023).

For each Y-homolog, we asked if the gene is conserved across 15 therian (placental mammalian) species where high-quality, contiguous sequence assemblies of the sex chromosomes are available. Specifically, for each Y-homolog we calculated a phylogenetic branch length – the sum of all branch lengths connecting species where the gene is present, and thus a measure of the gene's longevity on therian Y chromosomes. We also calculated survival fraction – the ratio of phylogenetic branch length to maximum possible branch length (Bellott & Page, 2021).

Among X-Y gene pairs, those with the highest dosage sensitivity should be expressed from Xi in females and be long-lived and universally retained on the Y chromosome across species, *i.e.*, have a survival fraction of 1. We find that, among the 17 human X-Y gene pairs, only *DDX3X(Y), KDM6A(UTY)*, and *ZFX(Y)* are expressed from Xi in human females and retain a Y-homolog in all 15 eutherian species examined (Table 1).

Table 1: Dosage-sensitivity of human X-Y pair genes across therian mammalian lineages. Xi expression is indicated for X-homologs, and survival fraction and branch length are calculated for the corresponding Y-homologs. Genes are sorted first by Xi expression, then by Y-homolog survival fraction, and finally by Y-homolog branch length.

Gene	Xi Expression	Y-homolog	Survival Fraction	Branch Length (MY)
DDX3X	Yes	*DDX3Y*	1.00	662.840
KDM6A	Yes	*UTY*	1.00	662.840
ZFX	Yes	*ZFY*	1.00	662.840
NLGN4X	Yes	*NLGN4Y*	1.00	140.340
USP9X	Yes	*USP9Y*	0.990	656.140
PRKX	Yes	*PRKY*	0.851	74.180
EIF1AX	Yes	*EIF1AY*	0.833	551.940
KDM5C	Yes	*KDM5D*	0.831	686.840
TXLNG	Yes	*TXLNGY*	0.664	440.040
RPS4X	Yes	*RPS4Y*	0.355	342.940
SOX3	No	*SRY*	1.000	966.840
RBMX	No	*RBMY*	0.943	911.840
HSFX1	No	*HSFY1*	0.834	806.040
TSPYL2	No	*TSPY*	0.776	641.940
AMELX	No	*AMELY*	0.685	453.740
TBL1X	No	*TBL1Y*	0.644	90.440
TMSB4X	No	*TMSB4Y*	0.465	308.040

We further profiled the sensitivity of *DDX3X* to dosage changes using two metrics: 1) P_{CT} scores, which measure the evolutionary conservation of microRNA

targeting sites in a gene's 3' UTR (Friedman et al., 2009), and 2) LOEUF values, the ratio of observed to expected loss-of-function variants in a gene in human populations (Karczewski et al., 2020). High conservation of miRNA targeting sites in a gene's 3' UTR implies sensitivity to over-expression (Naqvi et al., 2018), while a low LOEUF value demonstrates sensitivity to loss of function. For all non-PAR genes on the human X chromosome (San Roman et al., 2023), we calculated percentile ranks according to each of these two metrics, from most constrained (high percentile) to least constrained (low percentile). Among X-Y pair genes expressed from Xi, *DDX3X* has the highest combined sensitivity to over-expression and loss of function, implying that its level of expression is especially constrained (Fig. 1A).

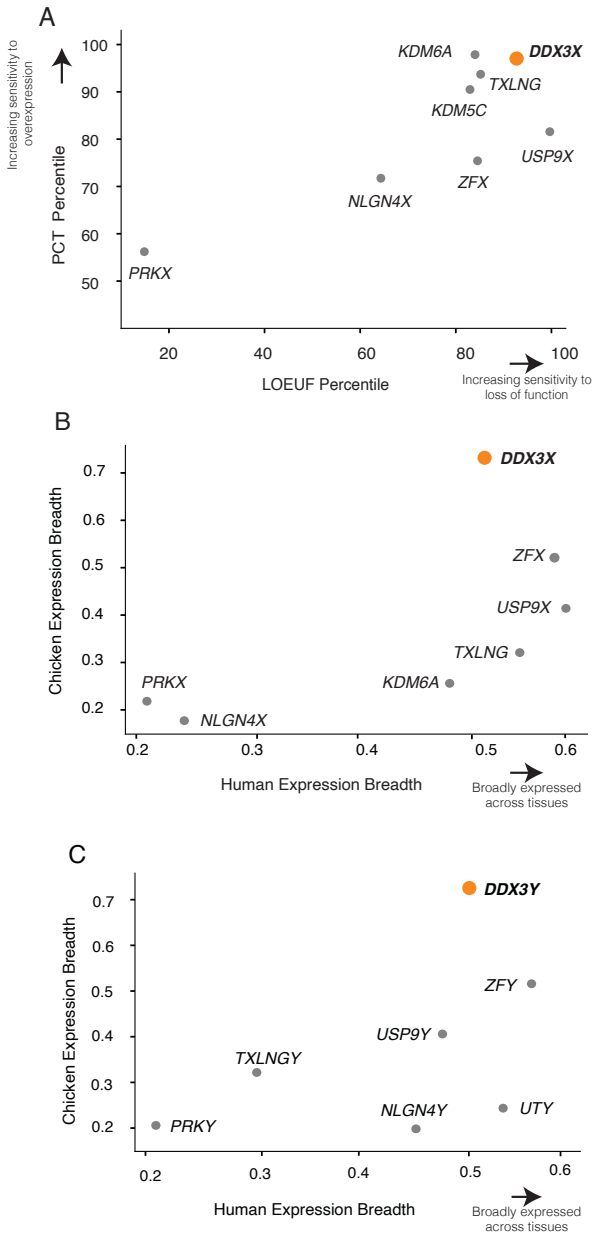

Fig 1: *DDX3X* is highly dosage sensitive and expressed broadly among human tissues. A) Among human X-Y pair genes, *DDX3X* ranks highest in combined sensitivity to over-expression (as judged by PCT percentile among all X-chromosome genes) and under-expression (as judged by LOEUF percentile among all X-chromosome genes). B) *DDX3X* and C) *DDX3Y* and their chicken ortholog display the highest expression breadth among, respectively, the X and Y members of human X-Y gene pairs.

We also assessed whether *DDX3X* and *DDX3Y* are expressed more broadly across the body than other X-Y gene pairs – another feature of highly dosage-sensitive genes (Bellott et al., 2014) – and if this breadth was present ancestrally. The ancestral state of sex-linked genes can be inferred from analyses of birds such as chickens, where the orthologs of human sex chromosomal genes are found on autosomes 1 and

4 (Bellott et al., 2010). For each gene pair for which expression data was available in humans (GTEx, 2017) and chickens (Bellott et al., 2014; Merkin et al., 2012), we measured how broadly the chicken gene and human gene pair were expressed across the body's various tissues. *DDX3X*, *DDX3Y*, and their autosomal chicken ortholog display the highest combined expression breadth across the two species, suggesting that their dosage is critical throughout the body (Fig. 1B, 1C).

DDX3X **and** ***DDX3Y*** **transcript levels fall as, respectively, Y-chromosome and X-chromosome copy numbers rise**

To identify mechanisms that regulate *DDX3X* and *DDX3Y* expression in human cells, we re-analyzed RNA-sequencing data from primary skin fibroblasts of human donors with sex chromosome aneuploidies (San Roman et al., 2023). We first assessed *DDX3X* and *DDX3Y* transcript levels in cells with a single X chromosome and increasing numbers of Y chromosomes. As expected, *DDX3Y* transcript levels rise with increasing numbers of Y chromosomes. However, *DDX3X* expression from the single X chromosome falls significantly (Fig. 2A, B). Conversely, in cells with a single Y chromosome and increasing numbers of X chromosomes, *DDX3X* transcript levels rise, as expected given its expression from both Xa and Xi. However, *DDX3Y* expression from the single Y chromosome falls significantly (Fig 2C, D).

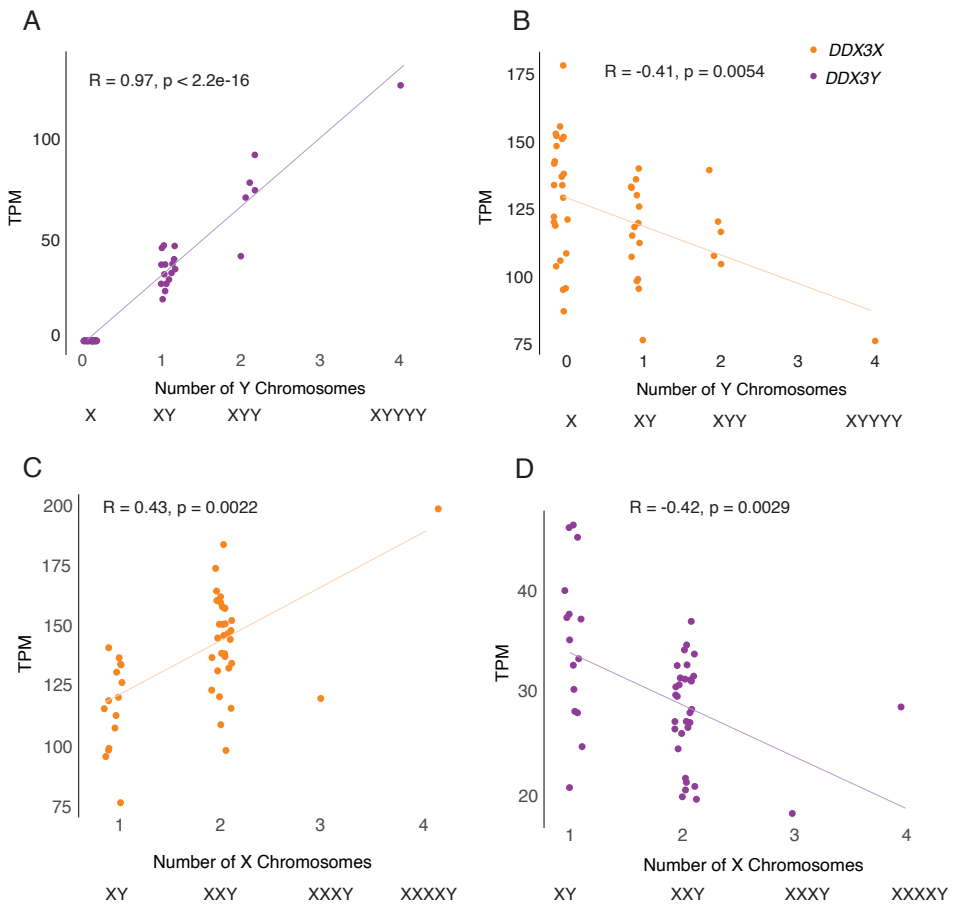

Fig. 2: *DDX3X* and *DDX3Y* expression is negatively responsive to, respectively, Y and X chromosome copy number. Scatterplots show *DDX3X* and *DDX3Y* transcript levels in cultured fibroblasts with the indicated sex chromosome constitutions. Each point represents a primary fibroblast culture from one individual. A,B) *DDX3Y* transcript levels are significantly elevated and *DDX3X* transcript levels significantly reduced in fibroblasts with multiple Y chromosomes. C,D) *DDX3X* transcript levels are significantly elevated and *DDX3Y* transcript levels significantly reduced in fibroblasts with multiple X chromosomes. R values and statistical significance calculated using Pearson correlation.

We asked whether this inverse relationship is common across all X-Y gene pairs, or is a special feature of *DDX3X* and *DDX3Y*. For each X-Y pair gene, we obtained values for the change in its transcript levels per extra Xi, and the change in its transcript levels per extra Y chromosome (San Roman et al., 2023). In both fibroblasts and lymphoblastoid cell lines (LCLs), *DDX3X* transcript levels fall significantly as Y chromosome copy number increases; conversely, *DDX3Y* transcript levels fall as X chromosome copy number increases (Table S1). This response is not observed with other X-Y pair genes; it is unique to *DDX3X* and *DDX3Y* (Table S1).

We considered the possibility that these decreases in *DDX3X* and *DDX3Y* transcript levels in response to changes in sex chromosome copy number might reflect a general cellular response to aneuploidy. To test this, we examined LCLs from individuals with trisomy 21. We observed no change in *DDX3X* or *DDX3Y* transcript levels in response to chromosome 21 copy number (Fig S1). We conclude that *DDX3X* and *DDX3Y* transcript levels are inversely related to Chr Y and Chr X copy number, respectively.

Perturbing *DDX3X* elicits a response in *DDX3Y*, and vice versa

We asked whether these effects of altering sex chromosome copy number are due to changes in *DDX3X* and *DDX3Y* expression. We examined naturally occurring mutations that affect *DDX3X* or *DDX3Y* expression as well as experimental knockdowns to capture the effects of perturbing *DDX3X* and *DDX3Y* transcript levels.

First, we quantified *DDX3X* transcripts in LCLs from azoospermic (infertile) males with *AZFa* micro-deletions. *AZFa* micro-deletions result from homologous recombination between endogenous retroviral elements on the human Y chromosome, and they remove the *DDX3Y* and *USP9Y* genes without affecting other genes (Fig. 3A) (Sun et al., 2000). We found that *DDX3X* transcript levels were significantly higher in LCLs from *AZFa*-deleted males compared to males with intact Y chromosomes (Fig. 3B). To test whether *DDX3X* transcript levels are elevated upon deletion of other Y-chromosome regions, we profiled LCLs from XY individuals whose Y-chromosomes retain *DDX3Y* but are missing several other genes, including the sex determining gene *SRY* (Schiebel et al., 1997). *DDX3X* transcript levels were unaltered in these individuals (Fig. S2),

demonstrating that *DDX3X* levels are elevated specifically in response to *DDX3Y* deletion.

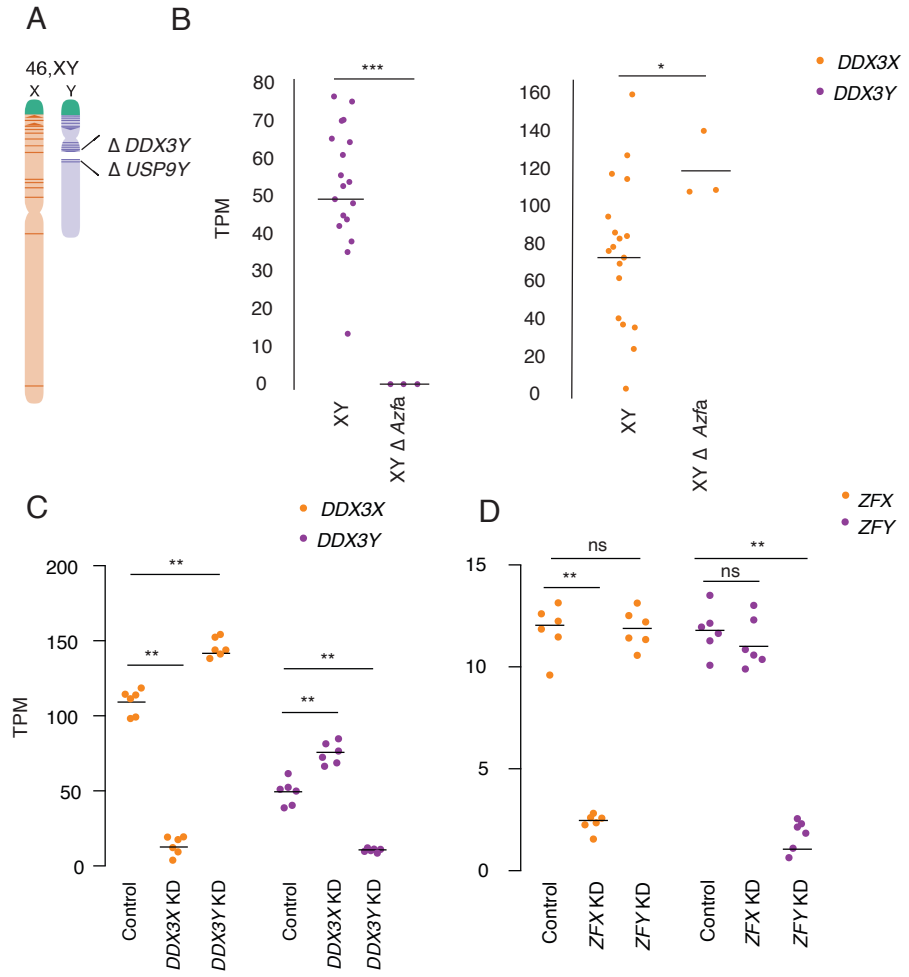

Fig. 3: *DDX3X* and *DDX3Y* each respond directly to perturbations in the other's expression. A) Schematic diagram of naturally occurring human Y-chromosome (AZFa) micro-deletion of *DDX3Y* and *USP9Y*. B) *DDX3X* transcript levels are significantly higher in *AZFa*-deleted 46,XY LCLs compared to Y-chromosome-intact 46,XY LCLs. Each point represents a sample from one individual. Statistical significance determined by Mann Whitney- U test, *** $p < 0.0001$, * $p < 0.05$ C) CRISPRi-mediated knockdown of *DDX3Y* using two independent gRNAs in three unrelated 46,XY fibroblast cultures results in significantly elevated *DDX3X* transcript levels. Conversely, *DDX3X* knockdown results in significantly elevated *DDX3Y* transcript levels. D) Re-analysis of CRISPRi knockdown of *ZFX* or *ZFY* (San Roman et al., 2023) demonstrates that knockdown of either gene does not result in significant elevation of the homolog's transcripts. Statistical significance determined by ANOVA, ** $p < 0.001$.

We then used CRISPRi to target *DDX3X* or *DDX3Y* for knockdown in primary 46,XY fibroblasts. *DDX3X* transcript levels rose significantly upon knockdown of *DDX3Y* (*DDX3Y* KD), and *DDX3Y* transcript levels responded in reciprocal fashion to *DDX3X* KD (Fig. 3C). This negative cross-regulation across X and Y homologs was specific to *DDX3X* and *DDX3Y*, as CRISPRi knockdowns of *ZFX* and *ZFY*, another broadly expressed, dosage-sensitive X-Y gene pair, did not show this pattern (Fig. 3D) (San Roman et al., 2023). We validated these findings in an independent dataset, the Cancer Cell Line Encyclopedia (CCLE), which catalogs mutational and expression data from hundreds of cancer cell lines (Ghandi et al., 2019). There we identified 491 different XY cell lines that retained the Y chromosome, and among these a set of 11 lines that harbored loss of function mutations in *DDX3X* (Table S2). *DDX3Y* transcript levels are significantly higher in these 11 cell lines compared to lines where *DDX3X* is presumed intact (Fig. S3). Thus, knockdowns or loss of function in either *DDX3X* or *DDX3Y* are consistently buffered by compensatory increases in the homolog's expression, demonstrating that *DDX3X* and *DDX3Y* are negatively cross-regulated.

Taken together, these three approaches show that *DDX3X* and *DDX3Y* are negatively cross-regulated in multiple cell types: in LCLs, in primary fibroblasts, and in cancer cell lines originating from five different tissues (Table S2), demonstrating that this is a general, global response independent of tissue type or disease state. This model readily explains compensatory increases in *DDX3Y* transcript levels that other investigators have observed 1) in *DDX3X*-mutant lymphomas, where it was interpreted as an oncogenic adaptation (Gong et al., 2021) and 2) in mouse models of *DDX3X*

syndrome and medulloblastoma (Gong et al., 2021; Hoye et al., 2022; Patmore et al., 2020). We conclude that negative cross-regulation of *DDX3X* and *DDX3Y* occurs in many if not all somatic tissues and cell types, in both humans and mice.

Negative cross-regulation of *DDX3X* buffers total levels of *DDX3X* and *DDX3Y*

We hypothesized that negative cross-regulation of *DDX3X* and *DDX3Y* serves to maintain the combined expression of the two genes in a narrow range, buffering total transcript levels against changes in gene dosage. To test this, we summed transcript levels for the two genes in our knockdown models and observed that, in the setting of *DDX3Y* knockdown, the increase in *DDX3X* transcript levels fully compensates and maintains the summed transcript levels of *DDX3X* and *DDX3Y* at control levels (Fig. 4A). However, in the setting of *DDX3X* knockdown – a larger perturbation -- the increase in *DDX3Y* transcript levels does not fully compensate. We confirmed these results at the protein level using a mass-spectrometry framework that enables sensitive protein quantification by multiplexing peptides and samples (Derks et al., 2022). To

measure summed expression of DDX3X and DDX3Y protein, we quantified peptides shared by DDX3X and DDX3Y (Fig. 4B).

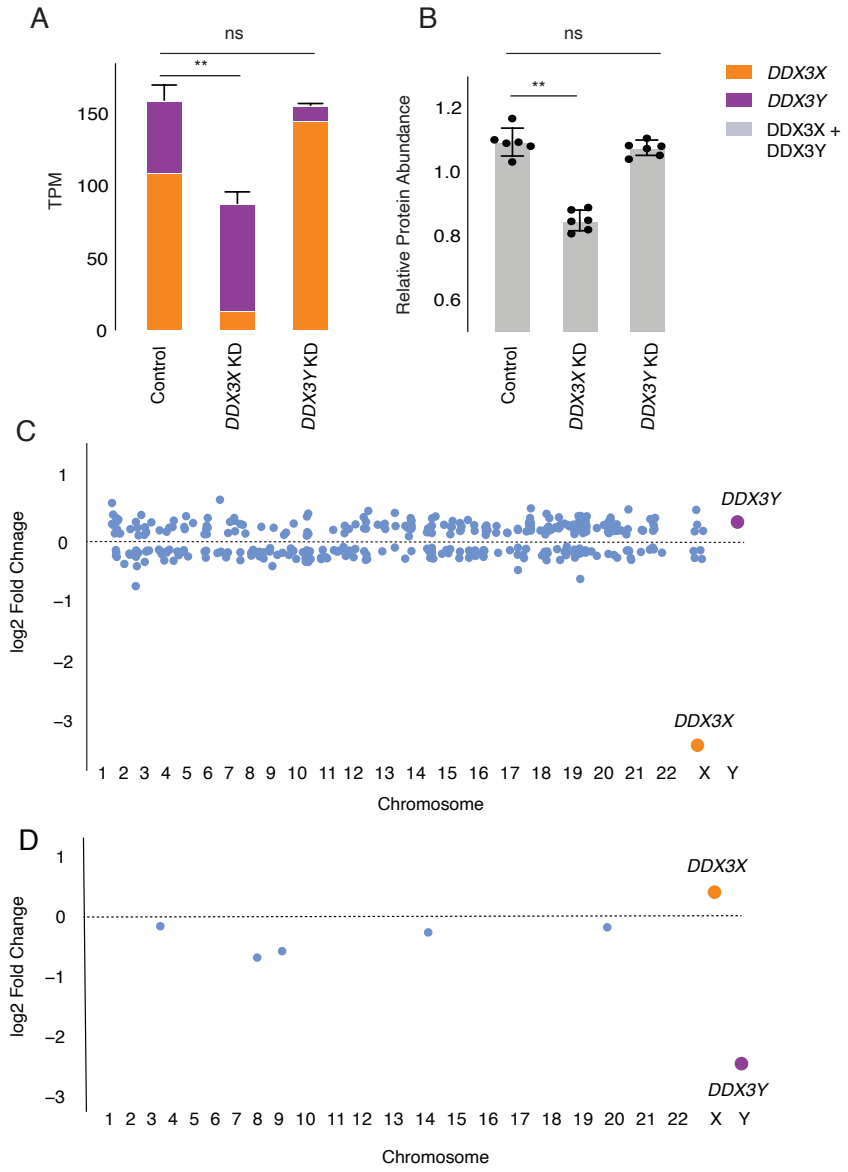

Fig 4: Increased expression of *DDX3X* fully compensates, at transcript and protein levels, for knockdown of *DDX3Y*, but the inverse is not true. A) Stacked bar graph showing summed TPM of *DDX3X* and *DDX3Y* in CRISPRi knockdowns using two independent gRNAs in three independent 46,XY fibroblast cultures. Statistical significance calculated by ANOVA, ** $p < 0.001$. B) Bar graph showing abundance of shared DDX3X and DDX3Y peptides in CRISPRi knockdowns with three technical replicates in two independent 46,XY fibroblast cultures. C) Differential gene expression analysis of control vs *DDX3X* knockdown reveals significant expression changes in 397 target genes across the genome, including *DDX3X* and *DDX3Y*. Genes with $p < 0.05$ (after multiple hypothesis correction) indicated in blue, with exception of *DDX3X* (in orange) and *DDX3Y* (in purple). D) Differential gene expression analysis of control vs *DDX3Y* knockdown reveals only six genes, including *DDX3X* and *DDX3Y*, that change significantly.

Given these results, we predicted that the incomplete compensation of summed DDX3X + DDX3Y protein levels seen with the *DDX3X* KD would result in genome-wide gene expression changes, while such changes would not occur with the *DDX3Y* KD. Indeed, the *DDX3X* KD significantly altered the expression of 379 genes (Fig. 4C), while

the *DDX3Y* KD significantly altered the expression of only six genes genome-wide, indicating nearly complete compensation through elevated *DDX3X* expression (Fig. 4D). The *DDX3X* knockdown has far-reaching consequences because of the limited ability of *DDX3Y* to compensate for diminished *DDX3X* expression.

We then asked whether negative cross-regulation of *DDX3X* and *DDX3Y* contributes to the genome-wide gene expression changes observed in individuals with sex chromosome aneuploidies. We found no significant overlap between 1) the set of genes responsive to increasing numbers of X chromosomes in the aneuploidy dataset (San Roman et al., 2023) and 2) the set of genes differentially expressed in our *DDX3X* KD (Fig. S4A). Unlike *ZFX*, which drives a large portion of the genome-wide response to X-chromosome copy number (San Roman et al., 2023), the elevated *DDX3X* expression observed with addition of Xi does not drive significant gene expression changes in the aneuploid lines. Indeed, the increase in summed *DDX3X* and *DDX3Y* transcript levels per additional sex chromosome (X or Y) is more modest than that of similarly constrained X-Y pairs (Fig. S4B,C,D), suggesting that *DDX3X* and *DDX3Y* are not major drivers of gene expression changes associated with sex chromosome aneuploidy.

DDX3X is auto-regulated in 46,XX cells

We hypothesized that negative cross-regulation of the *DDX3X*-*DDX3Y* gene pair evolved from an earlier system of negative auto-regulation in the autosomal ancestor of

this X-Y pair. Indeed, the yeast ortholog of *DDX3X* (*Ded1*) appears to be negatively auto-regulated (Silvia Marina, 2015). If negative cross-regulation in human XY cells evolved from negative auto-regulation, we might expect to observe negative auto-regulation of *DDX3X* in human XX cells. We set out to test for this, and, if present, whether it might be unique among the 17 human NPX genes with NPY homologs. For each X-Y pair gene where informative SNPs could be identified, we obtained its allelic ratio (AR), the ratio of Xi- and Xa-derived transcripts (San Roman et al., 2023). For each gene, we then compared its AR value to its ΔE_X value, the increment of change in a gene's expression per additional X, relative to Xa (San Roman et al., 2023). If an X-linked gene's expression from Xi and Xa are independent and additive, then the gene's AR should approximate its ΔE_X—and we found this to be true for all other NPX genes with NPY homologs. To the contrary, while *DDX3X* has an AR of 0.55 in LCLs and 0.42 in fibroblasts, it has a significantly lower ΔE_X of 0.26 in LCLs and 0.16 in fibroblasts (Fig 5A). In other words, while Xi contributes 55% or 42% as many transcripts as Xa does, *DDX3X* transcript levels increase by only 26% or 16% with each additional Xi. This strongly suggests that *DDX3X* is negatively auto-regulated in the absence of *DDX3Y*.

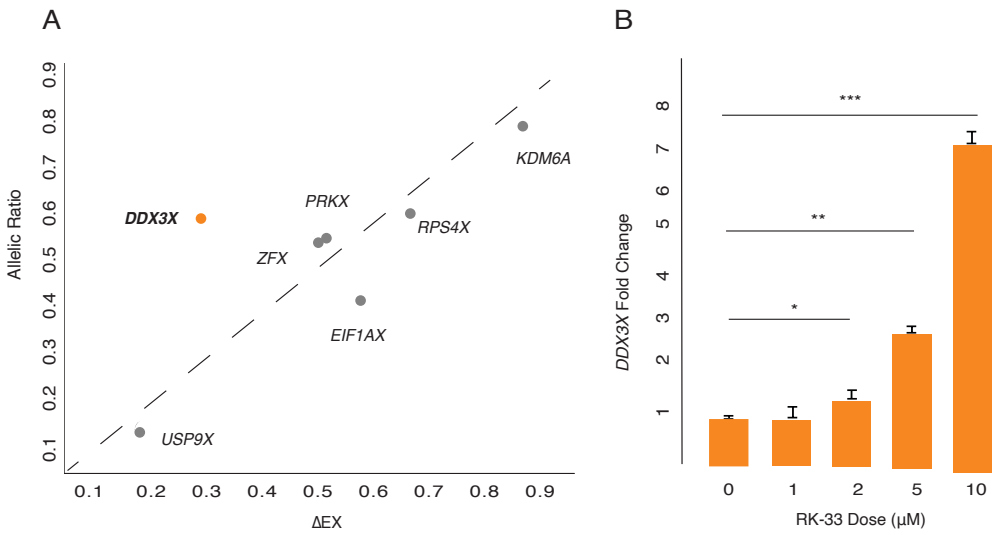

Fig 5: *DDX3X* is negatively auto-regulated in 46,XX cells. A) *DDX3X* 's allelic ratio (AR) is significantly higher than its ΔE_X value in LCLs, setting it apart it from all other Xi/Xa/Y-expressed X-Y pair genes, whose AR values approximate their ΔE_X values. B) *DDX3X* transcript levels (by qPCR) in 46,XX fibroblasts are significantly elevated in a dose-responsive manner upon treatment with DDX3 inhibitor RK-33. Statistical significance determined by one-sided t-test on delta Ct values. Error bars indicate standard deviation of three technical replicates. * $p < 0.05$, *** $p < 0.001$.

Moreover, we hypothesized that chemical inhibition of DDX3X protein activity could lead to increased *DDX3X* transcript levels. We directly perturbed *DDX3X* in XX fibroblasts using RK-33, a competitive inhibitor of DDX3X that binds its ATP-binding cleft and disrupts helicase function (Bol et al., 2015). Indeed, *DDX3X* transcript levels were significantly elevated, in a dose-dependent manner, in cells treated with RK-33 (Fig 5B). Increasing duration of RK-33 treatment also increased *DDX3X* transcript levels in a time-dependent manner (Fig S5). Together, these findings demonstrate that *DDX3X* transcript levels are negatively auto-regulated in XX cells.

In theory, our observations concerning auto- and cross-regulation could be explained by independent, parallel evolution of negative cross-regulation of *DDX3Y* by

DDX3X, and of *DDX3X* by *DDX3Y*, but this seems implausibly unlikely, especially given the absence of sexual recombination as an evolutionary enabler in the case of *DDX3Y*. A simpler hypothesis is that reciprocal cross-regulation of *DDX3X* and *DDX3Y* derives directly from a negative, post-transcriptional auto-regulatory mechanism that governed the ancestral (autosomal) *DDX3* gene. We conclude that this regulatory scheme was present in the *DDX3* gene in our amniote ancestors before the autosome carrying *DDX3* became part of today's mammalian sex chromosomes.

DDX3X **response is mediated by mRNA stability**

DDX3X encodes an RNA-binding protein known to bind its own transcripts (Van Nostrand et al., 2020). In yeast, the *DDX3* ortholog *Ded1* is negatively auto-regulated and this regulation is dependent on its 3'UTR, (Silvia Marina, 2015) indicating that *Ded1* mRNA stability is being modulated. We reasoned that the negative cross-regulation we observed between *DDX3X* and *DDX3Y* may involve mRNA stability. If *DDX3Y* destabilizes *DDX3X* transcripts, we would expect the half-life of *DDX3X* transcripts to decrease in response to increasing *DDX3Y* dosage. We tested this prediction by labeling nascent mRNAs in 46,XY and 49,XYYYY LCLs with 5-EU and sequencing these populations at discrete intervals to quantify mRNA half-life (Fig 6A). We calculated the ratio of nascent mRNA/ total mRNA normalized to steady-state levels, across time points, and observed a striking difference in *DDX3X* mRNA half-life between the two conditions. *DDX3X* mRNAs were 3-fold less stable in 49,XYYYY cells,

(Fig 6B) implying that DDX3Y directly or indirectly destabilizes *DDX3X* mRNAs, reducing the steady state levels of *DDX3X* transcripts. This result persists upon shortening 5EU labeling time (Fig. S5B). *DDX3X* steady state levels are lower in 49,XYYYY samples as predicted (Fig S5A).

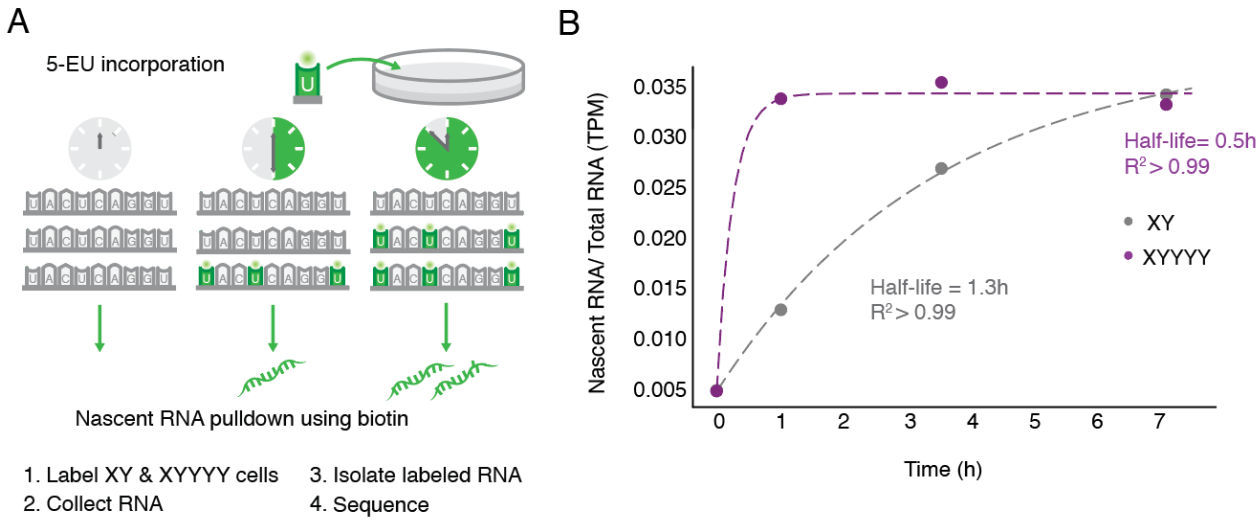

Fig 6: *DDX3X* mRNA stability is regulated. A) Schematic of experiment to determine half-lives of mRNAs. 46,XY and 49,XYYYY LCLs were incubated with 5-ethyl uridine to obtain nascent mRNAs. B) *DDX3X* is destabilized at least 3-fold in 49,XYYYY vs 46,XY LCLs.

Overall, these results support a model where ancestral (autosomal) *DDX3* destabilized its own transcripts to negatively auto-regulate its expression, foreshadowing the ability of mammalian *DDX3X* and *DDX3Y* to destabilize their own and each other's transcripts (Fig 7).

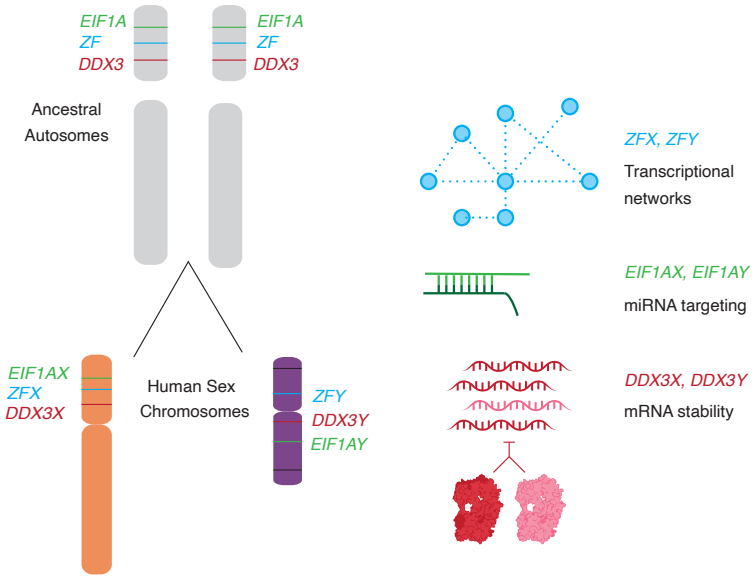

Fig 7: Coding sequences and gene regulatory mechanisms of X-Y gene pairs were preserved during sex chromosome evolution. The auto- and cross-regulation of *DDX3X* and *DDX3Y* likely originated from the auto-regulation of ancestral *DDX3*. Studies of other X-Y gene pairs such as *ZFX-ZFY* and *EIF1AX-EIF1AY* suggest that on a gene-by-gene basis, regulatory mechanisms also persist on the human X- and Y-chromosomes from the ancestral autosome.

Discussion:

DDX3X and DDX3Y are encoded by X- and Y-linked homologs and perform critical cellular roles in RNA metabolism (Soto-Rifo & Ohlmann, 2013). We report that *DDX3X* is negatively auto-regulated (Fig. 5) and that *DDX3X* and *DDX3Y* are negatively cross-regulated (Fig. 3). We also find that *DDX3X* transcript stability is modulated to achieve this regulation (Fig 6). These findings shed new light on the mechanisms by which dosage-sensitive genes on the sex chromosomes are regulated.

Gene regulatory mechanisms: preservation and modification during human sex chromosome evolution

We reasoned that such tight delimiting of *DDX3* gene expression likely pre-dated the divergence of the homologous genes *DDX3X* and *DDX3Y* on the sex chromosomes, supported by the auto- and cross-regulation of *DDX3X* and *DDX3Y* we observe in humans, and previous evidence of cross-regulation in mouse models (Hoye et al., 2022; Patmore et al., 2020). Strikingly, there is evidence that *Ded1*, the yeast ortholog of *DDX3X,* is similarly auto-regulated (Silvia Marina, 2015) suggesting that *DDX3X* regulation may be conserved over 1.3 billion years since the common ancestor of yeast and humans (Kumar et al., 2022). These data indicate that DDX3X's pre-existing gene regulatory mechanisms on the ancestral autosome were maintained on the human X and Y chromosomes (Fig 7), albeit with differences in the steady state transcript level of *DDX3X* and *DDX3Y* over at least 200 million years of evolution.

The ancestral origins of gene regulatory mechanisms on the sex chromosomes can also be seen in recent work studying other X-Y gene pairs. *ZFX* and *ZFY* dosage have similar genome-wide effects in LCLs and fibroblasts (San Roman et al., 2023), suggesting that their transcriptional networks have been preserved during sex chromosome evolution. However, the effects of *ZFX* are more potent than *ZFY* in knockdown studies, indicating a source of genome-wide sex differences (San Roman et al., 2023). Studies of miRNA sites provide further evidence for inferring the ancestral origin of X-Y gene pair regulatory elements; miRNA sites on avian Z-W chromosomes have been preserved on human sex chromosomes (Naqvi et al., 2018). *EIF1AX*, a key component of translation initiation, has retained a miR-1 site that is disrupted in *EIF1AY*, leading to 2-fold up-regulation of the Y-homolog in heart tissues (Godfrey et al., 2020).

Similarly, preservation of *DDX3X* and *DDX3Y* cross-regulation along with the differences in their steady state levels may underpin human disease phenotypes.

Implications for genetic disorders of *DDX3X* and *DDX3Y* in humans

Constitutional (germline) mutations in *DDX3X* and *DDX3Y* cause radically different phenotypes. In human males, reports of constitutional mutations in *DDX3X* are exceedingly rare; these are typically missense alleles that only partially reduce DDX3X protein function but nonetheless cause a neurodevelopmental disorder ('*DDX3X* syndrome') (Kellaris et al., 2018). By contrast, de novo deletions of the entire *DDX3Y* gene (so-called *AZFa* deletions) cause spermatogenic failure and thereby infertility but otherwise have no reported impact on somatic development, function, or health (Sun et al., 2000). As *DDX3X* accounts for the bulk of total *DDX3* expression in the male brain (Godfrey et al., 2020), we propose that elevated *DDX3X* transcript levels compensate for the absence of *DDX3Y* in the brain and other somatic tissues in *AZFa*-deleted males (Fig 4A,B), explaining why males with germline *DDX3Y* deletions display no neurodevelopmental consequences. In testicular germ cells, where *DDX3Y* predominates (Ramathal et al., 2015), DDX3X cannot compensate for the loss of *DDX3Y*, leading to azoospermia and male infertility.

Meanwhile, somatic loss-of-function mutations in *DDX3X* drive many male-biased lymphomas, medulloblastomas, and leukemias (Brandimarte et al., 2014; Gong et al., 2021; Patmore et al., 2020). The male bias is consistent with incomplete

compensation; *DDX3Y* levels are increased in *DDX3X* mutant cancer cell lines (Fig S3) but this increase is not sufficient to replace the larger contribution of *DDX3X* to their combined expression level. Unlike *DDX3X*, *DDX3Y* somatic mutations have not been identified as drivers in human cancers, suggesting that somatic loss of *DDX3Y* is fully compensated for by increased *DDX3X* levels.

Closing

While *DDX3X* and *DDX3Y* are a unique instance of X-Y gene pair cross-regulation, the preservation of this complex regulatory scheme implies the maintenance of ancestral gene regulatory mechanisms for other X-Y gene pairs such as *KDM6A/UTY* and *USP9X/USP9Y*, which demonstrate moderately high dosage sensitivity (Fig 1) and are associated with developmental disorders (Homann et al, 2014., Lederer et al 2012). Overall, this study demonstrates how studies of regulatory conservation can be used to understand and treat disorders caused by mutations of X-Y gene pairs.

Methods

Analysis of total branch length and survival fraction: For each gene, total branch length and survival fraction values in therian species were obtained from Bellott & Page (Bellott & Page, 2021). To obtain a gene's total branch length, all branch lengths in the most parsimonious tree connecting all species where the gene is present are summed from the last common ancestor. The survival fraction is the observed total branch length

divided by the maximum possible branch length. Survival fractions range from 0 (lost in all lineages) to 1 (retained in every lineage).

Analysis of constraint metrics: We downloaded LOEUF (loss-of-function observed/expected upper fraction) scores from gnomAD (v2.1.1.lof_metris.by_gene.txt;https://gnomad.broadinstitute.org/) and only used scores with a minimum of 10 expected LoF variants. For sensitivity to an increase in gene dosage, we used the per-gene average probability of conserved miRNA targeting scores (PCT) (Friedman et al.,2009). For each metric, we computed a percentile rank score, from most constrained to least constrained (San Roman et al., 2023).

Calculation of expression breadth: Human expression breadth was calculated from GTEx v8 using male samples. For each gene, expression breadth was calculated using TPM values as follows: Sum of expression across tissues/(Maximum expression in a tissue * Number of tissues). For each X-Y gene pair, expression breath values for the X-homolog and Y-homolog were averaged to generate a mean score. Chicken expression breadth values were obtained from Bellott et al using data from Merkin et al. (Bellott et al., 2010; Merkin et al., 2012).

Aneuploidy data: RNA-sequencing data from cultured cells of individuals with sex chromosome aneuploidy (San Roman et al., 2023) were downloaded from https://doi.org/10.1016/j.xgen.2023.100259.

Cell Culture: All LCLs were cultured in complete RPMI at 37C. Fibroblasts were cultured in high-glucose DMEM (Gibco), 20% FBS, L-Glutamine (MP Biomedicals), MEM Non-Essential Amino Acids (Gibco), 100 IU/ml Penicillin/Streptomycin (Lonza)).

CRISPRi: Three independent, unrelated 46,XY fibroblast cultures stably expressing a nuclease-dead Cas9 fused with a repressive KRAB domain (dCas9-KRAB) were obtained from Adrianna San Roman. gRNAs for control (intergenic), *DDX3X*, and *DDX3Y* were chosen from the human CRISPRi v2 library (Horlbeck et al., 2016) and cloned into the sgOpti lentiviral expression vector. Viral particles were generated and frozen as described in San Roman et al. Guide sequences were as follows:

Control 1: GACATATAAGAGGTTCCCCG

Control 2: AACGGCGGATTGACCGTAAT

DDX3X #1: GTCCCGTGAGAGGGCCTTCG

DDX3X #2: GCCCGGGACGAGCACAATGG

DDX3Y #1: GTTCGGTCTCACACCTACAG

DDX3Y #2: GAGTACTGGGCCTCACGCAA

Control and *DDX3X*- or *DDX3Y*-targeting gRNAs were transduced into the stably-expressing dCas9-KRAB fibroblasts, and cells were selected using 2 ug/mL puromycin (Sigma) beginning 24 h post infection. Cells were washed once with PBS and collected 72 h post infection. RNA was extracted with the RNeasy Mini Kit (Qiagen). RNA sequencing libraries were prepared using the KAPA mRNA HyperPrep Kit V2 (Roche).

Paired-end 100x100 bp sequencing was performed on a NovaSeq 6000 (Illumina). Reads were pseudoaligned with kallisto and imported into R using tximport. Differential gene expression analysis was performed using DESeq2 (Love et al., 2014). RNA-sequencing data from *ZFX* and *ZFY* knock-down experiments (San Roman et al., 2023) were downloaded from dbGaP Study Accession: phs002481.v2.p1.

Treatment with RK-33: 46,XX fibroblast cultures were treated with 0, 1, 2, 5, or 10 μM RK-33 in DMSO for 24 h. For the time course, they were treated with 2 μM RK-33 for 0, 1, 2, 4, or 24 h.

qPCR: Cells were washed once with PBS and collected 72 h post treatment. RNA was extracted with the RNeasy Mini Kit (Qiagen) and cDNAs prepared with Super-Script Vilo Master Mix (Thermo Fisher). *DDX3X* levels were quantified by qPCR using Fast Sybr Green Master Mix (Thermo Fisher). Primers for *DDX3X* and reference gene *ACTB* were as follows:

DDX3X F: GTGGAAGTGGATCAAGGGGA

DDX3X R: TGATTTGTCACACCAGCGAC

ACTB F: CACCAACTGGGACGACAT

ACTB R: ACAGCCTGGATAGCAACG

Analysis of Cancer Cell Line Expression dataset: Expression and mutation data for cancer cell lines were downloaded from the DepMap 22Q2 release

(https://depmap.org/portal/download/all/). Analysis was restricted to 46,XY cells by applying a log2TPM filter of > 0.2 *DDX3Y,* > 0.2 *RPS4Y*, < 2 *XIST*.

Sample preparation for mass spectrometry: Samples were prepared for proteomic analysis by mPOP (Minimal Proteomic Sample Preparation) as described in Specht et al (Specht et al., 2018). Briefly, cells were resuspended in MS-grade water and frozen. They were then heated and lysed. Proteins were reduced and treated with Trypsin Gold (Promega). The peptide abundance of each sample was measured and each sample was labeled with non-isobaric mass tags, mTRAQ Δ0, Δ4, or Δ8 (SciEx: 4440015, 4427698, 4427700) following the manufacturer's instructions. Reactions were quenched and pooled as a 3-plex with relative mass offsets of Δ0, Δ4, and Δ8.

Mass Spectrometry data acquisition: mTRAQ-labeled peptide sets were separated by reversed-phase UHPLC in 1 μl injections by a Dionex UltiMate 3000 using a 25 cm × 75 μm IonOpticks Aurora Series UHPLC column (AUR2-25075C18A). Buffer A was 0.1% formic acid in MS-grade water. Buffer B was 80% acetonitrile (ACN) with 0.1% formic acid, mixed in MS-grade water. The gradient was as follows: 4% Buffer B (minutes 0–11.5), 4–7% Buffer B (minutes 11.5–12), 7–32% Buffer B (minutes 12–75), 32–95% Buffer B (minutes 75–77), 95% Buffer B (minutes 77–80), 95–4% Buffer B (minutes 80–80.1), and 4% Buffer B until minute 95. The flowrate was 200 nL/min throughout.

Mass spectrometry data were acquired using a DIA method which utilizes frequent MS1-scans for quantitation, as previously described (Derks et al., 2022).

Mass spectrometry data analysis: Raw plexDIA data were processed with DIA-NN (version 1.8.1 beta 16) (Demichev et al., 2019) using the following settings and additional commands: {--window 1}, {--mass-acc 10.0}, {--mass-acc-ms1 5}, {--reanalyse}, {--rt-profiling}, {--peak-height}, {--fixed-mod mTRAQ, 140.0949630177, nK}, {--channels mTRAQ,0,nK,0:0; mTRAQ,4,nK,4.0070994:4.0070994; mTRAQ,8,nK,8.0141988132:8.0141988132}, {--peak-translation}, {--original-mods}, {--report-lib-info}, {--ms1-isotope-quant}, {--mass-acc-quant 5.0}.

The resulting data were filtered at 1% FDR for precursors and protein-groups. Precursors were further filtered for Translated.Q.Value < 0.01. MaxLFQ (Cox et al., 2014) was used to perform protein-group-level quantification for all samples. Each protein-group was normalized to the mean value in each LC-MS run, as each LC-MS run contained three technical replicates from each of the three conditions (control, *DDX3X* knockdown, and *DDX3Y* knockdown). Each sample was then normalized to its own respective median protein group value to account for differences in absolute protein abundances between samples. Finally, each protein-group was normalized to the mean value of the protein-group across all samples, for each cell-line. For each cell line, batch-correction was performed using Combat (Leek et al., 2012) with missing data imputed with a kNN algorithm (k=3), to correct biases produced by using different mass-tag offsets (e.g. Δ0, Δ4, and Δ8).

5-EU labeling and cell collection: LCLs were thawed and allowed to grow in T175 flasks. Cells were split with fresh LCL media and 5EU (Jena Bioscience) was added to a final concentration of 400 μM. Cells were collected 0, 0.5,1, 1.5, and 2, 3.5 and 7 h later, washed with PBS and pelleted prior to addition of TRIzol (Thermo Fisher Scientific) reagent. Cells were snap-frozen at -80 C. RNA was precipitated with isopropanol and 1ng of 5-EU EGFP positive control was added.

Biotinylation and pulldown: Biotinylation and pulldown were performed as described (Kingston & Bartel, 2019). Briefly, biotin was attached to metabolically labeled RNAs in a 10 μL reaction protected from light. The reaction was quenched and RNA precipitated. RNA was then incubated with blocked and pre-washed streptavidin bead slurry. Beads were washed once more and RNA was eluted with TCEP (tris(2-carboxyethyl) phosphine) and water. RNA was precipitated and libraries were then prepared using the SMART-Seq v4 Ultra Low Input RNA kit and sequenced on a NovaSeq 6000. Input RNAs were also sequenced to measure total RNA. TPMs were normalized to 5-EU positive EGFP spike-in. The normalized fraction of nascent/total *DDX3X* mRNA was fit to the equation $y = \alpha/\beta * 1\text{-}e^{\beta/t}$ to obtain β (half-life).

Statistical Methods: Various statistical tests were used to calculate p values as indicated in the methods section, figure legends, or text, where appropriate. Results were considered statistically significant when $p < 0.05$ or FDR < 0.05 when multiple

hypothesis correction was applied, unless stated otherwise. All statistics were calculated using R software, version 4.2.1 or Prism, version 9.4.1 unless stated otherwise.

Data Access: Original code for the analyses in this paper is deposited at https://github.com/shruthi3195/DDX3X_SR_2023. Raw reads for sequencing data were deposited at NCBI and can be accessed at dbGaP Study Accession: phs002481.v3.p1.

Acknowledgements: We thank members of the Page lab for advice, J. Adarme and S. Tocio for laboratory support, and A.K. San Roman and J. Hughes for comments on the manuscript . We thank the Whitehead Institute Genome Technology Core for advice and library preparation & sequencing. We thank Caitlin Rausch for illustration. Patient samples used to generate LCLs from *Azfa* donors are from Dr. R.A. Oates and Dr. S. Silber. Supported by the Howard Hughes Medical Institute, the Whitehead Institute, and philanthropic gifts from Brit and Alexander d'Arbeloff, Arthur W. and Carol Tobin Brill, Matthew Brill, Charles Ellis, the Barakett Foundation, the Howard P. Colhoun Foundation, and the Seedling Foundation.

References

Bellott, D. W., Hughes, J. F., Skaletsky, H., Brown, L. G., Pyntikova, T., Cho, T. J., Koutseva, N., Zaghlul, S., Graves, T., Rock, S., Kremitzki, C., Fulton, R. S., Dugan, S., Ding, Y., Morton, D., Khan, Z., Lewis, L., Buhay, C., Wang, Q., . . . Page, D. C. (2014). Mammalian y chromosomes retain widely expressed dosage-sensitive regulators. *Nature 508*, 494-499. https://doi.org/10.1038/nature13206

Bellott, D. W., & Page, D. C. (2021). Dosage-sensitive functions in embryonic development drove the survival of genes on sex-specific chromosomes in snakes, birds, and mammals. *Genome Research*, *31*(198).

Bellott, D. W., Skaletsky, H., Pyntikova, T., Mardis, E. R., Graves, T., Kremitzki, C., Brown, L. G., Rozen, S., Warren, W. C., Wilson, R. K., & Page, D. C. (2010). Convergent evolution of chicken Z and human X chromosomes by expansion and gene acquisition. *Nature 466*, 612-616. https://doi.org/10.1038/nature09172

Bol, G. M., Vesuna, F., Xie, M., Zeng, J., Aziz, K., Gandhi, K., Levine, A., Irving, A., Korz, D., Tantravedi, S., Heerma van Voss, M. R., Gabreilson, K., Bordt, E. A., Polster, B. M., Cope, L., van der Groep, P., Kondaskar, A., Rudek, M. A., Hosmane, R. S., . . . Raman, V. (2015). Targeting DDX3 with a small molecule inhibitor for
lung cancer therapy. *EMBO Molecular Medicine*.

Brandimarte, L., La Starza, R., Gianfelici, V., Barba, G., Pierini, V., Di Giacomo, D., Cools, J., Elia, L., Vitale, A., Luciano, L., Bardi, A., Chiaretti, S., Matteucci, C., Specchia, G., & Mecucci, C. (2014). DDX3X-MLLT10 fusion in adults with NOTCH1 positive T-cell acute lymphoblastic leukemia. *Hematologica*, *99*. https://doi.org/10.3324/haematol.2013.101725

Cox, J., Hein, M. Y., Luber, C. A., Paron, I., Nagaraj, N., & Mann, M. (2014). Accurate proteome-wide label-free quantification by delayed normalization and maximal peptide ratio extraction, termed MaxLFQ. *Molecular & Cellular Protemics*, *13*, 2513–2526.

Demichev, V., Messner, C. B., Vernardis, S. I., Lilley, K. S., & Ralser, M. (2019). DIA-NN: neural networks and interference correction enable deep proteome coverage in high throughput. *Nature Methods*(17), 41-44.

Derks, J., Leduc, A., Wallmann, G., Huffman, R. G., Willetts, M., Khan, S., Specht, H., Ralser, M., Demichev, V., & Slavov, N. (2022). Increasing the throughput of sensitive proteomics by plexDIA. *Nature Biotechnology*, *41*, 50-59.

Elbaum-Garfinkle, S., Kim, Y., Szczepaniak, K., Chen, C. C. H., Eckmann, C. R., Myong, S., & Brangwynne, C. P. (2015). The disordered P granule protein LAF-1 drives phase separation into droplets with tunable viscosity and dynamics. *PNAS*, *112*, 7189-7194. https://doi.org/10.1073/pnas.1504822112

Friedman, R. C., Farh, K. K. H., Burge, C. B., & Bartel, D. P. (2009). Most mammalian mRNAs are conserved targets of microRNAs. *Genome Research*, *19*, 92-105. https://doi.org/10.1101/gr.082701.108

Ghandi, M., Huang, F. W., Jané-Valbuena, J., Lo, C. C., McDonald, E. R., Barretina, J., Gelfand, E. T., Bielski, C. M., Li, H., Hu, K., Andreev-Drakhlin, A. Y., Kim, J., Hess, J. M., Haas, B. J., Aguet, F., Weir, B. A., Rothberg, M. V., Paolella, B. R., Lawrence, M. S., . . . Sellers, W. R. (2019). Next-generation characterization of the Cancer Cell Line Encyclopedia. *Nature*, *569*, 503-508. https://doi.org/10.1038/s41586-019-1186-3

Godfrey, A. K., Naqvi, S., Chmatal, L., Chick, J. M., Mitchell, R. N., Gygi, S. P., Skaletsky, H., & Page, D. C. (2020). Quantitative analysis of Y-Chromosome gene expression across 36 human tissues. *Genome Research*.

Gong, C., Krupka, J. A., Gao, J., Grigoropoulos, N. F., Screen, M., Usheva, Z., Cucco, F., Barrans, S., Painter, D., Mohammad Zaini, N., Haupl, r., Bornelo, S., Ruiz De Los Mozos, I., Meng, W., Zhou, P., Blain, A. E., Forde, S., Matthews, J., Tan Guet Khim, M., . . . Hodson, D. J.

(2021). Sequential inverse dysregulation of the RNA helicases DDX3X and DDX3Y facilitates MYC-driven lymphomagenesis. *Molecular Cell*.

GTEx. (2017). *Genetic effects on gene expression across human tissues*

Horlbeck, M. A., Gilbert, L. A., Villatla, J. E., Adamson, B., Pak, R. A., Chen, Y., Fields, A. P., Yon Park, C., Corn, J. E., Kampmann, M., & Weissman, J. S. (2016). Compact and highly active next-generation libraries for CRISPR-mediated gene repression and activation. *eLife*, *5*.

Hoye, M. L., Calviello, L., Poff, A. J., Ejimogu, N.-E., Newman, C. R., Montgomery, M. D., Ou Jianhong, Floor, S. N., & Silver, D. N. (2022). Aberrant cortical development is driven by impaired cell cycle and translational control in a DDX3X syndrome model. *eLife*.

Johnstone, O., Deuring, R., Bock, R., Linder, P., Fuller, M. T., & Lasko, P. (2005). Belle is a Drosophila DEAD-box protein required for viability and in the germ line. *Developmental Biology*, *277*, 92-101. https://doi.org/10.1016/j.ydbio.2004.09.009

Karczewski, K. J., Francioli, L. C., Tiao, G., Cummings, B. B., Alföldi, J., Wang, Q., Collins, R. L., Laricchia, K. M., Ganna, A., Birnbaum, D. P., Gauthier, L. D., Brand, H., Solomonson, M., Watts, N. A., Rhodes, D., Singer-Berk, M., England, E. M., Seaby, E. G., Kosmicki, J. A., . . . Xavier, R. J. (2020). The mutational constraint spectrum quantified from variation in 141,456 humans. *Nature*, *581*, 434-443. https://doi.org/10.1038/s41586-020-2308-7

Kellaris, G., Khan, K., Baig, S. M., Tsai, I. C., Zamora, F. M., Ruggieri, P., Natowicz, M. R., & Katsanis, N. (2018). A hypomorphic inherited pathogenic variant in DDX3X causes male intellectual disability with additional neurodevelopmental and neurodegenerative features. *Human Genomics*, *12*. https://doi.org/10.1186/s40246-018-0141-y

Kingston, E. R., & Bartel, D. P. (2019). Global analyses of the dynamics of mammalian microRNA metabolism. *Genome Research*, *29*, 1777-1790.

Kumar, S., Suleski, M., Craig, J. M., Kasprowicz, A. E., Sanderford, M., Li, M., Stecher, G., & Hedges, B. S. (2022). TimeTree 5: An Expanded Resource for Species Divergence Times. *Molecular Biology and Evolution*, *39*(8).

Lahn, B. T., & Page, D. C. (1997). Functional Coherence of theHuman Y Chromosome. *Science*, *278*(5338), 675-678.

Lahn, B. T., & Page, D. C. (1999). Four evolutionary strata on the human X chromosome. *Science*, *286*, 5441.

Leek, J. T., Johnson, W. E., Parker, H. S., Jaffe, A. E., & Storey, J. D. (2012). The sva package for removing batch effects and other unwanted variation in high-throughput experiments. *Bioinformatics*, *28*(6), 882-883.

Love, M. I., Huber, W., & Anders, S. (2014). Moderated estimation of fold change and dispersion for RNA-seq data with DESeq2. *Genome Biology*.

Merkin, J., Russell, C., Chen, P., Burge, C. B., & (2012). Evolutionary dynamics of gene and isoform regulation in mammalian tissues. *Science*, *338*, 1593-1599. https://doi.org/10.1126/science.1228186

Naqvi, S., Bellott, D. W., Lin, K. S., & Page, D. C. (2018). Conserved microRNA targeting reveals preexisting gene dosage sensitivities that shaped amniote sex chromosome evolution. *Genome Research*, *28*(474).

Patmore, D. M., Jassim, A., Nathan, E., Gilbertson, R. J., Tahan, D., Hoffmann, N., Tong, Y., Smith, K. S., Kanneganti, T. D., Suzuki, H., Taylor, M. D., Northcott, P., & Gilbertson, R. J. (2020). DDX3X Suppresses the Susceptibility of Hindbrain Lineages to Medulloblastoma. *Developmental Cell*, *54*, 455-470.e455. https://doi.org/10.1016/j.devcel.2020.05.027

Ramathal, C., Angulo, B., Sukhwani, M., Cui, J., Durruthy-Durruthy, J., Fang, F., Schanes, P., Turek, P. J., Orwing, K. E., & Reijo Pera, R. (2015). DDX3Y gene rescue of a Y chromosome AZFa deletion restores germ cell formation and transcriptional programs. *Nature Scientific Reports*.

Rosner, A., & Rinkevich, B. (2007). The DDX3 Subfamily of the DEAD Box Helicases: Divergent Roles as Unveiled by Studying Different Organisms and In Vitro Assays. *Current Medicinal Chemistry*, *14*, 2517-2525.

San Roman, A. K., Godfrey, A. K., Skaletsky, H., Bellott, D. W., Groff, A. F., Harris, H. L., Blanton, L. V., Hughes, J. F., Brown, L., Phou, S., Buscetta, A., Kruszka, P., Banks, N., Dutra, A., Pak, E., Lasutschinkow, P. C., Keen, C., Davis, S. M., Tartaglia, N. R., . . . Page, D. C. (2023). The human inactive X chromosome modulates expression of the active X chromosome. *Cell Genomics*, *3*, 100259. https://doi.org/10.1016/j.xgen.2023.100259

San Roman, A. K., Skaletsky, H., Godfrey, A. K., Bokil, N. V., Teitz, L., Singh, I., Blanton, L. V., Bellott, D. W., Pyntikova, T., Lange, J., Koutseva, N., Hughes, J. F., Brown, L., Phou, S., Buscetta, A., Kruszka, P., Banks, N., Dutra, A., Pak, E., . . . Page, D. C. (2023). The human Y and inactive X chromosomes similarly modulate autosomal gene expression. *BiorXiv*.

Schiebel, K., Winkelmann, M., Mertz, A., Xu, X., Page, D. C., Weil, D., Petit, C., & Rappold, G. A. (1997). Abnormal XY interchange between a novel isolated protein kinase gene, PRKY, and its homologue, PRKX, accounts for one third of all (Y+)XX males and (Y-)XY females. *Human Molecular Genetics*, *6*.

Sekiguchi, T., Iida, H., Fukumara, J., & Nishimoto, T. (2004). Human DDX3Y, the Y-encoded isoform of RNA helicase DDX3, rescues a hamster temperature-sensitive ET24 mutant cell line with a DDX3X mutation. *Experimental Cell Research*, *300*(1), 213-222.

Sharma, D., Putnam, A. A., & Jankowsky, E. (2017). Biochemical Differences and Similarities between the DEAD-Box Helicase Orthologs DDX3X and Ded1p. *Journal of Molecular Biology*, *429*, 3730-3742. https://doi.org/10.1016/j.jmb.2017.10.008

Shen, H., Yanas, A., Owens, M. C., Zhang, C., Fritsch, C., Fare, C. M., Copley, K. E., Shorter, J., Goldman, Y. E., & Liu, K. F. (2022). Sexually dimorphic RNA helicases DDX3X and DDX3Y differentially regulate RNA metabolism through phase separation. *Molecular Cell*, *82*(14), 2588-2603.

Silvia Marina, D. (2015). *A synthetic approach to study function and expression of the Saccharomyces cerevisiae RNA helicase Ded1* ETH Zurich]. https://doi.org/10.3929/ethz-a-010603399

Snijders Blok, L., Madsen, E., Juusola, J., Gilissen, C., Baralle, D., Reijnders, M. R. F., Venselaar, H., Helsmoortel, C., Cho, M. T., Hoischen, A., Vissers, L. E. L. M., Koemans, T. S., Wissink-Lindhout, W., Eichler, E. E., Romano, C., Van Esch, H., Stumpel, C., Vreeburg, M., Smeets, E., . . . Kleefstra, T. (2015). Mutations in DDX3X Are a Common Cause of Unexplained Intellectual Disability with Gender-Specific Effects on Wnt Signaling. *American Journal of Human Genetics*, *97*, 343-352. https://doi.org/10.1016/j.ajhg.2015.07.004

Soto-Rifo, R., & Ohlmann, T. (2013). The role of the DEAD-box RNA helicase DDX3 in mRNA metabolism. *Wiley interdisciplenary reviews. RNA*, *4*, 369-385. https://doi.org/10.1002/wrna.1165

Specht, H., Harmange, G., Perlman, D. H., Emmott, E., Niziolek, Z., Budnik, B., & Slavov, N. (2018). Automated sample preparation for high-throughput single-cell proteomics. *BiorXiv*.

Sun, C., Skaletsky, H., Rozen, S., Gromoll, J., Nieschlag, E., Oates, R., & Page, D. C. (2000). Deletion of azoospermia factor a (AZFa) region of human Y chromosome caused by recombination between HERV15 proviruses. *Human Molecular Genetics*, *9*, 2291-2296. http://ftp.genome.washington.edu/RM/

Tukiainen, T., Villani, A.-C., Yen, A., Rivas, M. A., Marshall, J. L., Satija, R., Aguirre, M., Gauthier, L., Fleharty, M., Kirby, A., Cummings, B. B., Castel, S. E., Karczewski, K. J., Aguet, F., Byrnes, A., Consortium, G., Laapalainen, T., Regev, A., Ardlie, K. G., . . . MacArthur, D. G. (2017). Landscape of X chromosome inactivation across human tissues. *Nature*(550), 244-248.

Valentin-Vega, Y. A., Wang, Y. D., Parker, M., Patmore, D. M., Kanagaraj, A., Moore, J., Rusch, M., Finkelstein, D., Ellison, D. W., Gilbertson, R. J., Zhang, J., Kim, H. J., & Taylor, J. P. (2016). Cancer-associated DDX3X mutations drive stress granule assembly and impair global translation. *Nature Scientific Reports*, *6*. https://doi.org/10.1038/srep25996

Van Nostrand, E. L., Freese, P., Pratt, G. A., Wang, X., Wei, X., Xiao, R., Blue, S. M., Chen, J.-Y., Cody, N. A. L., Dominguez, D., Olson, S., Sundararaman, B., Zhan, L., Bazile, C., Philip

Benoit Bouvrette, L., Bergalet, J., Duff, M. O., Garcia, K. E., Gelboin-Burkhart, C., . . . Yeo, G. W. (2020). A large-scale binding and functional map of human RNA-binding proteins. *Nature*(583), 711-719.

Venkataramanan, S., Gadek, M., Calviello, L., Wilkins, K., & Floor, S. N. (2021). DDX3X and DDX3Y are redundant in protein synthesis. *RNA*.

SUPPLEMENTARY MATERIAL

Expression of the human sex-linked RNA helicases *DDX3X* and *DDX3Y* is buffered by post-transcriptional auto- and cross-regulation

Shruthi Rengarajan, Jason Derks, Daniel W. Bellott, Nikolai Slavov, David C. Page

SUPPLEMENTARY FIGURES

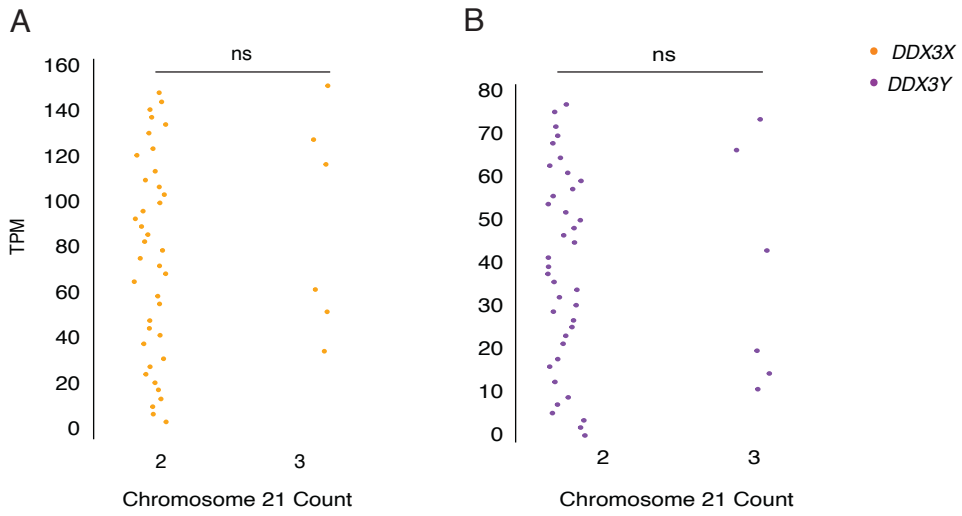

Supplemental Figure S1: Chromosome 21 copy number does not affect *DDX3X* or *DDX3Y* levels. Each point represents a lymphoblastoid cell line from one XX or XY individual with either 2 or 3 copies of chromosome 21 demonstrating that A) *DDX3X* and B) *DDX3Y* levels don't respond to aneuploidy. Statistical significance was determined by Mann Whitney- U test.

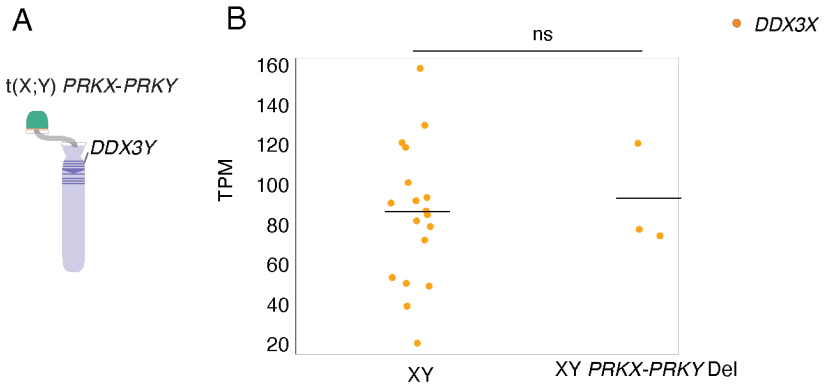

Supplementary Figure S2: *DDX3X* levels are unchanged in cells with other Y chromosome abnormalities. A) Abnormal recombination between *PRKX* and *PRKY* results in a X-Y translocation and deletion of the Y chromosome which leaves DDX3Y intact. B) LCLs derived from individuals with *PRKX-PRKY* translocations have the same levels of *DDX3X* transcripts as WT XY individuals. Statistical significance was determined by Mann Whitney- U test.

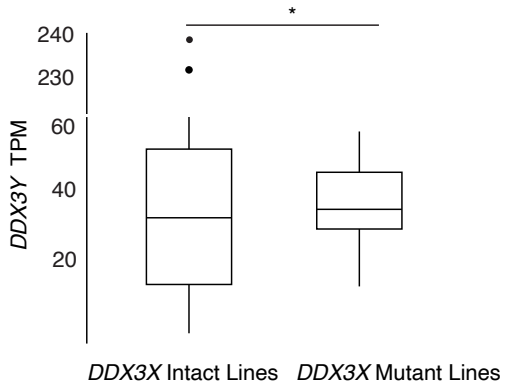

Supplementary Figure S3: *DDX3Y* transcripts are higher in XY cancer cell lines with damaging *DDX3X* mutations. 480 DDX3X intact XY lines and 11 DDX3X damaged XY lines are plotted. Statistical significance was determined by one tailed t-test, **$p < 0.05$

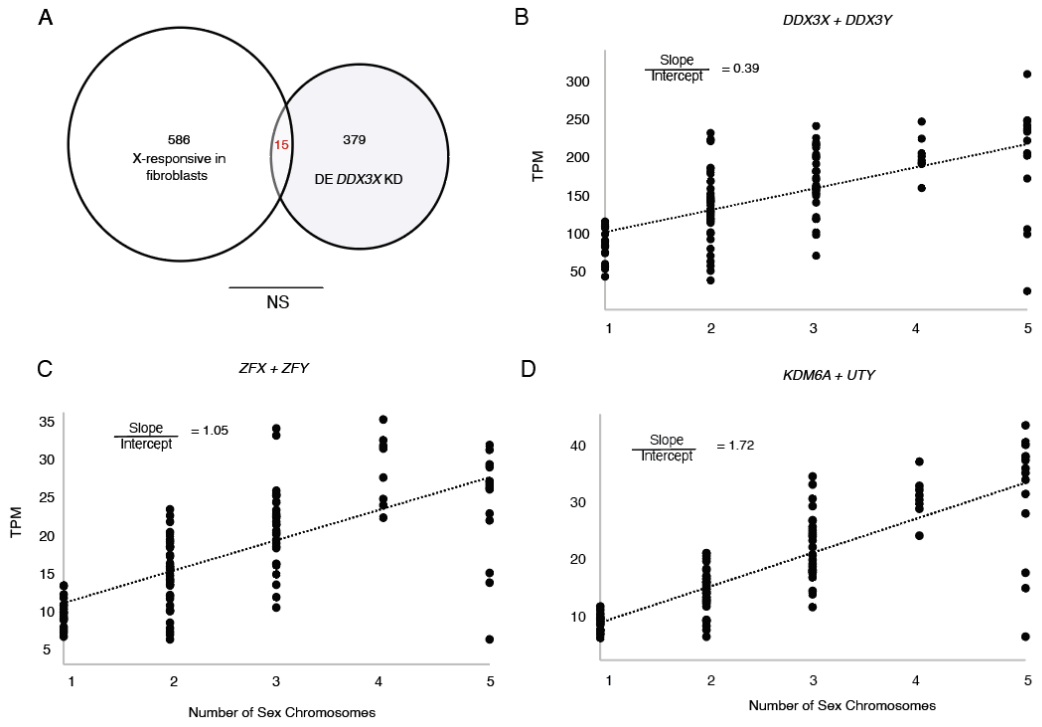

Supplementary Figure S4: *DDX3X* and *DDX3Y* levels are not major contributors to gene expression changes in sex chromosome aneuploidy. A) There is no overlap between genes that are differentially expressed upon *DDX3X* KD in XY fibroblasts and those that respond to X-chromosome dosage in fibroblasts with X chromosome aneuploidies. Hypergeometric test was used to assess statistical significance. B) The increase in the total expression of *DDX3X* + *DDX3Y* with sex chromosome copy number is buffered compared to similarly constrained X-Y pair genes *ZFX*/*ZFY* (C) and *KDM6A*/*UTY* (D).

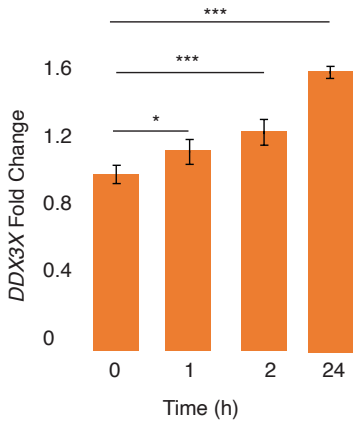

Supplementary Figure S5: *DDX3X* transcript levels (by qPCR) in XX fibroblasts are significantly elevated when treated with 2μM DDX3 inhibitor RK-33, proportional to duration of treatment. Statistical significance was determined by one-sided t-test on delta Ct values. Error bars indicate standard deviation of three technical replicates. * = p <0.05, *** = p < 0.001.

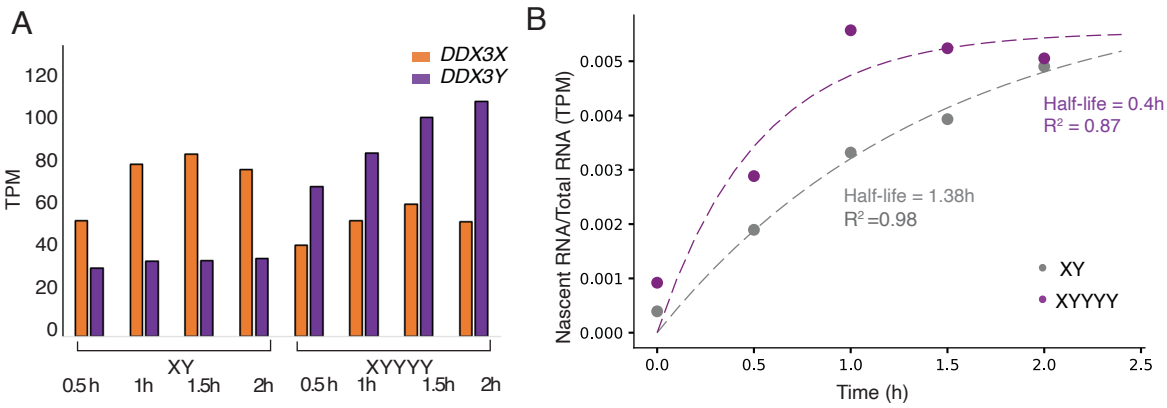

Supplementary Figure S6: A) *DDX3Y* levels are elevated and *DDX3X* levels are decreased in XYYYY LCLs compared to XY LCLs. B) *DDX3X* remains destabilized 3-fold in XYYYY LCLs when labeled for up to 7 hours. Normalized fraction of nascent/total *DDX3X* mRNA were fit to the equation $y = \alpha/\beta * 1\text{-}e^{\beta/t}$ to obtain β (half-life)

SUPPLEMENTAL TABLES

Table S1: Change in gene expression of X and Y homologs per additional Y or X chromosome respectively, in fibroblasts and LCLs. Genes are sorted by adjusted p value.

Fibroblast	Gene	Change per Y Chr	Adjusted p value
	DDX3X	-0.1325	4.21E-06
	PRKX	-0.0964	0.2351
	ZFX	-0.0801	0.2743
	KDM6A	-0.028	0.5569
	USP9X	-0.0455	0.5831
	KDM5C	0.0225	0.8089
	EIF1AX	-0.0079	0.9671

	Gene	Change per X Chr	Adjusted p value
	DDX3Y	-0.1318	0.1743
	ZFY	-0.0667	0.6812
	USP9Y	0.0483	0.706
	PRKY	0.0445	0.706
	KDM5D	0.0429	0.706
	UTY	-0.039	0.706
	EIF1AY	0.0358	0.706

LCL	Gene	Change per Y Chr	Adjusted p value
	DDX3X	-0.1089	9.21E-04
	ZFX	-0.0928	0.0517
	PRKX	-0.072	0.3306
	USP9X	-0.0343	0.4446
	KDM6A	0.0141	0.8804
	EIF1AX	-0.003	0.9259
	KDM5C	0.0045	0.9697

	Gene	Change per X Chr	Adjusted p value
	DDX3Y	-0.0796	0.0768
	KDM5D	0.1095	0.231
	USP9Y	0.0641	0.3028
	EIF1AY	-0.0312	0.4497
	ZFY	-0.0292	0.4497
	PRKY	-0.0198	0.7594
	UTY	-0.0128	0.7594

DepMap ID	Cell Line	Tumor type	Tissue of origin	*DDX3X* Mutation
ACH-000534	WSUDLCL2	Burkitt Lymphoma	Lymphoid	p.V657fs
ACH-001563	MM127	Melanoma	Skin	p.R292*
ACH-002055	TL1	Burkitt Lymphoma	Lymphoid	p.S410fs
ACH-000654	RAJI	Burkitt Lymphoma	Lymphoid	p.P297P
ACH-001610	NP5	Diffuse Glioma	CNS/Brain	p.M391T
ACH-001097	KARPAS384	Adult T-Cell Leukemia/Lymphoma	T-Cell	p.R46*
ACH-000402	BL70	Burkitt Lymphoma	Lymphoid	p.Y343*
ACH-000056	DOHH2	Diffuse Large B-Cell Lymphoma	Lymphoid	_
ACH-000619	PECAPJ15	Oral Cavity Squamous Cell Carcinoma	Head and Neck	pQ477*
ACH-001617	OCILY7	Diffuse Large B-Cell Lymphoma	Lymphoid	_
ACH-000766	NCIH1648	Lung Adenocarcinoma	Lung	pE196fs

Table S2: List of CCLE cell lines annotated with *DDX3X* loss of function

Table S3: LOEUF and PCT scores for X homologs of X-Y pair genes. Genes are ordered by combined LOEUF and PCT score.

Gene	LOEUF	LOEUF X rank	Pct	PCT X rank	Combined Score
DDX3X	0.118	92.89	0.338	97.38	134.5786629
KDM6A	0.161	84.08	0.379	98.15	129.2395795
USP9X	0.051	99.61	0.186	81.82	128.9056418
TXLNG	0.158	85.26	0.284	93.99	126.8991241
KDM5C	0.166	83.03	0.245	90.76	123.009587
ZFX	0.16	84.61	0.16	75.65	113.4979057

NLGN4X	0.249	64.34	0.135	71.96	96.52915207
PRKX	0.895	14.74	0.074	56.39	58.28464378

Table S4: Expression breadth scores for human X-Y pair genes and their chicken orthologs. Genes are ordered by combined expression breadth.

Gene	Chicken Breadth	Human X Breadth	Combined Breadth
DDX3X	0.730304257	0.471391844	0.869226425
ZFX	0.5212655	0.546732732	0.755403469
USP9X	0.414073276	0.556244707	0.693444195
TBL1X	0.586347148	0.355482986	0.685690259
TXLNG	0.32053212	0.517916258	0.609079708
KDM6A	0.255477286	0.459713152	0.52593234
PRKX	0.217633361	0.208370734	0.301301581
NLGN4X	0.176577057	0.239367661	0.297449717

Y homolog	Chicken Breadth	Human Y Breadth	Combined Breadth
DDX3Y	0.730304257	0.479998852	0.873924027
ZFY	0.5212655	0.523221583	0.738565194
TBL1Y	0.586347148	0.355482986	0.685690259
USP9Y	0.414073276	0.465701179	0.623164718
UTY	0.255477286	0.49371075	0.555894728
NLGN4Y	0.176577057	0.448771995	0.482261092
TXLNGY	0.32053212	0.339798978	0.467123309
PRKY	0.217633361	0.261896003	0.340519891

Table S5: *DDX3X* and *DDX3Y* expression from filtered XY CCLE cell lines

XY Cell Line	*DDX3X* Damage (1 = Yes)	*DDX3X* log2 TPM	*DDX3Y* log 2 TPM
ACH-000534	1	6.248496886	4.865423978
ACH-001563	1	3.537296067	5.09000653
ACH-002055	1	4.06091205	5.628190335
ACH-000654	1	7.640751056	6.451705665
ACH-001610	1	7.184379486	5.032982417
ACH-001097	1	2.049630768	4.00270252
ACH-000402	1	4.367371066	5.878234879
ACH-000056	1	6.637349411	5.487357715
ACH-000619	1	6.200849575	3.861955364
ACH-001617	1	4.764473551	5.341630009

ACH-000766	1	5.325530332	5.192588722
ACH-000267	0	6.798828178	4.986410935
ACH-000750	0	6.715344295	0.214124805
ACH-000544	0	4.788685711	1.847996907
ACH-000045	0	5.626439137	5.262282806
ACH-000774	0	6.721235931	4.438292852
ACH-000892	0	6.982195024	5.838447593
ACH-001648	0	5.746850183	4.437627248
ACH-000948	0	6.738767837	5.241077458
ACH-000883	0	7.376689765	5.549361133
ACH-000479	0	7.168922782	5.785812075
ACH-000005	0	6.713420885	7.175225173
ACH-000130	0	7.252854626	6.285217246
ACH-000765	0	7.12649799	5.634012356
ACH-000836	0	6.895181422	3.336283388
ACH-001385	0	5.140369671	4.50589093
ACH-001454	0	6.012792122	3.365972428
ACH-001685	0	6.607034346	5.221103725
ACH-000120	0	7.303963356	6.515226746
ACH-000659	0	6.543341212	6.801417366
ACH-000904	0	7.931742144	5.67468662
ACH-001560	0	7.301861967	4.947198584
ACH-000452	0	6.989593185	0.443606651
ACH-000953	0	7.707497182	5.324810603
ACH-001634	0	4.842476063	3.583759754
ACH-000365	0	6.465648026	4.985955755
ACH-001818	0	6.048541366	4.216454865
ACH-000317	0	6.075104722	5.396433531
ACH-000508	0	7.7524141	0.250961574
ACH-001164	0	5.66448284	4.100977648
ACH-000859	0	8.155324229	0.344828497
ACH-000577	0	6.619853147	5.63284983
ACH-000167	0	6.841218374	0.201633861
ACH-000514	0	7.771423441	5.239168879
ACH-000151	0	7.198101209	5.956289027
ACH-000955	0	7.204473331	5.324450605
ACH-000611	0	7.130724991	0.22650853
ACH-000997	0	7.631540867	5.577730931
ACH-001412	0	7.09244003	2.657640005
ACH-000446	0	6.494575617	6.109151579
ACH-001407	0	7.198985184	5.671859468

ACH-002018	0	6.07489072	4.642123916
ACH-000095	0	6.713420885	5.8928767
ACH-000172	0	6.738632747	6.044612693
ACH-000335	0	7.082042565	5.758356483
ACH-000067	0	7.412612185	5.479295243
ACH-000238	0	5.884109451	4.882643049
ACH-000907	0	6.482686971	4.234194723
ACH-000336	0	6.07317756	0.713695815
ACH-000115	0	6.98436149	5.226893814
ACH-000760	0	6.698079537	1.599317794
ACH-000257	0	7.196233261	5.99095486
ACH-001532	0	5.98208091	4.819668183
ACH-000512	0	6.695854658	5.001802243
ACH-000608	0	7.496494307	0.367371066
ACH-000545	0	7.16651461	0.659924558
ACH-000252	0	6.675815931	5.11727946
ACH-000122	0	7.443358004	0.333423734
ACH-000208	0	6.615298579	5.819923596
ACH-001570	0	5.854494418	4.499527024
ACH-000253	0	7.275472718	4.135042286
ACH-000028	0	6.83541884	0.389566812
ACH-000648	0	6.675392543	5.455820365
ACH-000386	0	7.126394738	6.107897062
ACH-000822	0	6.839329782	5.559185866
ACH-000803	0	7.536441505	0.321928095
ACH-000128	0	7.046141782	4.780835002
ACH-000716	0	6.95419631	5.57500972
ACH-000664	0	7.775116404	4.392317423
ACH-000893	0	7.274913895	5.755688777
ACH-000126	0	6.442445929	5.994353437
ACH-000249	0	6.844737144	4.742006211
ACH-000742	0	6.726422541	4.252476214
ACH-000976	0	6.413966352	3.367371066
ACH-000974	0	7.521207816	0.201633861
ACH-001751	0	6.560256398	5.126394738
ACH-001270	0	6.661635602	4.542877099
ACH-000533	0	6.575614878	5.928370323
ACH-000269	0	6.94204526	4.630521963
ACH-001528	0	6.420212891	5.402585758
ACH-000078	0	6.268284667	6.847370601
ACH-000752	0	7.077777073	5.165107985

ACH-000868	0	6.39694722	3.03562391
ACH-000027	0	7.180505944	6.718772592
ACH-001338	0	6.920888742	5.220329955
ACH-001807	0	6.262094845	3.773996325
ACH-001229	0	5.605553595	5.165510018
ACH-001303	0	5.641256999	3.839959587
ACH-000316	0	7.380157992	6.004501392
ACH-000786	0	4.152183419	5.942983598
ACH-000756	0	7.065873847	5.504620392
ACH-000913	0	8.021146554	0.214124805
ACH-000436	0	6.151168794	5.813268142
ACH-000343	0	8.021535249	0.831877241
ACH-001999	0	5.749534268	4.712045449
ACH-000559	0	7.523953939	0.286881148
ACH-000131	0	7.120393416	4.472487771
ACH-000054	0	7.05126333	6.069745124
ACH-000154	0	7.437960088	6.049630768
ACH-000839	0	5.785027362	3.809414444
ACH-000815	0	7.03683298	0.23878686
ACH-001142	0	6.628190335	4.980939266
ACH-000499	0	7.069208067	6.769771739
ACH-000070	0	6.363521544	4.801158656
ACH-000726	0	7.131136719	0.454175893
ACH-000498	0	6.522306893	5.509379149
ACH-000778	0	7.015582312	5.276496666
ACH-000622	0	7.447331233	0.250961574
ACH-000558	0	6.893968869	5.788685711
ACH-000065	0	6.582706527	5.443606651
ACH-000495	0	6.938638658	0.23878686
ACH-000706	0	7.141391916	5.240314329
ACH-001347	0	6.429113779	3.388189537
ACH-000084	0	7.70120248	6.263410059
ACH-000999	0	6.963705307	5.49441561
ACH-000284	0	7.315602457	5.410069692
ACH-000757	0	8.999323578	3.109360559
ACH-000241	0	7.256255873	6.377644358
ACH-001997	0	6.689997971	3.496973581
ACH-001134	0	3.812498225	5.051372102
ACH-001557	0	7.167217409	5.13093087
ACH-000041	0	7.423914268	6.325350433
ACH-000206	0	7.001239284	5.972233124

ACH-000429	0	5.674404154	5.083213368
ACH-001562	0	7.421307468	5.663629259
ACH-000074	0	6.837438715	7.169524197
ACH-000063	0	6.991408467	5.483815777
ACH-000387	0	6.745237332	7.91336816
ACH-000649	0	7.267161218	6.158256229
ACH-000437	0	7.379378367	5.865423978
ACH-000214	0	6.738902914	4.946262984
ACH-000255	0	7.520186495	0.389566812
ACH-000221	0	7.216163813	0.23878686
ACH-000245	0	6.921126849	5.558573776
ACH-000158	0	6.664056113	6.279657007
ACH-000787	0	6.434294618	5.870857864
ACH-001745	0	6.400196342	4.762348816
ACH-000340	0	7.083319758	6.010332283
ACH-000399	0	6.829595899	6.792725233
ACH-000549	0	7.062316027	4.993221467
ACH-000891	0	7.095397023	5.088735246
ACH-000307	0	7.102238194	4.956985925
ACH-000656	0	6.436794812	0.201633861
ACH-002014	0	6.157245867	2.22650853
ACH-000439	0	5.778471434	4.526694846
ACH-000728	0	7.045268215	2.09423607
ACH-000723	0	5.833143096	4.361768359
ACH-000053	0	7.12722055	5.194165869
ACH-000421	0	7.291216754	0.847996907
ACH-000882	0	6.73403214	5.697106574
ACH-001737	0	6.413627929	5.60940039
ACH-000312	0	7.059723	6.020591095
ACH-000981	0	6.781884235	5.608809243
ACH-000530	0	7.854182707	2.606442228
ACH-001430	0	7.008428622	5.406672716
ACH-000261	0	7.148629106	0.23878686
ACH-000938	0	6.849999259	6.388361768
ACH-001414	0	5.98208091	5.087038457
ACH-000518	0	6.693486957	6.607774152
ACH-001688	0	4.371558863	3.835924074
ACH-000964	0	6.751276249	6.0725346
ACH-000615	0	6.676380255	0.22650853
ACH-000165	0	7.000563443	5.539158811
ACH-000707	0	7.078524445	5.627315001

ACH-001863	0	6.818262608	4.553360503
ACH-001197	0	6.520422249	6.315240153
ACH-000698	0	7.781031791	0.214124805
ACH-000396	0	7.594473905	5.116447936
ACH-001841	0	6.59812696	3.061776198
ACH-000354	0	6.104965605	0.201633861
ACH-001190	0	7.07734983	6.061992154
ACH-000371	0	6.689019541	4.292781749
ACH-000770	0	6.628919374	5.545041683
ACH-000661	0	7.031990609	6.205548911
ACH-000458	0	7.798569004	4.185866545
ACH-000338	0	7.517590658	0.23878686
ACH-000218	0	6.840840853	5.122672719
ACH-000632	0	7.6121313	4.933100475
ACH-000420	0	7.477920131	1.475084883
ACH-000833	0	6.520107902	3.087462841
ACH-000062	0	7.743959212	6.154818109
ACH-000914	0	7.584737062	6.30833903
ACH-000677	0	7.533018186	0.378511623
ACH-000652	0	7.121533517	0.411426246
ACH-001568	0	4.399171094	3.837943242
ACH-000801	0	6.846117173	5.747924416
ACH-001605	0	6.700717133	4.14404637
ACH-000951	0	6.800641097	5.267161218
ACH-001977	0	7.010108453	4.403267722
ACH-000671	0	6.721099189	5.593652558
ACH-001959	0	7.692580633	4.916476644
ACH-000080	0	6.409221197	6.186857067
ACH-000522	0	6.189231549	0.22650853
ACH-002045	0	6.090641752	5.664198369
ACH-002065	0	7.325530332	5.390942773
ACH-000368	0	6.965668864	4.773468928
ACH-001649	0	5.815063017	4.507160349
ACH-000703	0	7.215581534	4.975905274
ACH-001415	0	7.405652061	3.078951341
ACH-000575	0	6.959074601	5.364572432
ACH-001200	0	6.487357715	6.057883449
ACH-000853	0	6.754085782	6.299208018
ACH-000546	0	6.417515003	0.411426246
ACH-001845	0	6.507160349	4.181897643
ACH-000486	0	5.928607199	0.378511623

ACH-000400	0	6.753551055	1.66448284
ACH-000118	0	6.599020177	4.10349764
ACH-000487	0	6.019924261	5.882887553
ACH-000465	0	6.700300991	5.741466986
ACH-001558	0	7.362645218	5.473137488
ACH-000909	0	7.825785627	0.263034406
ACH-000921	0	7.38663853	0.22650853
ACH-000271	0	5.87774425	4.909773104
ACH-000266	0	6.388706169	4.891419187
ACH-000362	0	6.301587647	5.657068301
ACH-001556	0	7.254083779	6.164102412
ACH-000977	0	6.485587833	6.151371776
ACH-001020	0	6.651195236	5.143230135
ACH-000087	0	7.391372492	5.499845887
ACH-001624	0	5.070389328	3.334854269
ACH-000932	0	7.010891706	5.595145568
ACH-000036	0	6.87835751	6.5360529
ACH-000597	0	6.872705657	6.23476954
ACH-001609	0	6.242030802	5.001351893
ACH-000310	0	7.089476964	5.878480131
ACH-000197	0	7.08182959	6.432458385
ACH-001796	0	6.229780167	4.709290636
ACH-000059	0	7.443275112	6.439290681
ACH-000089	0	6.61205756	1.280956314
ACH-001283	0	6.733625498	4.546585829
ACH-001669	0	5.125981654	1.570462931
ACH-000306	0	6.475571321	4.880195729
ACH-001566	0	5.886062338	4.64038956
ACH-000274	0	6.85586515	4.333423734
ACH-001814	0	6.867402306	4.460742564
ACH-000209	0	5.538538164	5.279099802
ACH-000848	0	7.585112774	5.767654798
ACH-000331	0	7.264911693	6.273329387
ACH-000318	0	5.66732447	0.454175893
ACH-000463	0	7.190713617	5.867402306
ACH-000736	0	7.001914808	4.142413438
ACH-000099	0	6.823621998	5.087462841
ACH-000422	0	7.385948658	4.806839582
ACH-000007	0	6.374517881	4.741466986
ACH-000150	0	7.181400762	5.444600814
ACH-000970	0	6.978424465	0.298658316

ACH-000971	0	7.83586093	4.609991295
ACH-000290	0	7.287804709	5.463360886
ACH-000655	0	6.792074462	3.349082146
ACH-000190	0	6.129076903	6.403608584
ACH-001035	0	6.499048598	5.666756592
ACH-000600	0	6.443109313	5.230356745
ACH-000995	0	6.405141463	3.986410935
ACH-001533	0	4.459431619	4.072963272
ACH-001982	0	6.71259578	4.969472865
ACH-001329	0	6.862699341	4.754887502
ACH-001524	0	7.459267667	4.125981654
ACH-001036	0	7.193870285	4.848497755
ACH-000543	0	6.809671678	4.893847558
ACH-000638	0	6.916237768	3.255500733
ACH-000101	0	7.312610723	5.590961241
ACH-000240	0	6.996275749	5.719457275
ACH-000511	0	7.337265086	0.201633861
ACH-001673	0	6.301221805	5.945326777
ACH-001228	0	6.607922067	3.792855352
ACH-000829	0	6.96474517	6.037821465
ACH-000389	0	6.968205979	5.82858081
ACH-000616	0	7.655494946	5.842224613
ACH-000767	0	7.991861931	4.517275693
ACH-001339	0	6.206135253	5.146492307
ACH-000650	0	7.03496399	5.687060688
ACH-001310	0	6.797012978	5.642412773
ACH-000277	0	7.178316272	0.214124805
ACH-000873	0	6.757823336	4.936873462
ACH-000427	0	6.682432841	5.266786541
ACH-000954	0	7.727852401	0.35614381
ACH-000604	0	5.765799923	0.201633861
ACH-000088	0	7.422653501	6.060263599
ACH-000459	0	6.838321521	5.876271361
ACH-000813	0	6.412104045	3.742006211
ACH-000743	0	7.025693274	4.605849867
ACH-000612	0	7.263691734	7.005512273
ACH-000227	0	7.15035658	5.837691
ACH-000289	0	6.385431037	5.001351893
ACH-000469	0	7.245552706	0.298658316
ACH-001603	0	6.258141996	4.778208576
ACH-000614	0	6.764340847	4.758622982

ACH-000692	0	6.344650989	0.411426246
ACH-000975	0	6.910252963	5.676662335
ACH-000015	0	7.059723	3.407352751
ACH-001207	0	6.754219433	5.054848477
ACH-000064	0	6.685519722	5.996840648
ACH-000747	0	7.00495076	5.848247353
ACH-001740	0	7.08236197	4.211790976
ACH-000102	0	7.792009369	6.159871337
ACH-001638	0	5.766330131	4.027684877
ACH-000837	0	6.940401698	4.862451391
ACH-000734	0	7.133604623	5.9795681
ACH-001523	0	7.317955218	5.510329019
ACH-000950	0	6.808127587	4.751142325
ACH-000370	0	6.715618859	5.113950482
ACH-000729	0	7.156335937	6.287065907
ACH-000956	0	7.003264909	5.742275748
ACH-001619	0	5.719731057	0.201633861
ACH-000482	0	6.498250868	5.869377924
ACH-001109	0	6.813909425	5.593652558
ACH-002048	0	6.11997861	5.057016965
ACH-002044	0	7.747924416	3.532316959
ACH-000326	0	6.561173365	6.041549645
ACH-000531	0	6.591709333	0.201633861
ACH-000415	0	5.391973883	2.575312331
ACH-000748	0	7.117487266	6.141800612
ACH-000403	0	6.587515014	4.669593751
ACH-001057	0	6.067165427	5.935459748
ACH-000718	0	7.138118178	4.969472865
ACH-000580	0	7.185866545	5.811471031
ACH-000233	0	7.199966742	4.712045449
ACH-000466	0	6.490890979	0.263034406
ACH-000710	0	5.913607512	2.166715445
ACH-000175	0	6.904604518	5.64096791
ACH-000489	0	6.478324711	4.207892852
ACH-000896	0	6.760620161	4.638073837
ACH-001232	0	7.45112867	5.54225805
ACH-000576	0	5.852498299	3.301587647
ACH-000424	0	7.143026004	5.533563348
ACH-000133	0	7.177718511	6.112491636
ACH-001973	0	6.590961241	5.242221395
ACH-001701	0	6.225737653	1.077242999

ACH-000135	0	6.705010253	5.622637567
ACH-000292	0	7.243745235	5.739578112
ACH-000401	0	6.304145941	6.06091205
ACH-000562	0	6.590362488	4.991861931
ACH-000321	0	5.875042803	6.150762744
ACH-000334	0	7.014355293	5.879950768
ACH-001699	0	5.845991771	3.198494154
ACH-000966	0	7.299391206	0.378511623
ACH-001346	0	6.323370069	5.106432078
ACH-000799	0	6.318678374	5.43496176
ACH-000980	0	8.022256832	0.23878686
ACH-000125	0	7.468501862	6.670160514
ACH-001059	0	6.830229967	6.128664587
ACH-000464	0	6.609991295	5.09085343
ACH-000472	0	5.92552477	2.711494907
ACH-000550	0	6.714657657	5.610286657
ACH-000346	0	6.861459166	5.543495883
ACH-000588	0	6.793245639	4.663913842
ACH-000234	0	7.17602351	5.820178962
ACH-000817	0	6.493134922	4.793895883
ACH-001848	0	5.618238656	3.473786912
ACH-000773	0	7.4325419	4.596338864
ACH-000788	0	6.898450233	5.723558561
ACH-000251	0	6.776498832	5.77452353
ACH-000987	0	6.889473543	5.706530553
ACH-000641	0	7.616769366	5.909293086
ACH-000854	0	6.196134881	5.737416366
ACH-000140	0	6.938168151	5.532940288
ACH-002800	0	6.593503172	5.404971224
ACH-000949	0	6.823112437	0.622930351
ACH-000623	0	6.819540461	5.569551851
ACH-000405	0	6.6043679	5.495375381
ACH-000682	0	7.055390905	4.875780063
ACH-000170	0	6.702934532	6.1278396
ACH-001509	0	5.618532334	2.9202933
ACH-000634	0	7.243650042	5.63314055
ACH-000105	0	7.097926773	5.486714373
ACH-000232	0	7.135965742	5.075960413
ACH-001378	0	3.521050737	2.744161096
ACH-001129	0	6.405822221	5.131754091
ACH-000068	0	6.771753554	5.153400028

ACH-000762	0	6.23476954	0.344828497
ACH-000571	0	6.825404046	3.234194723
ACH-000960	0	7.263785614	0.201633861
ACH-000984	0	7.511752654	0.464668267
ACH-000858	0	5.932155684	0.23878686
ACH-000867	0	6.646450706	6.086401646
ACH-000288	0	7.219458967	0.201633861
ACH-000525	0	7.002027365	6.155627816
ACH-000538	0	7.240886714	6.081936082
ACH-000819	0	7.091065078	6.034523875
ACH-000502	0	6.604664415	0.286881148
ACH-002080	0	6.333065878	2.757023247
ACH-000198	0	6.628044483	5.523875551
ACH-000645	0	6.555049213	5.081936082
ACH-001707	0	4.893362211	3.607626221
ACH-000905	0	7.214416269	2.974529312
ACH-000096	0	7.569703738	6.005399988
ACH-001622	0	5.411765185	4.032982417
ACH-000359	0	6.798180154	6.222263604
ACH-001992	0	7.057233635	5.464668267
ACH-001386	0	7.284014345	5.561020578
ACH-000516	0	7.859534786	4.616475329
ACH-000583	0	7.107583262	5.745775149
ACH-000477	0	6.794155898	4.837438715
ACH-001494	0	5.227664073	3.781359714
ACH-001239	0	7.151879107	0.495695163
ACH-000242	0	7.374343989	4.998646839
ACH-001289	0	7.289004456	5.318316841
ACH-000004	0	6.305970521	6.728600811
ACH-000156	0	7.626512146	3.753818443
ACH-000332	0	7.246408087	5.440952198
ACH-001569	0	5.403949364	4.59275601
ACH-000681	0	7.759089238	5.458447627
ACH-000826	0	6.969933275	0.82374936
ACH-001496	0	6.819029455	4.841973119
ACH-001574	0	4.078097423	3.941106311
ACH-000254	0	6.075318693	4.915998852
ACH-000484	0	6.439290681	5.668743189
ACH-000548	0	6.499048598	5.356495988
ACH-001647	0	6.412442825	4.614709844
ACH-000959	0	7.375387027	5.920055055

ACH-001530	0	6.890081838	4.919340082
ACH-001050	0	6.970738639	5.439955517
ACH-000113	0	6.428611418	5.751945682
ACH-000917	0	7.010108453	0.40053793
ACH-000146	0	6.577126661	6.088735246
ACH-000055	0	6.967514481	5.484138131
ACH-000040	0	7.273702369	5.236492618
ACH-002461	0	6.017921908	4.312519967
ACH-000092	0	7.106850796	6.317412614
ACH-001567	0	5.770829046	4.782408565
ACH-000330	0	7.132988043	0.23878686
ACH-000942	0	6.591709333	6.344828497
ACH-000738	0	7.528336893	0.695993813
ACH-000166	0	6.308156975	6.568336182
ACH-000313	0	6.80464733	5.814550423
ACH-000451	0	6.694044413	6.312338439
ACH-001061	0	6.758622982	4.587964989
ACH-001054	0	6.543341212	4.790772038
ACH-001366	0	6.274448044	4.761817143
ACH-000211	0	7.673768403	0.23878686
ACH-000373	0	6.789207575	3.54225805
ACH-000152	0	6.880195729	5.394033895
ACH-000627	0	7.178216662	4.595145568
ACH-000810	0	6.96127604	6.010779839
ACH-000935	0	5.925049965	0.263034406
ACH-000457	0	6.460906348	0.23878686
ACH-001277	0	6.593652558	4.820689561
ACH-000695	0	6.562547724	5.444600814
ACH-000789	0	7.097189387	5.231893162
ACH-001038	0	7.081083929	5.369466484
ACH-001016	0	7.433543714	5.478648295
ACH-001450	0	7.054305845	5.097189387
ACH-000670	0	6.445263208	6.349966747
ACH-000843	0	6.916118315	5.491853096
ACH-001750	0	6.837438715	5.484138131
ACH-000591	0	7.1017131	6.278356528
ACH-000952	0	7.18814373	5.06436554
ACH-000162	0	7.740725224	6.262658655
ACH-000159	0	7.216551869	6.006298024
ACH-001522	0	7.143842354	5.09085343
ACH-000367	0	7.344473459	5.851998837

ACH-000586	0	8.058749412	5.4747605
ACH-000991	0	7.60932651	0.464668267
ACH-000220	0	7.70887696	6.128252152
ACH-000447	0	7.664625055	0.321928095
ACH-000827	0	6.752882366	4.568032105
ACH-001196	0	6.661493093	5.376776572
ACH-001520	0	4.547203025	3.642701572
ACH-000968	0	6.128870759	4.061776198
ACH-000077	0	6.947549278	6.628481994
ACH-001549	0	6.354557947	4.587364991
ACH-000072	0	6.376602952	7.858664869
ACH-000483	0	7.236588285	5.695158678
ACH-000825	0	6.280028357	0.201633861
ACH-000161	0	6.605553595	4.877253454
ACH-000741	0	6.9175511	0.321928095
ACH-000358	0	7.509062386	5.85224859
ACH-000075	0	7.05126333	1.298658316
ACH-000553	0	6.68846014	5.078951341
ACH-000181	0	6.553053253	5.873813198
ACH-002659	0	6.484621527	1.622930351
ACH-001453	0	6.791944272	4.673556424
ACH-000739	0	6.422064766	5.501439145
ACH-000388	0	5.653919873	5.358607249
ACH-000860	0	7.143026004	4.750070486
ACH-000319	0	7.514359007	6.582254908
ACH-000455	0	6.932155684	6.425761401
ACH-001711	0	6.403608584	5.297191417
ACH-001529	0	6.794935663	4.151371776
ACH-000493	0	7.512068826	5.781097381
ACH-000341	0	6.931801228	6.09212285

Table S6: Normalized abundance of peptides that are common to DDX3X & DDX3Y

	R1	R2	R3	R4	R5	R6
Control	1.09127177	1.08166782	1.03229697	1.1682261	1.09425885	1.1015297
DDX3XKD	0.8820274	0.84627154	0.8895345	0.82010613	0.80777338	0.84994896
DDX3YKD	1.04069377	1.09574025	1.08388533	1.07434965	1.10609464	1.06136908

Table S7: DESeq2 output of significantly differentially expressed genes upon *DDX3X* knockdown. Significance is determined by adjusted p value < 0.05.

	baseMean	log2FoldChange	lfcSE	stat	pvalue	padj

DDX3X	14898.473	-3.411	0.297	-11.484	1.592E-30	2.239E-26
PARP6	1036.253	0.479	0.054	8.905	5.321E-19	3.743E-15
DLG5	7252.634	0.231	0.031	7.385	1.521E-13	7.132E-10
TCFL5	957.737	-0.298	0.041	-7.180	6.953E-13	2.446E-09
IRAK1	6181.261	0.570	0.082	6.967	3.234E-12	9.100E-09
ERLEC1	11229.619	-0.308	0.044	-6.922	4.441E-12	1.041E-08
PLCD3	3685.770	0.440	0.068	6.495	8.309E-11	1.670E-07
PRKRA	2423.253	0.257	0.041	6.320	2.620E-10	4.608E-07
RUBCN	2174.268	0.342	0.057	6.033	1.606E-09	2.054E-06
SETD3	5093.532	0.255	0.042	6.039	1.548E-09	2.054E-06
ZMYND19	627.915	0.360	0.061	5.911	3.408E-09	3.996E-06
TRIM8	7854.255	0.402	0.069	5.822	5.821E-09	6.101E-06
ZNF703	3579.195	0.528	0.091	5.815	6.071E-09	6.101E-06
BAG1	1162.234	0.493	0.087	5.682	1.333E-08	1.123E-05
RAPGEF1	3970.699	0.405	0.071	5.679	1.353E-08	1.123E-05
TCF20	2307.297	0.284	0.050	5.679	1.356E-08	1.123E-05
RUNX3	444.205	0.414	0.075	5.488	4.068E-08	3.180E-05
PHC1	884.522	0.374	0.069	5.451	5.004E-08	3.706E-05
SLC25A43	3205.496	0.190	0.035	5.439	5.348E-08	3.763E-05
UBAC1	1682.791	0.225	0.042	5.362	8.224E-08	5.510E-05
MAP3K3	4507.077	0.234	0.044	5.331	9.766E-08	5.808E-05
MGST1	5273.417	-0.262	0.049	-5.328	9.907E-08	5.808E-05
TCF3	2699.991	0.332	0.063	5.267	1.388E-07	7.509E-05
MAPKAPK 2	8199.483	0.253	0.048	5.232	1.674E-07	8.215E-05
SDCCAG3	1651.691	0.294	0.056	5.230	1.693E-07	8.215E-05
SHB	1541.163	0.272	0.052	5.243	1.578E-07	8.215E-05
ITPK1	2312.786	0.331	0.064	5.168	2.368E-07	1.075E-04
MON1B	2417.502	-0.167	0.032	-5.171	2.327E-07	1.075E-04
ANAPC5	7715.387	0.192	0.038	5.093	3.533E-07	1.554E-04
ARCN1	33084.931	-0.158	0.031	-5.055	4.294E-07	1.831E-04
MAZ	6687.960	0.290	0.057	5.049	4.446E-07	1.840E-04
LINC01420	2011.874	-0.264	0.053	-5.034	4.815E-07	1.936E-04
FAM53B	924.893	0.434	0.087	5.015	5.312E-07	2.076E-04
ZBTB42	130.355	0.570	0.116	4.927	8.340E-07	3.088E-04
ZNF592	3014.298	0.264	0.054	4.932	8.125E-07	3.088E-04
CSRNP2	2734.160	0.192	0.039	4.890	1.006E-06	3.629E-04
FAM219B	2503.299	0.233	0.048	4.867	1.135E-06	3.983E-04
PLEKHO1	1618.110	0.341	0.070	4.862	1.161E-06	3.983E-04
RAB7B	557.174	-0.331	0.068	-4.856	1.198E-06	4.014E-04
CD63	68122.511	-0.202	0.042	-4.809	1.517E-06	4.673E-04

KCMF1	4941.495	0.245	0.051	4.807	1.528E-06	4.673E-04
PLCG1	3644.730	0.220	0.046	4.799	1.594E-06	4.673E-04
RPS6KC1	3417.535	0.157	0.033	4.809	1.517E-06	4.673E-04
TEAD2	1348.081	0.225	0.047	4.820	1.438E-06	4.673E-04
ZNF496	840.073	0.334	0.070	4.800	1.584E-06	4.673E-04
PLCB3	3227.973	0.255	0.053	4.789	1.672E-06	4.740E-04
TIMM8A	450.206	0.294	0.061	4.788	1.685E-06	4.740E-04
FAHD1	2143.229	0.246	0.052	4.766	1.881E-06	5.191E-04
GHITM	10300.856	-0.151	0.032	-4.699	2.617E-06	7.081E-04
AGO2	6020.721	0.311	0.066	4.686	2.779E-06	7.110E-04
DGKD	649.197	0.323	0.069	4.688	2.753E-06	7.110E-04
PRICKLE4	120.187	0.482	0.103	4.690	2.736E-06	7.110E-04
CREBRF	1851.340	-0.282	0.060	-4.663	3.123E-06	7.709E-04
KIAA1147	636.678	0.301	0.064	4.665	3.084E-06	7.709E-04
COPB2	29774.683	-0.166	0.036	-4.640	3.486E-06	8.191E-04
GIT1	2078.965	0.440	0.095	4.637	3.539E-06	8.191E-04
ITPR3	3826.796	0.433	0.093	4.633	3.599E-06	8.191E-04
WNK4	3686.667	0.288	0.062	4.641	3.472E-06	8.191E-04
ZNF618	2062.280	0.242	0.052	4.633	3.610E-06	8.191E-04
CTNND1	23077.280	-0.115	0.025	-4.613	3.974E-06	8.876E-04
GABARAP	11134.970	-0.178	0.039	-4.608	4.061E-06	8.928E-04
MGST3	5289.065	-0.180	0.039	-4.593	4.379E-06	9.478E-04
TNFRSF10D	18922.180	0.342	0.075	4.588	4.472E-06	9.534E-04
DAZAP1	3025.025	0.173	0.038	4.584	4.568E-06	9.593E-04
GATAD2A	5566.275	0.347	0.076	4.569	4.896E-06	1.013E-03
ETS1	7031.563	0.265	0.058	4.561	5.096E-06	1.039E-03
SPAG7	1749.665	-0.138	0.030	-4.552	5.317E-06	1.054E-03
USP31	677.582	0.419	0.092	4.547	5.437E-06	1.062E-03
KRTAP1-5	2973.425	-0.618	0.136	-4.531	5.883E-06	1.123E-03
RFNG	1688.438	0.436	0.096	4.530	5.906E-06	1.123E-03
SAMD1	2103.051	0.230	0.051	4.509	6.505E-06	1.220E-03
MORF4L1	28028.860	-0.185	0.041	-4.505	6.645E-06	1.230E-03
AAAS	1459.628	-0.214	0.048	-4.448	8.656E-06	1.542E-03
DVL1	4585.184	0.660	0.149	4.440	8.977E-06	1.579E-03
PLEKHM2	5544.373	0.277	0.063	4.428	9.497E-06	1.650E-03
AP3D1	14032.809	0.192	0.043	4.422	9.792E-06	1.680E-03
ZNF74	208.919	0.390	0.088	4.406	1.052E-05	1.783E-03
CDR2L	4347.768	0.358	0.081	4.398	1.092E-05	1.808E-03
HYOU1	8724.941	0.190	0.043	4.398	1.091E-05	1.808E-03
SERINC2	3423.428	-0.248	0.056	-4.387	1.152E-05	1.884E-03

EPRS	23398.834	-0.144	0.033	-4.383	1.173E-05	1.897E-03
MTMR12	2392.374	0.243	0.056	4.359	1.305E-05	2.062E-03
SENP2	3555.594	0.155	0.036	4.361	1.295E-05	2.062E-03
POFUT1	7043.627	0.132	0.030	4.350	1.359E-05	2.101E-03
RAD51D	742.997	0.355	0.082	4.313	1.614E-05	2.469E-03
MICALL1	3112.260	0.333	0.077	4.300	1.707E-05	2.582E-03
HMBS	793.504	0.323	0.075	4.290	1.790E-05	2.679E-03
PKN1	6270.278	0.373	0.087	4.278	1.890E-05	2.799E-03
RNF19B	758.983	0.217	0.051	4.268	1.969E-05	2.857E-03
BRPF3	2765.488	0.170	0.040	4.226	2.381E-05	3.317E-03
MFHAS1	718.927	0.422	0.100	4.227	2.373E-05	3.317E-03
BTBD6	3069.288	0.322	0.077	4.210	2.559E-05	3.530E-03
FBXO17	1127.315	0.290	0.069	4.186	2.844E-05	3.818E-03
GTF2IRD1	899.028	0.278	0.066	4.189	2.800E-05	3.818E-03
TMED8	2070.881	0.182	0.043	4.185	2.849E-05	3.818E-03
CERK	6260.885	0.222	0.053	4.182	2.893E-05	3.840E-03
ABHD6	629.659	0.245	0.059	4.164	3.131E-05	4.089E-03
IQCE	1851.848	0.208	0.050	4.163	3.139E-05	4.089E-03
GPX8	22910.342	-0.213	0.052	-4.130	3.627E-05	4.640E-03
PPP1R26	746.976	0.359	0.087	4.130	3.623E-05	4.640E-03
CDK16	6143.801	0.183	0.044	4.119	3.800E-05	4.817E-03
MTA1	2398.876	0.222	0.054	4.117	3.847E-05	4.832E-03
BAG2	6435.615	-0.284	0.069	-4.113	3.910E-05	4.868E-03
PRKAR2A	7521.342	0.219	0.053	4.107	4.007E-05	4.905E-03
RAB3GAP1	12882.719	-0.156	0.038	-4.107	4.009E-05	4.905E-03
CREB3L1	20068.518	-0.185	0.045	-4.100	4.130E-05	5.010E-03
HIST1H2BD	799.495	-0.270	0.066	-4.095	4.230E-05	5.087E-03
KDELR2	39561.303	-0.134	0.033	-4.082	4.474E-05	5.334E-03
UBE2H	11857.315	-0.252	0.062	-4.077	4.568E-05	5.401E-03
ATP6V1E1	8440.182	-0.125	0.031	-4.058	4.955E-05	5.809E-03
CEP170B	4336.611	0.284	0.070	4.050	5.115E-05	5.851E-03
DUSP7	1861.287	0.276	0.068	4.053	5.048E-05	5.851E-03
LSM11	387.097	0.314	0.078	4.051	5.107E-05	5.851E-03
ANO8	418.186	0.415	0.103	4.047	5.196E-05	5.895E-03
STARD10	384.169	0.358	0.089	4.030	5.585E-05	6.237E-03
MCM3AP	6175.466	0.196	0.049	4.024	5.725E-05	6.258E-03
PTGFR	1428.093	-0.365	0.091	-4.025	5.709E-05	6.258E-03
SYNE1	12398.416	-0.250	0.062	-4.022	5.782E-05	6.258E-03
SHANK3	240.178	0.409	0.102	4.015	5.937E-05	6.376E-03
CHMP2A	3700.699	-0.260	0.065	-3.994	6.510E-05	6.939E-03

FDFT1	5454.299	-0.152	0.038	-3.984	6.764E-05	7.156E-03
HIST1H4H	544.842	-0.270	0.068	-3.966	7.314E-05	7.622E-03
PABPC1L	88.367	0.551	0.139	3.966	7.307E-05	7.622E-03
AADAT	406.657	0.260	0.066	3.953	7.714E-05	7.865E-03
ABHD4	2111.898	-0.211	0.053	-3.954	7.693E-05	7.865E-03
HIVEP3	990.404	0.381	0.096	3.956	7.619E-05	7.865E-03
NCK2	1494.815	0.256	0.065	3.950	7.818E-05	7.914E-03
ABCC9	3851.629	-0.231	0.059	-3.943	8.045E-05	8.085E-03
NUDT18	420.857	-0.298	0.076	-3.938	8.224E-05	8.206E-03
SGPL1	2380.479	0.167	0.042	3.934	8.344E-05	8.267E-03
CLK3	1490.841	-0.177	0.045	-3.928	8.565E-05	8.427E-03
CAT	4340.164	-0.131	0.033	-3.924	8.706E-05	8.485E-03
GOLPH3L	1990.804	-0.189	0.048	-3.923	8.744E-05	8.485E-03
KCNK2	10463.281	-0.158	0.041	-3.904	9.450E-05	9.107E-03
SLC7A1	21582.848	0.272	0.070	3.895	9.809E-05	9.388E-03
EPHB4	1814.502	0.225	0.058	3.893	9.920E-05	9.423E-03
ZNF274	999.787	0.192	0.049	3.889	1.005E-04	9.423E-03
RIT1	2272.419	-0.179	0.046	-3.877	1.057E-04	9.848E-03
GARS	27038.900	-0.152	0.039	-3.871	1.082E-04	9.894E-03
KHSRP	6559.052	0.152	0.039	3.872	1.078E-04	9.894E-03
ZKSCAN1	8993.789	-0.197	0.051	-3.871	1.083E-04	9.894E-03
KIAA0196	5039.951	-0.154	0.040	-3.863	1.121E-04	9.920E-03
MMP14	40005.655	0.225	0.058	3.866	1.104E-04	9.920E-03
WBP2	3210.200	-0.174	0.045	-3.865	1.110E-04	9.920E-03
ZBTB38	14726.921	-0.160	0.041	-3.863	1.119E-04	9.920E-03
CCDC85C	1332.051	0.407	0.105	3.858	1.142E-04	1.005E-02
TBC1D1	3797.415	0.307	0.080	3.851	1.176E-04	1.027E-02
DGKQ	775.252	0.409	0.106	3.842	1.218E-04	1.051E-02
GBF1	12788.291	-0.094	0.025	-3.844	1.212E-04	1.051E-02
CACNB3	993.681	0.288	0.075	3.840	1.232E-04	1.052E-02
DYNLRB1	7456.410	-0.141	0.037	-3.838	1.241E-04	1.052E-02
EPN1	7286.726	0.301	0.079	3.839	1.237E-04	1.052E-02
CAMSAP1	3096.465	0.242	0.063	3.827	1.299E-04	1.082E-02
IFFO2	2146.582	0.148	0.039	3.828	1.293E-04	1.082E-02
ATP5E	8151.648	-0.266	0.070	-3.812	1.377E-04	1.126E-02
IRF2	941.689	-0.274	0.072	-3.814	1.367E-04	1.126E-02
PDGFC	9770.930	-0.160	0.042	-3.812	1.376E-04	1.126E-02
RBPMS	3022.308	-0.284	0.075	-3.808	1.401E-04	1.140E-02
SOX12	1774.488	0.198	0.052	3.806	1.412E-04	1.142E-02
PRR13	4730.575	-0.148	0.039	-3.788	1.520E-04	1.222E-02
GTF3A	4203.605	0.159	0.042	3.776	1.597E-04	1.277E-02

IFNGR2	4025.030	-0.165	0.044	-3.772	1.616E-04	1.285E-02
ARSJ	6156.395	-0.187	0.050	-3.768	1.645E-04	1.300E-02
NSF	6970.648	-0.149	0.040	-3.763	1.679E-04	1.313E-02
TAF10	1800.407	-0.195	0.052	-3.764	1.674E-04	1.313E-02
PTPRF	9226.105	0.154	0.041	3.760	1.702E-04	1.323E-02
MINK1	7589.883	0.137	0.036	3.753	1.746E-04	1.345E-02
VPS72	1792.170	-0.160	0.043	-3.753	1.749E-04	1.345E-02
AMZ2	4115.813	-0.169	0.045	-3.748	1.786E-04	1.365E-02
SGMS2	5069.612	-0.226	0.060	-3.746	1.800E-04	1.369E-02
CCNH	1651.593	-0.178	0.048	-3.735	1.876E-04	1.389E-02
EPHB1	233.946	0.714	0.191	3.736	1.867E-04	1.389E-02
NSMF	1649.142	0.259	0.069	3.735	1.876E-04	1.389E-02
ZFYVE9	4216.755	0.147	0.039	3.738	1.858E-04	1.389E-02
ACAT2	970.763	-0.271	0.073	-3.720	1.993E-04	1.457E-02
ANXA4	7116.245	-0.155	0.042	-3.719	1.998E-04	1.457E-02
MYPOP	509.872	0.259	0.070	3.722	1.980E-04	1.457E-02
FBXW2	6594.163	0.100	0.027	3.713	2.047E-04	1.485E-02
SERINC3	20828.996	-0.135	0.036	-3.712	2.058E-04	1.485E-02
HSBP1L1	294.543	0.290	0.078	3.708	2.092E-04	1.486E-02
RBMS2	9788.836	-0.230	0.062	-3.709	2.082E-04	1.486E-02
SLC35B3	2886.136	-0.168	0.045	-3.709	2.077E-04	1.486E-02
COPZ1	7214.860	-0.138	0.037	-3.701	2.151E-04	1.505E-02
HIST1H2AC	3542.890	-0.329	0.089	-3.701	2.145E-04	1.505E-02
LRRC2	1068.705	-0.260	0.070	-3.703	2.134E-04	1.505E-02
MAN2A1	7404.676	0.161	0.044	3.699	2.160E-04	1.505E-02
AVEN	1648.643	0.198	0.054	3.695	2.198E-04	1.524E-02
VPS52	2725.968	-0.136	0.037	-3.691	2.234E-04	1.541E-02
POLR3E	1045.289	0.233	0.063	3.686	2.277E-04	1.563E-02
BLVRA	1837.236	-0.140	0.038	-3.684	2.292E-04	1.565E-02
PNO1	1611.612	0.176	0.048	3.678	2.354E-04	1.592E-02
FCF1	3480.164	-0.112	0.031	-3.673	2.399E-04	1.615E-02
HIRIP3	405.924	-0.299	0.081	-3.671	2.415E-04	1.618E-02
CCDC127	2159.887	-0.149	0.041	-3.667	2.451E-04	1.634E-02
NFIC	14695.869	-0.197	0.054	-3.666	2.464E-04	1.635E-02
LRRK1	1819.182	0.211	0.058	3.660	2.524E-04	1.667E-02
ZZEF1	4822.443	0.190	0.052	3.654	2.583E-04	1.699E-02
ANKS6	1168.097	0.275	0.075	3.651	2.608E-04	1.707E-02
B4GALT4	3231.938	-0.181	0.050	-3.650	2.626E-04	1.711E-02
TAPBP	6657.141	0.109	0.030	3.648	2.642E-04	1.713E-02
CHKA	356.027	0.259	0.071	3.634	2.788E-04	1.799E-02
BRI3BP	993.530	0.282	0.078	3.633	2.805E-04	1.801E-02

C2orf88	142.294	0.439	0.121	3.628	2.855E-04	1.801E-02
MAN2A2	2664.403	0.199	0.055	3.629	2.846E-04	1.801E-02
POGK	4073.162	0.115	0.032	3.628	2.853E-04	1.801E-02
PTDSS1	4880.744	0.295	0.081	3.631	2.828E-04	1.801E-02
MLLT6	1922.946	0.220	0.061	3.625	2.886E-04	1.805E-02
SHC1	24835.512	-0.157	0.043	-3.626	2.874E-04	1.805E-02
UBA2	5562.043	0.188	0.052	3.621	2.935E-04	1.827E-02
HOXA9	1299.158	-0.159	0.044	-3.617	2.982E-04	1.840E-02
ZNF558	739.995	0.216	0.060	3.617	2.978E-04	1.840E-02
ALG13	1034.357	-0.282	0.078	-3.615	3.007E-04	1.848E-02
C11orf95	1975.123	0.266	0.074	3.610	3.057E-04	1.870E-02
PCNT	2039.038	0.197	0.055	3.604	3.136E-04	1.910E-02
ETFDH	1704.993	-0.238	0.066	-3.602	3.152E-04	1.912E-02
SLC25A37	1378.784	0.228	0.063	3.601	3.166E-04	1.912E-02
VSIG10	925.715	0.252	0.070	3.598	3.206E-04	1.928E-02
UBE2V1	15555.392	-0.151	0.042	-3.597	3.221E-04	1.929E-02
GFPT1	18072.105	-0.174	0.048	-3.593	3.273E-04	1.952E-02
RPS27L	10302.534	-0.167	0.047	-3.585	3.369E-04	2.000E-02
PSMC2	6258.134	-0.140	0.039	-3.582	3.415E-04	2.019E-02
PTPN14	29006.445	0.175	0.049	3.575	3.499E-04	2.051E-02
MICU1	5616.677	-0.109	0.031	-3.570	3.564E-04	2.081E-02
ARL1	10357.524	-0.204	0.057	-3.566	3.631E-04	2.102E-02
GORASP2	14499.015	-0.163	0.046	-3.566	3.629E-04	2.102E-02
AKT1	10593.548	0.195	0.055	3.563	3.670E-04	2.116E-02
KLHL12	2532.303	0.123	0.035	3.559	3.720E-04	2.136E-02
MTX2	1788.348	-0.135	0.038	-3.547	3.894E-04	2.205E-02
TMCO3	10795.588	-0.135	0.038	-3.547	3.902E-04	2.205E-02
TMEM251	299.829	0.287	0.081	3.548	3.876E-04	2.205E-02
MRPL43	1950.766	-0.148	0.042	-3.532	4.118E-04	2.306E-02
STRAP	12939.178	-0.140	0.040	-3.531	4.146E-04	2.306E-02
TRMO	398.243	-0.277	0.078	-3.532	4.126E-04	2.306E-02
SYT11	7170.403	-0.192	0.054	-3.527	4.201E-04	2.327E-02
EDF1	9634.125	-0.150	0.042	-3.526	4.222E-04	2.329E-02
MLEC	22992.607	0.124	0.035	3.523	4.259E-04	2.341E-02
KIFC3	1647.248	0.314	0.089	3.521	4.306E-04	2.348E-02
WDR48	2935.489	-0.155	0.044	-3.521	4.302E-04	2.348E-02
PCGF2	2015.922	-0.192	0.055	-3.516	4.385E-04	2.382E-02
TRAFD1	2156.292	-0.144	0.041	-3.513	4.430E-04	2.398E-02
CRABP2	5469.956	-0.403	0.115	-3.510	4.481E-04	2.416E-02
CTNNA1	37570.013	-0.104	0.030	-3.509	4.500E-04	2.416E-02
ALG3	1614.331	-0.171	0.049	-3.508	4.523E-04	2.420E-02

S100A10	14132.105	-0.141	0.040	-3.505	4.565E-04	2.433E-02
ZFYVE27	985.459	0.270	0.077	3.503	4.603E-04	2.444E-02
FAM114A1	17413.752	-0.169	0.048	-3.497	4.705E-04	2.461E-02
SEMA3C	14354.327	-0.231	0.066	-3.499	4.666E-04	2.461E-02
SPG21	3764.401	0.132	0.038	3.499	4.671E-04	2.461E-02
NCOR2	17232.428	0.201	0.058	3.492	4.797E-04	2.490E-02
ZNF768	927.106	0.262	0.075	3.493	4.783E-04	2.490E-02
MOCOS	826.967	-0.230	0.066	-3.480	5.020E-04	2.587E-02
DNAJC3	10070.357	0.162	0.047	3.476	5.097E-04	2.610E-02
SUPT3H	347.086	-0.247	0.071	-3.475	5.101E-04	2.610E-02
ACAP3	1452.502	0.307	0.089	3.457	5.453E-04	2.770E-02
CDYL2	2159.002	0.287	0.083	3.453	5.547E-04	2.798E-02
NLGN1	2776.442	-0.255	0.074	-3.453	5.548E-04	2.798E-02
CDH10	429.629	-0.402	0.116	-3.451	5.576E-04	2.802E-02
FBXO3	2468.590	-0.148	0.043	-3.445	5.708E-04	2.858E-02
AP1G1	14561.316	-0.075	0.022	-3.442	5.770E-04	2.879E-02
B3GNT9	2831.734	-0.219	0.064	-3.439	5.839E-04	2.891E-02
ERRFI1	4275.687	0.466	0.135	3.438	5.857E-04	2.891E-02
LMNA	51639.659	-0.168	0.049	-3.438	5.853E-04	2.891E-02
ARNT	3735.062	-0.146	0.043	-3.433	5.967E-04	2.905E-02
LTBP1	26547.979	-0.170	0.050	-3.434	5.939E-04	2.905E-02
NPM3	492.456	0.276	0.080	3.434	5.952E-04	2.905E-02
WIPF1	6234.625	-0.152	0.044	-3.430	6.042E-04	2.932E-02
ZNF710	725.615	0.241	0.070	3.427	6.101E-04	2.950E-02
CYTH1	899.639	0.179	0.052	3.424	6.163E-04	2.966E-02
SMPDL3A	646.845	-0.285	0.083	-3.423	6.195E-04	2.966E-02
SSFA2	14086.185	0.221	0.065	3.423	6.198E-04	2.966E-02
CNOT8	3031.626	-0.148	0.043	-3.421	6.237E-04	2.975E-02
PRPH2	399.723	-0.331	0.097	-3.418	6.302E-04	2.986E-02
TOP1MT	464.030	0.223	0.065	3.418	6.302E-04	2.986E-02
CBLN3	165.226	-0.469	0.137	-3.416	6.352E-04	2.997E-02
ZC3H6	762.427	-0.312	0.091	-3.415	6.368E-04	2.997E-02
USP36	1945.322	0.236	0.069	3.414	6.393E-04	2.999E-02
PSD4	334.110	0.364	0.107	3.410	6.488E-04	3.033E-02
ZEB2	9506.064	-0.218	0.064	-3.406	6.590E-04	3.070E-02
MTMR4	2044.587	0.154	0.045	3.402	6.696E-04	3.102E-02
TMEM248	9177.249	-0.079	0.023	-3.401	6.702E-04	3.102E-02
FAM114A2	2179.011	-0.142	0.042	-3.398	6.789E-04	3.132E-02
HOXC6	2842.753	-0.189	0.056	-3.394	6.878E-04	3.163E-02
COG6	3677.468	-0.178	0.053	-3.393	6.907E-04	3.165E-02
TMEM260	1443.407	-0.213	0.063	-3.392	6.950E-04	3.175E-02

NTPCR	1595.970	-0.141	0.041	-3.390	6.989E-04	3.179E-02
SLC41A2	1111.975	-0.224	0.066	-3.389	7.004E-04	3.179E-02
SH3BGRL3	38481.086	-0.226	0.067	-3.388	7.040E-04	3.185E-02
BNIP3L	12952.881	-0.211	0.062	-3.386	7.100E-04	3.191E-02
ZNF318	2512.493	0.141	0.042	3.385	7.120E-04	3.191E-02
RBFOX2	14345.711	-0.089	0.026	-3.383	7.174E-04	3.204E-02
CTDSPL	2588.537	0.134	0.040	3.381	7.226E-04	3.207E-02
SMU1	4306.077	-0.090	0.026	-3.381	7.226E-04	3.207E-02
ATPIF1	3104.573	-0.176	0.052	-3.378	7.290E-04	3.215E-02
TXN2	2900.899	-0.114	0.034	-3.378	7.288E-04	3.215E-02
FHOD3	3111.112	0.239	0.071	3.370	7.511E-04	3.278E-02
KIT	744.879	0.292	0.087	3.371	7.499E-04	3.278E-02
ZFP91	9276.858	0.133	0.040	3.372	7.460E-04	3.278E-02
KHNYN	2518.690	0.204	0.061	3.369	7.549E-04	3.278E-02
ARFGAP3	7504.763	-0.121	0.036	-3.366	7.624E-04	3.280E-02
CTSK	1766.283	-0.246	0.073	-3.367	7.608E-04	3.280E-02
SEC24D	21505.830	-0.129	0.038	-3.367	7.595E-04	3.280E-02
CD68	7593.359	-0.259	0.077	-3.360	7.797E-04	3.325E-02
CRMP1	621.303	0.184	0.055	3.361	7.755E-04	3.325E-02
FARP1	17310.118	0.153	0.046	3.360	7.794E-04	3.325E-02
AIMP1	3449.723	-0.180	0.053	-3.359	7.828E-04	3.328E-02
CKAP4	74616.364	-0.133	0.040	-3.355	7.942E-04	3.341E-02
HIF1A	77205.026	-0.268	0.080	-3.354	7.955E-04	3.341E-02
MKRN1	4498.096	-0.113	0.034	-3.357	7.893E-04	3.341E-02
PAF1	3320.928	-0.215	0.064	-3.355	7.936E-04	3.341E-02
GPSM1	1994.614	0.267	0.080	3.353	8.004E-04	3.352E-02
TMEM263	14961.960	-0.248	0.074	-3.348	8.139E-04	3.398E-02
EDA2R	1776.682	-0.177	0.053	-3.345	8.241E-04	3.431E-02
CSNK1E	5671.119	0.193	0.058	3.339	8.417E-04	3.493E-02
CFAP20	1161.417	-0.161	0.048	-3.334	8.565E-04	3.544E-02
MORN2	563.235	-0.205	0.062	-3.327	8.778E-04	3.622E-02
MARCKSL1	1106.616	0.351	0.106	3.324	8.869E-04	3.636E-02
MFAP1	2741.662	-0.223	0.067	-3.323	8.891E-04	3.636E-02
PRRC1	9561.895	-0.215	0.065	-3.325	8.850E-04	3.636E-02
RBM7	2464.877	-0.268	0.081	-3.319	9.024E-04	3.679E-02
ARL3	2239.110	-0.185	0.056	-3.310	9.338E-04	3.786E-02
ETS2	1173.026	0.206	0.062	3.304	9.532E-04	3.854E-02
LDOC1	2336.918	-0.135	0.041	-3.301	9.639E-04	3.881E-02
NEDD8	6771.052	-0.091	0.028	-3.300	9.654E-04	3.881E-02
PSMD10	3023.756	-0.149	0.045	-3.295	9.834E-04	3.922E-02
TBC1D16	3514.421	0.281	0.085	3.296	9.797E-04	3.922E-02

TICRR	240.567	0.407	0.124	3.295	9.839E-04	3.922E-02
SYNRG	2795.153	-0.106	0.032	-3.292	9.954E-04	3.956E-02
COLGALT2	1113.445	0.458	0.139	3.291	9.989E-04	3.957E-02
NAV2	2754.180	0.294	0.089	3.289	1.004E-03	3.957E-02
PUM2	6176.780	-0.126	0.038	-3.290	1.002E-03	3.957E-02
IMMT	5582.112	-0.127	0.039	-3.284	1.022E-03	4.017E-02
BBIP1	656.587	-0.276	0.084	-3.282	1.032E-03	4.044E-02
MPV17	2001.258	-0.146	0.044	-3.281	1.035E-03	4.044E-02
DRAM1	6765.917	-0.176	0.054	-3.275	1.056E-03	4.116E-02
DMWD	2137.601	0.193	0.059	3.271	1.071E-03	4.162E-02
FAM101B	4358.021	0.298	0.091	3.270	1.076E-03	4.171E-02
GSTM4	461.245	-0.190	0.058	-3.269	1.080E-03	4.174E-02
SNUPN	1115.374	-0.155	0.047	-3.263	1.104E-03	4.243E-02
TMEM14A	1312.678	-0.153	0.047	-3.260	1.115E-03	4.261E-02
GJA1	10860.576	-0.260	0.080	-3.255	1.132E-03	4.318E-02
TMA7	5310.940	-0.144	0.044	-3.253	1.142E-03	4.342E-02
C19orf12	2001.963	0.200	0.062	3.250	1.155E-03	4.369E-02
ST3GAL1	5106.623	0.276	0.085	3.248	1.164E-03	4.377E-02
ZSCAN26	861.410	-0.184	0.057	-3.248	1.163E-03	4.377E-02
RNF135	801.661	0.225	0.069	3.245	1.175E-03	4.396E-02
TMEM120B	1098.742	0.269	0.083	3.245	1.174E-03	4.396E-02
PFN1	57803.402	-0.125	0.038	-3.242	1.185E-03	4.408E-02
PINX1	392.457	0.233	0.072	3.242	1.187E-03	4.408E-02
STX7	5047.023	-0.129	0.040	-3.243	1.182E-03	4.408E-02
SLC22A15	453.450	0.220	0.068	3.234	1.222E-03	4.512E-02
WHSC1	3230.022	0.361	0.112	3.232	1.231E-03	4.533E-02
MTRR	2291.936	-0.155	0.048	-3.229	1.243E-03	4.565E-02
ADCY3	3449.457	0.200	0.062	3.222	1.275E-03	4.659E-02
ANKIB1	10454.665	-0.159	0.050	-3.221	1.276E-03	4.659E-02
C3orf67	139.613	0.409	0.127	3.221	1.278E-03	4.659E-02
SENP8	294.098	-0.304	0.094	-3.219	1.287E-03	4.667E-02
MYL12B	40464.640	-0.154	0.048	-3.215	1.302E-03	4.699E-02
ZNF597	373.038	0.247	0.077	3.216	1.300E-03	4.699E-02
HIST2H4A	266.576	-0.739	0.230	-3.214	1.309E-03	4.712E-02
RNF166	398.884	0.268	0.083	3.212	1.318E-03	4.728E-02
SOCS7	1207.899	0.211	0.066	3.211	1.321E-03	4.728E-02
PPRC1	2923.872	0.155	0.048	3.210	1.329E-03	4.734E-02
DDX51	601.496	0.205	0.064	3.207	1.343E-03	4.753E-02
SUMO1	8010.159	-0.239	0.075	-3.208	1.339E-03	4.753E-02
UFSP2	1532.767	-0.170	0.053	-3.206	1.345E-03	4.753E-02

TXNDC11	3422.091	-0.116	0.036	-3.205	1.351E-03	4.765E-02
TMEM110	2240.705	0.137	0.043	3.197	1.388E-03	4.872E-02
LNPEP	6178.102	0.123	0.039	3.194	1.402E-03	4.896E-02
CTTNBP2NL	8091.532	-0.211	0.066	-3.192	1.412E-03	4.919E-02
COG1	2313.968	-0.136	0.043	-3.191	1.416E-03	4.921E-02
PPP1R3C	14369.752	-0.262	0.082	-3.190	1.425E-03	4.939E-02
ADAMTS4	623.243	0.243	0.076	3.188	1.431E-03	4.946E-02
RNF111	3984.200	-0.164	0.051	-3.187	1.437E-03	4.955E-02
MARCH6	11168.605	-0.099	0.031	-3.184	1.454E-03	4.987E-02
POM121	4194.894	0.152	0.048	3.182	1.460E-03	4.987E-02
SMIM14	5309.909	-0.303	0.095	-3.183	1.460E-03	4.987E-02
ZNF202	479.526	0.198	0.062	3.184	1.453E-03	4.987E-02
RUFY3	1511.116	0.147	0.046	3.181	1.467E-03	4.993E-02
TMEM50A	23453.582	-0.132	0.042	-3.180	1.473E-03	4.993E-02

Table S8: DESeq2 output of significantly differentially expressed genes upon *DDX3Y* knockdown. Significance is determined by adjusted p value < 0.05.

	baseMean	log2FoldChange	lfcSE	stat	pvalue	padj
DDX3Y	6452.045	-2.393	0.094	-25.553	5.046E-144	2.115E-139
PPP1R21	1373.113	-0.174	0.032	-5.434	5.518E-08	2.891E-04
TMEM154	997.563	-0.696	0.148	-4.720	2.360E-06	3.956E-03
POLR3G	255.766	-0.590	0.138	-4.290	1.789E-05	2.343E-02
HERC4	11286.374	-0.278	0.066	-4.216	2.483E-05	3.096E-02
SOCS6	3243.938	-0.193	0.046	-4.214	2.512E-05	3.096E-02

Table S9: Allelic ratio values and change in gene expression per extra Xi for X-homologs of X-Y pair genes.

Gene	AR	Change per X Chr
DDX3X	0.56870922	0.257
EIF1AX	0.36436038	0.511
KDM6A	0.77139428	0.829
PRKX	0.53241182	0.467
RPS4X	0.58405489	0.604
USP9X	0.09544748	0.137
ZFX	0.52802306	0.453

Table S10: Ct values for qPCR of RK-33 treatment dose response of XX fibroblasts.

Sample	Target	CT
Dose 0 Rep 1	*ACTB*	17.342
Dose 0 Rep 2	*ACTB*	17.055
Dose 0 Rep 3	*ACTB*	17.090
Dose 1 Rep 1	*ACTB*	17.136
Dose 1 Rep 2	*ACTB*	17.096
Dose 1 Rep 3	*ACTB*	16.836
Dose 2 Rep 1	*ACTB*	17.309
Dose 2 Rep 2	*ACTB*	17.354
Dose 2 Rep 3	*ACTB*	17.294
Dose 5 Rep 1	*ACTB*	17.962
Dose 5 Rep 2	*ACTB*	17.796
Dose 5 Rep 3	*ACTB*	17.927
Dose 10 Rep 1	*ACTB*	19.191
Dose 10 Rep 2	*ACTB*	19.109
Dose 10 Rep 3	*ACTB*	19.132
Dose 0 Rep 1	*DDX3X*	21.953
Dose 0 Rep 2	*DDX3X*	21.749
Dose 0 Rep 3	*DDX3X*	21.732
Dose 1 Rep 1	*DDX3X*	21.969
Dose 1 Rep 2	*DDX3X*	21.710
Dose 1 Rep 3	*DDX3X*	21.597
Dose 2 Rep 1	*DDX3X*	21.503
Dose 2 Rep 2	*DDX3X*	21.449
Dose 2 Rep 3	*DDX3X*	21.561
Dose 5 Rep 1	*DDX3X*	21.136
Dose 5 Rep 2	*DDX3X*	20.985
Dose 5 Rep 3	*DDX3X*	20.995
Dose 10 Rep 1	*DDX3X*	21.165
Dose 10 Rep 2	*DDX3X*	20.992
Dose 10 Rep 3	*DDX3X*	20.852

Table S11: Ct values for qPCR of RK-33 treatment time response of XX fibroblasts.

Sample	Target	CT
Time 0 Rep 1	*ACTB*	17.416
Time 0 Rep 2	*ACTB*	17.377
Time 0 Rep 3	*ACTB*	17.459
Time 1 Rep 1	*ACTB*	17.603

Time 1 Rep 2	*ACTB*	17.598
Time 1 Rep 3	*ACTB*	17.714
Time 2 Rep 1	*ACTB*	17.829
Time 2 Rep 2	*ACTB*	17.706
Time 2 Rep 3	*ACTB*	17.745
Time 4 Rep 1	*ACTB*	17.977
Time 4 Rep 2	*ACTB*	17.625
Time 4 Rep 3	*ACTB*	17.916
Time 24 Rep 1	*ACTB*	17.970
Time 24 Rep 2	*ACTB*	17.875
Time 24 Rep 3	*ACTB*	17.758
Time 0 Rep 1	*DDX3X*	21.675
Time 0 Rep 2	*DDX3X*	21.542
Time 0 Rep 3	*DDX3X*	21.704
Time 1 Rep 1	*DDX3X*	21.726
Time 1 Rep 2	*DDX3X*	21.615
Time 1 Rep 3	*DDX3X*	21.699
Time 2 Rep 1	*DDX3X*	21.823
Time 2 Rep 2	*DDX3X*	21.539
Time 2 Rep 3	*DDX3X*	21.634
Time 4 Rep 1	*DDX3X*	21.800
Time 4 Rep 2	*DDX3X*	21.838
Time 4 Rep 3	*DDX3X*	21.718
Time 24 Rep 1	*DDX3X*	21.545
Time 24 Rep 2	*DDX3X*	21.442
Time 24 Rep 3	*DDX3X*	21.255

Chapter 3
Y chromosome-encoded regulators are essential in cancer cell lines

Shruthi Rengarajan[1,2], Erik C. Owen[1,3], David C. Page[1,2,4]

Affiliations:

1. Whitehead Institute, Cambridge, MA 02142, USA
2. Department of Biology, Massachusetts Institute of Technology, Cambridge, MA 02139, USA
3. Department of Computational & Systems Biology, Massachusetts Institute of Technology, Cambridge, MA 02139, USA
4. Howard Hughes Medical Institute, Whitehead Institute, Cambridge, MA 02142, USA

Abstract

The Y chromosome, which encodes broadly expressed regulatory genes, has been systematically excluded from genome-wide screens of essentiality. Here we use functional genomics data from the Cancer Dependency Map to test the essentiality of eight Y-chromosomal genes and identify > 80 cell lines which require one or more of these genes for proliferation. Particularly, we note that *DDX3Y* is required for viability in 25 cancer cell lines, including solid tumors, lymphomas and leukemias. Most cancers that require *DDX3Y* present with loss-of-function mutations in the X-chromosome homolog, *DDX3X,* and have elevated *DDX3Y* expression compared to *DDX3X* WT cell lines, uncovering a novel dependency in male tumors.

Keywords: Short Report, Y chromosome, Sex Chromosomes, Essentiality, Cancer

Author Contributions

S.R., D.C.P designed the experiments. E.O. and S.R. performed computational analyses. S.R. and D.C.P. wrote the manuscript.

Background

The Cancer Dependency Map (Depmap) is a repository of high-throughput loss-of-function screens that identify genes essential for proliferation in thousands of cancer cell lines, combined with deep genomic and transcriptomic characterization of the lines (Cancer Cell Line Encyclopedia) (Dempster et al., 2021; Ghandi et al., 2019; Tsherniak et al., 2017). This source has yielded many insights into the genetic changes that contribute to tumorigenesis. The genes on the Y chromosome have long posed a problem for such screens; as these genes are only expressed from a single copy in cell lines with a Y chromosome, they require specialized analyses. Y chromosome genes are also thought to be dispensable outside the male reproductive tract, furthering their exclusion. However, the Y chromosome contains several broadly-expressed genes (Bellott et al., 2014) , meriting their inclusion in genome-wide essentiality screens. Indeed, Y chromosome loss is common in cancers, making these dosage-sensitive regulators attractive tumor suppressor candidates (Forsberg et al., 2014). Recent work has shown that loss of Y drives tumor growth and severity in many cancer types (Abdel-Hafiz et al., 2023). Furthermore, the majority of cancers are male-biased in incidence and severity, and studying the role of Y chromosome genes in tumorigenesis could provide insight into how this bias arises (Lopes-Ramos et al., 2020).

The human X and Y chromosomes evolved from two ordinary pairs of autosomes over the past 200 million years (Ohno, 1967). Due to a series of inversions and the suppression of crossing over between the proto-X and Y chromosomes, the Y

chromosome was subject to large-scale genetic decay, such that only 3% of the genetic content remains (Skaletsky et al., 2003). The surviving Y chromosome genes were preserved by selection to maintain the ancestral dosage of regulators of key cellular processes, making them highly dosage-sensitive and necessary for male viability and cellular function (Bellott et al., 2014).

Here, we re-analyze these Y chromosome regulators in the Depmap dataset, identifying 81 novel genetic dependencies across a wide range of cancer cell types.

Results & Discussion

We first identified a subset of cell lines that contain a Y chromosome and do not have aberrant X inactivation, denoted ChrYPos (Fig S1, Table S1, Methods). These cells contain a single copy of the X chromosome. We also selected a control population of cell lines that did not contain Y chromosomes, denoted ChrYNeg (FigS1, Table S1). We evaluated all gRNAs for Y-encoded genes that were present in the AVANA guide library used by Depmap. We evaluated gRNAs for the following genes: *DDX3Y, USP9Y, EIF1AY, KDM5D, UTY, NLGN4Y, ZFY, RPS4Y*1. In our analyses, we only include gRNAs for Y-chromosome genes that do not also target their X-homologs (Table S2, Methods).

We identified 81 dependencies on Y-chromosome encoded regulators that are present in ChrYPos cells and not in ChrYNeg cells (Fig 1, Table S3). In particular,

DDX3Y, EIF1AY, ZFY or *RPS4Y1* knockdown have large deleterious effects in a number of ChrYPos lines. Many of these genes encode components of the translation initiation and ribosomal complexes, suggesting that such complexes are especially important to the survival and proliferation of cancer cell lines. Conversely, we see fewer dependencies on *KDM5D, USP9Y, UTY* or *NLGN4Y*. These genes consist of histone demethylases, a peptidase and a membrane protein suggesting that chromatin remodeling and signaling genes on the Y chromosome are not as crucial for the proliferation of ChrYPos cell lines as genes involved in translation. Moreover, we do not see any differences in the dependencies of known autosomal regulators between the ChrYPos and ChrYNeg subsets, demonstrating that these dependencies are specific to the presence or absence of a Y chromosome. (Fig S2).

Among the Y chromosome regulators we profiled, *DDX3Y* loss had a deleterious effect in the largest number of cell lines. We identified 25 ChrYPos lines with a *DDX3Y* dependency (Fig 1). These cell lines spanned 13 cancer tissue types, with a slight enrichment for skin and lymphoid tissues, demonstrating that *DDX3Y* is essential in cancers across the body (Fig 2A). Interestingly, its X-chromosome homolog *DDX3X* is mutated in many cancer types; *DDX3X* loss-of-function (LOF) mutations are known drivers of lymphomas and leukemias (Brandimarte et al., 2014; Gong et al., 2021), and other cancer types, including melanomas and medulloblastomas present with deleterious *DDX3X* mutations (Patmore et al., 2020; Phung et al., 2019; Valentin-Vega et al., 2016). *DDX3X* and *DDX3Y* negatively cross-regulate each other's expression levels and *DDX3Y* levels are elevated in cells with *DDX3X* mutations (Chapter 2). We

thus hypothesized that cell lines with *DDX3Y* dependencies reflected a *DDX3X-DDX3Y* interaction.

We asked if *DDX3Y* dependent lines were enriched for deleterious *DDX3X* mutations. We used PROVEAN (Protein Variation Effect Analyzer) (Choi et al., 2012) to analyze if a given *DDX3X* mutation was deleterious and 'damaging' to protein function; we then compared cell lines with these mutations to those with a dependency on *DDX3Y*. There was a significant overlap between cell lines with *DDX3X* damage and cell lines with *DDX3Y* dependency (Fig 2B). Meanwhile, cell lines without *DDX3Y* dependency showed no such overlap. We conclude that *DDX3X* LOF in ChrYPos cancer cell lines induces *DDX3Y* upregulation (Chapter 2), resulting in these cells becoming reliant on *DDX3Y* expression.

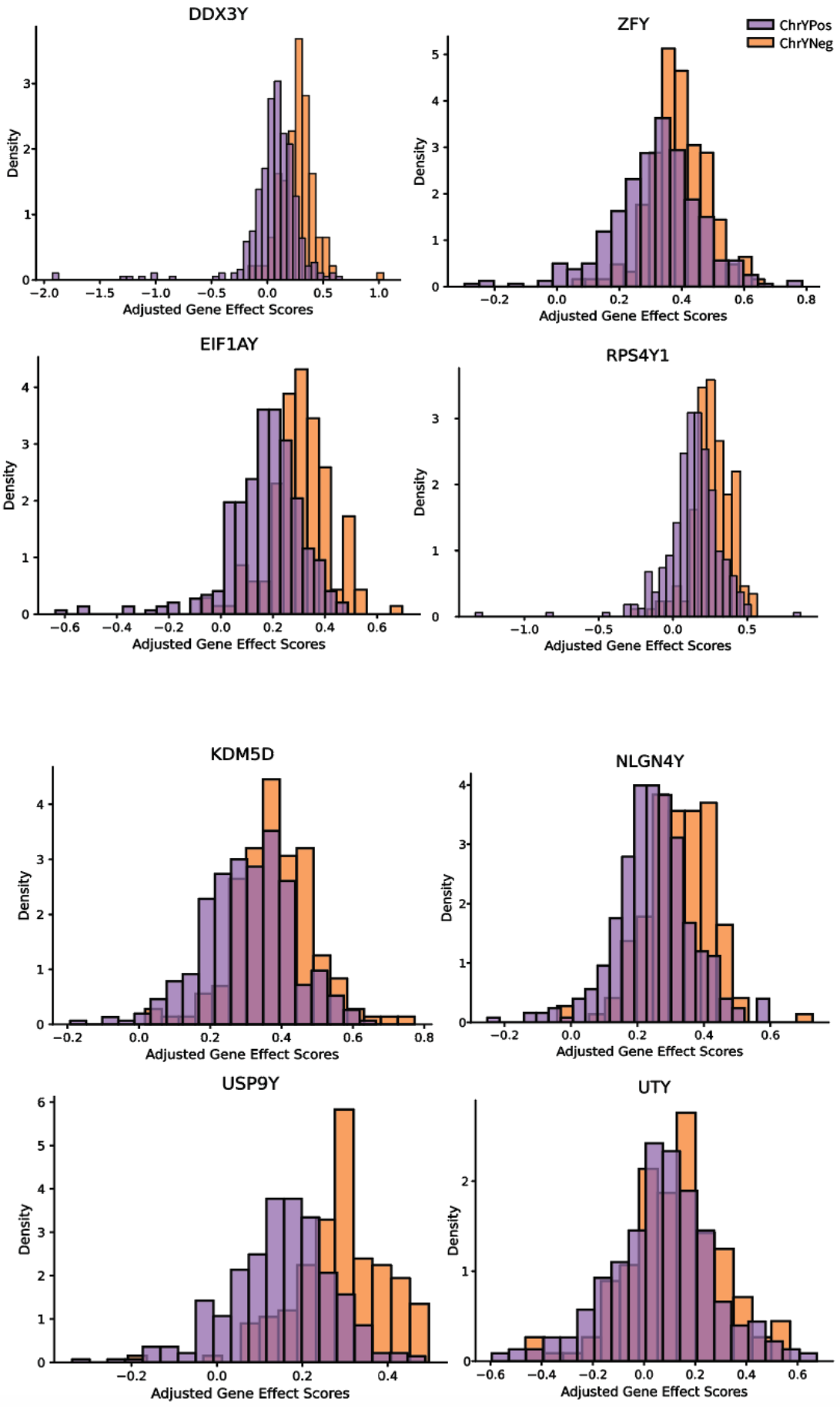
DDX3Y
ZFY
ChrYPos
ChrYNeg
EIF1AY
RPS4Y1
KDM5D
NLGN4Y
USP9Y
UTY
Density
Adjusted Gene Effect Scores

Fig 1: Genetic dependencies of Depmap cell lines on Y chromosome regulators. Histograms show the distribution of gene effect scores for eight Y encoded genes in ChrYPos lines (purple) and ChrYNeg lines (orange). A negative gene effect score indicates a negative fitness effect upon loss of the indicated gene.

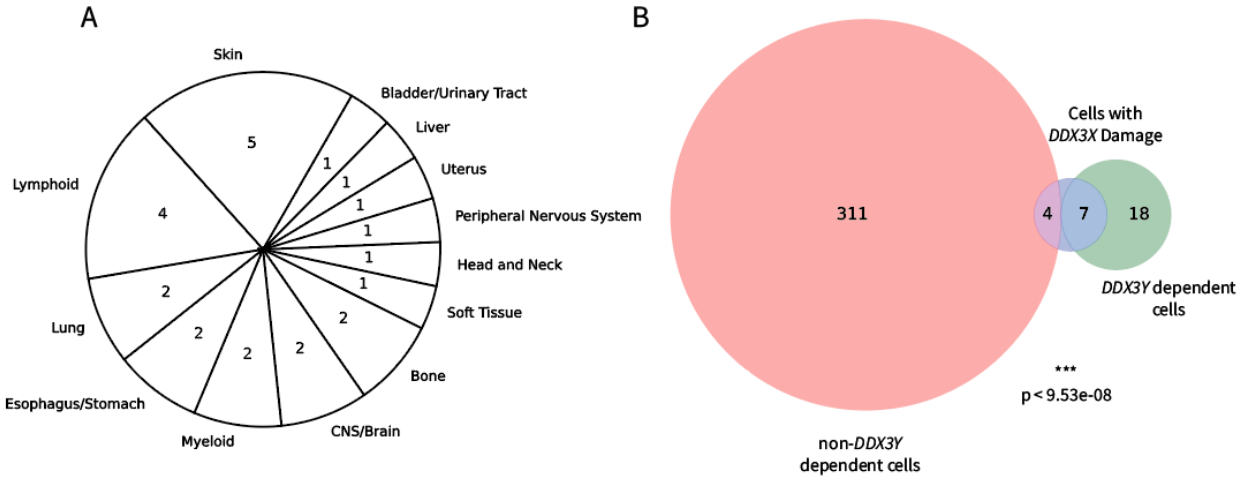

Fig 2: Characterization of cell lines with *DDX3Y* dependencies. A) Tissue of origin distribution of *DDX3Y*-dependent cancer cell lines. B) Venn Diagram showing significant enrichment of cell lines with *DDX3Y* dependency and cell lines with damaging *DDX3X* mutations (ChrYpos). Statistical significance calculated using hypergeometric test.

This study highlights the role of Y chromosome regulators in the proliferation of cancer cells. Particularly, *DDX3Y* emerges as a key dependency in *DDX3X* mutant cancers, making it a candidate drug target in male lymphomas, leukemias, melanomas and medulloblastomas. The incorporation of these broadly expressed regulators in future cancer research projects, including tumor sequencing and CRISPR screening will improve our understanding of the male bias in cancer diagnoses and severity.

Methods

Filtering of cell lines: ChrYPos cells were filtered using a log2TPM filter of *DDX3Y* > 0.2, *RPS4Y1* > 0.2, *Xist* < 2. ChrYNeg cells were filtered using a log2TPM filter of *DDX3Y* <= 0, *RPS4Y1* <= 0.

Filtering of gRNAs: Y chromosome gRNAs were processed using CRISPRoff (https://rth.dk/resources/crispr/) (Alkan et al., 2018). gRNAs that had favorable free energy binding to X-homologs within one mismatch of the seed sequence were excluded. Valid Y chromosome gRNAs were mapped to the AvanaRawReadcounts file and checked for quality in the pDNA batches. These guide RNAs were concatenated to AvanaGuideMap DataFrame. The sequence map was created by filtering for sequences from the Avana library that passed the Chronos quality control workflow. The sequence map was then subdivided into subsets, for ChrYPos cells and ChrYNeg cells.

Chronos: Chronos was run as specified in https://github.com/broadinstitute/chronos. The chronos model was trained in a Conda environment containing the packages: 'crispr-chronos' (2.0.6), 'nvidia-cudnn-cu11' (8.5.0.163), and 'tensorflow-gpu' (2.12.1) along with other necessary dependencies. Clonal outgrowths were first NaN'd for each set of DataFrames and then quality control reports were generated for each cell line set. Positive and negative controls were added from 'AchillesCommonEssentialControls.csv' and 'AchillesNonessentialControls.csv' and then a Chronos model was trained for 501

epochs for each cell line set. A high-performance computer cluster with RTX-2080Ti GPUs and 64 GB of RAM was used for training the models.

Copy Number Correction: Gene Effects were scaled so the median score of all common essential genes = -1 and the median of all nonessential genes = 0. A custom copy number matrix was generated with estimates for genes in cells that were not subject to WGS. For ChrYPos cells, copy number was estimated using the following rules: Autosomal genes = 1.0, X or Y chromosomal genes = 0.5. For ChrYNeg cells, copy number was estimated using the following rules: Autosomal genes == 1.0, X chromosomal genes = 1.0. The copy number correction module in Chronos was run on each gene effect DataFrame to get the resultant scaled and copy-number corrected gene effect matrix that was used for downstream analysis.

Availability of data: All data is downloaded from the Depmap 23Q4 release at https://depmap.org/portal/download/all/. Original code is deposited at https://github.com/shruthi3195/YDependencyMap.

Ethics Declaration: The authors declare no conflicts of interest

References

Abdel-Hafiz, H. A., Schafer, J. M., Chen, X., Xiao, T., Gauntner, T. D., Li, Z., & Theodorescu, D. (2023). Y chromosome loss in cancer drives growth by evasion of adaptive immunity. *Nature*, *619*(7970), 624–631. https://doi.org/10.1038/s41586-023-06234-x

Alkan, F., Wenzel, A., Anthon, C., Havgaard, J. H., & Gorodkin, J. (2018). CRISPR-Cas9 off-targeting assessment with nucleic acid duplex energy parameters. *Genome Biology*, *19*(1), 177. https://doi.org/10.1186/s13059-018-1534-x

Bellott, D. W., Hughes, J. F., Skaletsky, H., Brown, L. G., Pyntikova, T., Cho, T.-J., Koutseva, N., Zaghlul, S., Graves, T., Rock, S., Kremitzki, C., Fulton, R. S., Dugan, S., Ding, Y., Morton, D., Khan, Z., Lewis, L., Buhay, C., Wang, Q., … Page, D. C. (2014). Mammalian Y chromosomes retain widely expressed dosage-sensitive regulators. *Nature*, *508*(7497), 494–499. https://doi.org/10.1038/nature13206

Brandimarte, L., La Starza, R., Gianfelici, V., Barba, G., Pierini, V., Di Giacomo, D., Cools, J., Elia, L., Vitale, A., Luciano, L., Bardi, A., Chiaretti, S., Matteucci, C., Specchia, G., & Mecucci, C. (2014). DDX3X-MLLT10 fusion in adults with NOTCH1 positive T-cell acute lymphoblastic leukemia. *Haematologica*, *99*(5), 64–66. https://doi.org/10.3324/haematol.2013.101725

Choi, Y., Sims, G. E., Murphy, S., Miller, J. R., & Chan, A. P. (2012). Predicting the Functional Effect of Amino Acid Substitutions and Indels. *PLoS ONE*, *7*(10), e46688. https://doi.org/10.1371/journal.pone.0046688

Dempster, J. M., Boyle, I., Vazquez, F., Root, D. E., Boehm, J. S., Hahn, W. C., Tsherniak, A., & McFarland, J. M. (2021). Chronos: A cell population dynamics model of CRISPR experiments that improves inference of gene fitness effects. *Genome Biology*, *22*(1), 343. https://doi.org/10.1186/s13059-021-02540-7

Forsberg, L. A., Rasi, C., Malmqvist, N., Davies, H., Pasupulati, S., Pakalapati, G., Sandgren, J., de Ståhl, T. D., Zaghlool, A., Giedraitis, V., Lannfelt, L., Score, J., Cross, N. C. P., Absher, D., Janson, E. T., Lindgren, C. M., Morris, A. P., Ingelsson, E., Lind, L., & Dumanski, J. P. (2014). Mosaic loss of chromosome Y in peripheral blood is associated with shorter survival and higher risk of cancer. *Nature Genetics*, *46*(6), 624–628. https://doi.org/10.1038/ng.2966

Ghandi, M., Huang, F. W., Jané-Valbuena, J., Kryukov, G. V., Lo, C. C., McDonald, E. R., Barretina, J., Gelfand, E. T., Bielski, C. M., Li, H., Hu, K., Andreev-Drakhlin, A. Y., Kim, J., Hess, J. M., Haas, B. J., Aguet, F., Weir, B. A., Rothberg, M. V., Paolella, B. R., … Sellers, W. R. (2019). Next-generation characterization of the Cancer Cell Line Encyclopedia. *Nature*, *569*(7757), 503–508. https://doi.org/10.1038/s41586-019-1186-3

Gong, C., Krupka, J. A., Gao, J., Grigoropoulos, N. F., Giotopoulos, G., Asby, R., Screen, M., Usheva, Z., Cucco, F., Barrans, S., Painter, D., Zaini, N. B. M., Haupl, B., Bornelöv, S., Ruiz De Los Mozos, I., Meng, W., Zhou, P., Blain, A. E., Forde, S., … Hodson, D. J. (2021). Sequential inverse dysregulation of the RNA helicases DDX3X and DDX3Y facilitates MYC-driven lymphomagenesis. *Molecular Cell*, *81*(19), 4059-4075.e11. https://doi.org/10.1016/j.molcel.2021.07.041

Lopes-Ramos, C. M., Quackenbush, J., & DeMeo, D. L. (2020). Genome-Wide Sex and Gender Differences in Cancer. *Frontiers in Oncology*, *10*, 597788. https://doi.org/10.3389/fonc.2020.597788

Ohno, S. (1967). *Sex Chromosomes and Sex-Linked Genes* (Vol. 1). Springer. https://doi.org/10.1007/978-3-642-88178-7

Patmore, D. M., Jassim, A., Nathan, E., Gilbertson, R. J., Tahan, D., Hoffmann, N., Tong, Y., Smith, K. S., Kanneganti, T.-D., Suzuki, H., Taylor, M. D., Northcott, P., & Gilbertson, R. J. (2020). DDX3X Suppresses the Susceptibility of Hindbrain Lineages to Medulloblastoma. *Developmental Cell*, *54*(4), 455-470.e5. https://doi.org/10.1016/j.devcel.2020.05.027

Phung, B., Cieśla, M., Sanna, A., Guzzi, N., Beneventi, G., Cao Thi Ngoc, P., Lauss, M., Cabrita, R., Cordero, E., Bosch, A., Rosengren, F., Häkkinen, J., Griewank, K., Paschen, A., Harbst, K., Olsson, H., Ingvar, C., Carneiro, A., Tsao, H., … Jönsson, G. (2019). The X-Linked DDX3X RNA Helicase Dictates Translation Reprogramming and Metastasis in Melanoma. *Cell Reports*, *27*(12), 3573-3586.e7. https://doi.org/10.1016/j.celrep.2019.05.069

Skaletsky, H., Kuroda-Kawaguchi, T., Minx, P. J., Cordum, H. S., Hillier, L., Brown, L. G., Repping, S., Pyntikova, T., Ali, J., Bieri, T., Chinwalla, A., Delehaunty, A., Delehaunty, K., Du, H., Fewell, G., Fulton, L., Fulton, R., Graves, T., Hou, S.-F., … Page, D. C. (2003). The male-specific region of the human Y chromosome is a mosaic of discrete sequence classes. *Nature*, *423*(6942), 825–837. https://doi.org/10.1038/nature01722

Tsherniak, A., Vazquez, F., Montgomery, P. G., Weir, B. A., Kryukov, G., Cowley, G. S., Gill, S., Harrington, W. F., Pantel, S., Krill-Burger, J. M., Meyers, R. M., Ali, L., Goodale, A., Lee, Y., Jiang, G., Hsiao, J., Gerath, W. F. J., Howell, S., Merkel, E., … Hahn, W. C. (2017). Defining a Cancer Dependency Map. *Cell*, *170*(3), 564-576.e16. https://doi.org/10.1016/j.cell.2017.06.010

Valentin-Vega, Y. A., Wang, Y.-D., Parker, M., Patmore, D. M., Kanagaraj, A., Moore, J., Rusch, M., Finkelstein, D., Ellison, D. W., Gilbertson, R. J., Zhang, J., Kim, H. J., & Taylor, J. P. (2016). Cancer-associated DDX3X mutations drive stress granule assembly and impair global translation. *Scientific Reports*, *6*, 25996. https://doi.org/10.1038/srep25996

SUPPLEMENTARY MATERIAL

Y chromosome-encoded regulators are essential in a subset of XY cancer cell lines

Shruthi Rengarajan, Erik C. Owen, David C. Page

SUPPLEMENTARY FIGURES

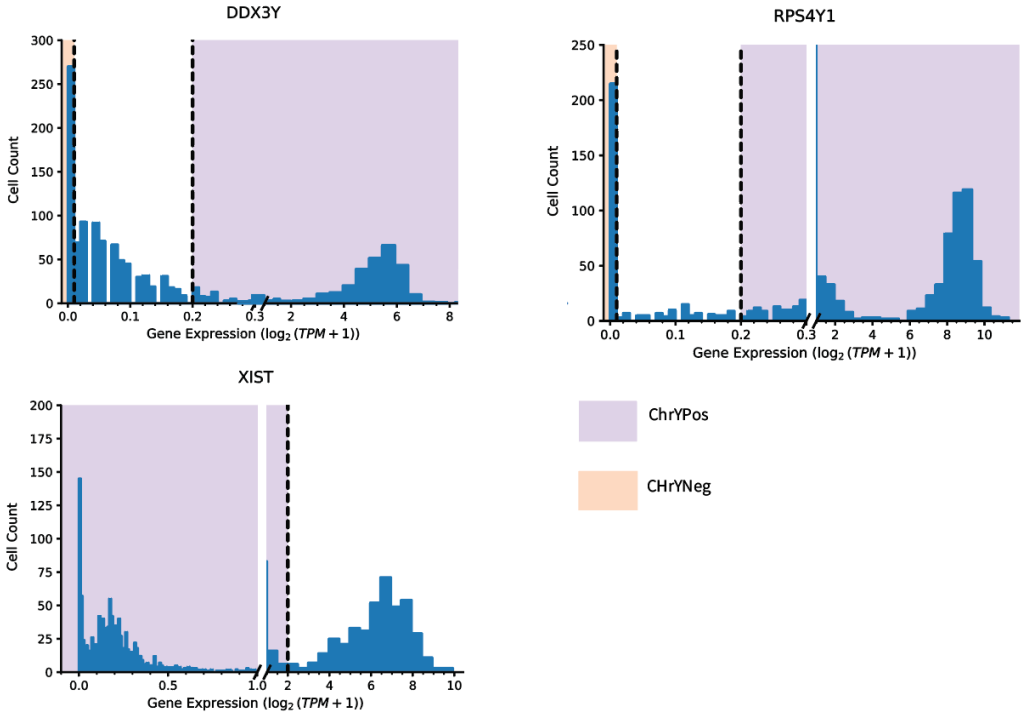

Fig S1. Expression filters for selecting Y bearing (ChrYPos) cells and non-Y bearing cells (ChrYNeg). ChrYPos cells are selected for high *DDX3Y* and *RPS4Y1* expression as well as low *Xist* expression (purple). ChrYNeg cells have no expression of *DDX3Y* & *RPS4Y1* (orange).

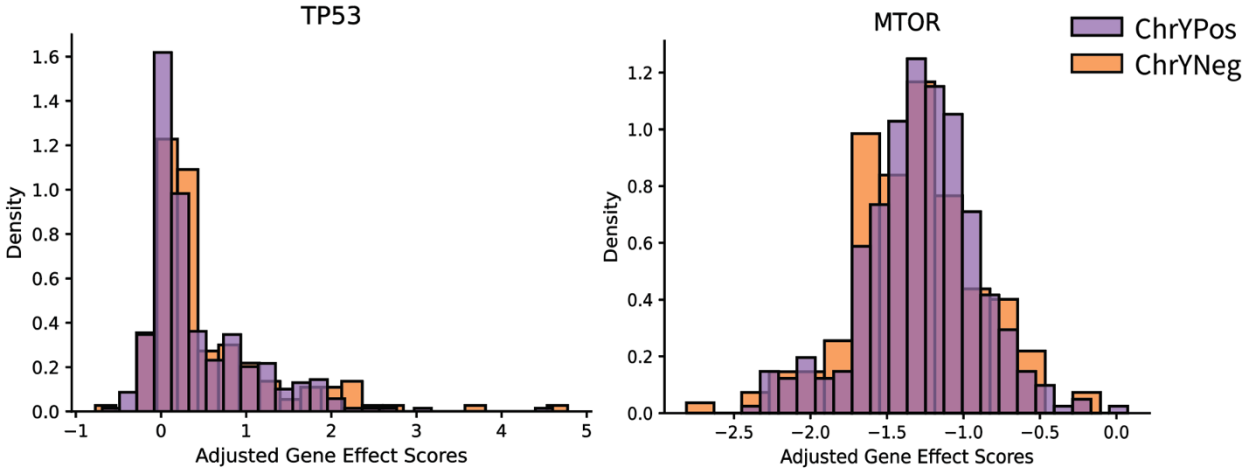

Fig S2: Genetic dependencies of Depmap cell lines on autosomal regulators. Histograms show the distribution of gene effect scores for 2 known autosomal regulators in ChrYPos lines (purple) and ChrYNeg lines (orange). There is no difference in the distribution of dependencies between ChrYPos and ChrYNeg lines.

SUPPLEMENTARY TABLES

Table S1: List of Y bearing (ChrYPos) cell lines

ModelID	PatientID	CellLineName
ACH-000004	PT-q4K2cp	HEL
ACH-000005	PT-q4K2cp	HEL 92.1.7
ACH-000007	PT-NOXwpH	LS513
ACH-000015	PT-ffwajI	NCI-H1581
ACH-000028	PT-viJKnw	KPL-1
ACH-000036	PT-llPs5J	U343
ACH-000040	PT-5XnRfQ	U-118 MG
ACH-000041	PT-3yDaRJ	RD-ES
ACH-000045	PT-zb7Sx0	MV4-11
ACH-000053	PT-nECHHn	KARPAS-299
ACH-000054	PT-cVfhmE	HT-1080
ACH-000055	PT-xKYZGz	D283 Med
ACH-000067	PT-25yL7C	Hs 683
ACH-000070	PT-0yrZJC	697
ACH-000074	PT-FJahu6	KU812
ACH-000075	PT-59c3mE	U-87 MG
ACH-000077	PT-brIUSU	MJ
ACH-000078	PT-Vot01h	MHH-NB-11
ACH-000092	PT-GaubVg	NCI-H2452
ACH-000095	PT-nsjOrX	D341 Med
ACH-000099	PT-JpfhsL	SIMA
ACH-000101	PT-6Sunyd	KE-37
ACH-000113	PT-OA9fna	OCI-AML2
ACH-000115	PT-O15HlH	VCaP
ACH-000118	PT-jYcdmK	HUP-T3
ACH-000120	PT-6jhjWI	CHP-212
ACH-000128	PT-mUWSlp	LN-319
ACH-000133	PT-PvBEqK	Hs 729
ACH-000146	PT-Sv45MF	THP-1
ACH-000151	PT-t7KWtB	JM1
ACH-000152	PT-DK2CQc	M059K
ACH-000159	PT-T2g8EU	OS-RC-2
ACH-000161	PT-G4xjbZ	COR-L105
ACH-000190	PT-YCDBvf	HD-MY-Z
ACH-000198	PT-FYT6ze	EOL-1
ACH-000206	PT-vEZ2Aw	C8166
ACH-000209	PT-xTQ9GQ	SNU-1079

ACH-000211	PT-5fvUg8	Daoy
ACH-000221	PT-7v9ThA	SNU-398
ACH-000227	PT-N9Xbr1	KP-N-YN
ACH-000232	PT-88IC1n	U-251 MG
ACH-000233	PT-zshCzw	DEL
ACH-000234	PT-A9d4DI	Caki-2
ACH-000238	PT-Kf5TA3	SCC-4
ACH-000251	PT-l5gD1h	NCI-H2887
ACH-000252	PT-XQHvQF	LS1034
ACH-000253	PT-BLAWlD	COLO 201
ACH-000255	PT-cxJQjg	LMSU
ACH-000257	PT-7LsK3v	COR-L279
ACH-000261	PT-9jciof	RERF-LC-AI
ACH-000266	PT-UWtyIo	SNU-213
ACH-000274	PT-QbMSjm	Hs 852.T
ACH-000277	PT-osxHUh	HCC1419
ACH-000288	PT-hgWgpg	BT-549
ACH-000290	PT-DzY90c	NCI-H209
ACH-000292	PT-x8fAhk	NCI-H841
ACH-000307	PT-rg0sYD	PK-1
ACH-000310	PT-2Urqss	IMR-32
ACH-000312	PT-k4Daz3	SK-N-BE(2)
ACH-000313	PT-Hd1kAu	KMRC-3
ACH-000316	PT-f7BtKr	SNU-886
ACH-000317	PT-ARX9yV	TUHR14TKB
ACH-000318	PT-8hgOdH	TE-10
ACH-000319	PT-5z2CJx	MPP 89
ACH-000326	PT-mEKuqA	JURL-MK1
ACH-000330	PT-ykXL80	EFM-19
ACH-000331	PT-ThvuiE	IST-MES2
ACH-000332	PT-Lio3jT	YAPC
ACH-000334	PT-mgfMcU	DB
ACH-000335	PT-MFqmhR	MSTO-211H
ACH-000336	PT-0F4qCF	OCI-AML3
ACH-000341	PT-I4N9IW	SK-N-FI
ACH-000343	PT-6ukZx4	NCI-H522
ACH-000346	PT-Qpiidf	JVM-3
ACH-000359	PT-qWqYVi	MG-63
ACH-000362	PT-H3wdRq	MOLM-13
ACH-000365	PT-I24dRR	SU-DHL-4
ACH-000368	PT-U0kXHW	SNU-1105
ACH-000370	PT-HHIjR4	SNU-626

ACH-000371	PT-B4jW32	RL
ACH-000387	PT-JUL0sC	TF-1
ACH-000389	PT-9RF4Fl	H4
ACH-000396	PT-jGS2bl	J82
ACH-000401	PT-hf4hbl	COLO-800
ACH-000402	PT-ieu86J	BL-70
ACH-000403	PT-cabct5	NCI-H747
ACH-000405	PT-2VMlkL	MEC-1
ACH-000415	PT-Typnjw	BICR 6
ACH-000420	PT-zjdwU2	SNU-449
ACH-000421	PT-M67oxD	SW837
ACH-000422	PT-UjP297	SNU-475
ACH-000424	PT-BIG8te	TC-71
ACH-000427	PT-e4bHZ8	NCI-N87
ACH-000436	PT-vvCo6J	OCI-My7
ACH-000437	PT-uhtVUf	SW 1088
ACH-000452	PT-xIsO4O	TE-8
ACH-000455	PT-XOGcZJ	LN-428
ACH-000458	PT-CfuEas	CJM
ACH-000459	PT-myAfV5	TUHR10TKB
ACH-000463	PT-gfHIRD	NCI-H460
ACH-000464	PT-3nLBts	CAS-1
ACH-000466	PT-IGNlGv	SNU-216
ACH-000469	PT-hzuTX4	YH-13
ACH-000472	PT-MxVfNi	HSC-2
ACH-000477	PT-A0Pe6P	Malme-3M
ACH-000479	PT-hM3DN4	KNS-81
ACH-000483	PT-YTIYsu	SNU-182
ACH-000484	PT-BHz6vU	VMRC-RCW
ACH-000486	PT-W6AZYO	KU-19-19
ACH-000487	PT-fzbPIv	F-36P
ACH-000489	PT-EtFrRG	SW1116
ACH-000493	PT-nNGWmq	SNU-423
ACH-000495	PT-GcbNSr	TUHR4TKB
ACH-000499	PT-m8xCzo	EW8
ACH-000502	PT-HGOuqa	TCC-PAN2
ACH-000511	PT-R4QjAn	Calu-1
ACH-000512	PT-H09155	INA6
ACH-000514	PT-Jj10yy	NCI-H1092
ACH-000516	PT-gEiUjw	CAL-78
ACH-000518	PT-czsVU5	CAL-33
ACH-000522	PT-sPPqcj	UM-UC-3

ACH-000525	PT-NNs10U	NCI-H2171
ACH-000532	PT-663aNr	SNU-61
ACH-000533	PT-x2jmX9	NCI-H2004 RT
ACH-000544	PT-SDTBu5	OE21
ACH-000545	PT-LSFu4z	VM-CUB1
ACH-000548	PT-p0K5QM	BHY
ACH-000549	PT-1JhWBd	SNU-1076
ACH-000550	PT-Wg8rkx	IGR-39
ACH-000559	PT-xIjoai	NCI-H1836
ACH-000571	PT-dw7sni	T98G
ACH-000576	PT-EvS9IW	KMS-27
ACH-000577	PT-DNXpFr	JHH-2
ACH-000580	PT-Dlqu1U	C32
ACH-000588	PT-wXGfqR	KMS-26
ACH-000591	PT-8XX4Me	LN-235
ACH-000597	PT-XDzUk4	TTC-709
ACH-000604	PT-yTztZ0	KYO-1
ACH-000608	PT-Ir2HyG	COV644
ACH-000614	PT-Zy2EsL	RVH-421
ACH-000616	PT-8WpAkT	Hs 746T
ACH-000619	PT-UF0NQM	PE/CA-PJ15
ACH-000622	PT-25ATIE	KNS-42
ACH-000623	PT-llEy7t	SNU-201
ACH-000627	PT-Rd3J4D	LCLC-103H
ACH-000632	PT-CeiJLF	Hs 944.T
ACH-000634	PT-FYoibe	LN-340
ACH-000638	PT-xglezn	NCI-H441
ACH-000645	PT-igc1W1	JL-1
ACH-000648	PT-pVwyuS	NCI-H28
ACH-000649	PT-4QH2lI	786-O
ACH-000652	PT-ETHfq8	SUIT-2
ACH-000654	PT-WEYO1e	Raji
ACH-000655	PT-ZQKvHU	SF268
ACH-000661	PT-VxRt2m	WM1799
ACH-000664	PT-jm7IYN	SU-DHL-1
ACH-000671	PT-TtIXsL	HuH-6
ACH-000677	PT-Z9x3iF	SW 1573
ACH-000681	PT-cqv92I	A549
ACH-000682	PT-Svdo1R	SNU-1066
ACH-000695	PT-WHXDvG	COR-L47
ACH-000698	PT-ERlBcq	DMS 53
ACH-000706	PT-srkn4o	EKVX

ACH-000716	PT-EhboSJ	TT2609-C02
ACH-000718	PT-8wDCNH	NCI-H2291
ACH-000734	PT-s6JoAb	JHH-5
ACH-000736	PT-2GXHBV	SNU-601
ACH-000738	PT-8oCN4x	GB-1
ACH-000739	PT-qL6HtY	Hep G2
ACH-000741	PT-iooYtf	U-BLC1
ACH-000747	PT-CmsNht	NCI-H1703
ACH-000748	PT-OexHxF	SJSA-1
ACH-000756	PT-cJo3y3	GI-1
ACH-000757	PT-kI5CjI	A427
ACH-000760	PT-zboiLS	LNZ308
ACH-000762	PT-M2rHki	YD-38
ACH-000765	PT-mH5ckQ	WM983B
ACH-000766	PT-wZGKqJ	NCI-H1648
ACH-000767	PT-1nXRn7	NCI-H526
ACH-000770	PT-7N6azV	P31/FUJ
ACH-000773	PT-vEVB0H	Ki-JK
ACH-000774	PT-lbbkFm	RERF-LC-Ad2
ACH-000778	PT-XJviYz	HSC-3
ACH-000787	PT-w7dxuB	LXF-289
ACH-000788	PT-ZSJTWI	A2058
ACH-000799	PT-mZ69Vl	Hs 695T
ACH-000801	PT-1I8hCi	Hs 936.T
ACH-000810	PT-1TshCj	SK-MEL-30
ACH-000817	PT-pWj35D	RPMI 8226
ACH-000819	PT-1DyLm0	LN-18
ACH-000822	PT-n2hnAf	SK-MEL-24
ACH-000827	PT-L3eOYW	WM793
ACH-000829	PT-h5fVs5	HuNS1
ACH-000833	PT-lbYOig	RH-30
ACH-000836	PT-ZS5SNw	YD-15
ACH-000837	PT-9eMhTl	NCI-H322
ACH-000839	PT-l3KlxJ	SCaBER
ACH-000843	PT-gQzNzd	HARA
ACH-000848	PT-WkfAGI	JHH-7
ACH-000853	PT-FGrsoV	NCI-H661
ACH-000858	PT-obWM4y	KNS-62
ACH-000859	PT-603OA3	HCC1954
ACH-000860	PT-W8OaFq	NCI-H358
ACH-000867	PT-3nyeTa	ChaGo-K-1
ACH-000873	PT-8iaWjG	KYSE-270

ACH-000882	PT-MRf5jM	IGR-1
ACH-000896	PT-bDT6oy	647-V
ACH-000905	PT-nC0LDL	5637
ACH-000907	PT-20TYLm	SNU-349
ACH-000913	PT-6MnPg3	ESS-1
ACH-000914	PT-zrYGap	HT
ACH-000917	PT-2HckVI	TE-4
ACH-000921	PT-jKAU6d	NCI-H157-DM
ACH-000932	PT-3F7Xgi	SNU-1
ACH-000935	PT-snQqpb	MDST8
ACH-000938	PT-rgsUoa	NALM-6
ACH-000948	PT-VDIRwk	23132/87
ACH-000950	PT-6USEGU	LoVo
ACH-000953	PT-Zkuf8L	SUP-T1
ACH-000959	PT-ulmNPq	SNU-C4
ACH-000960	PT-N5YXV2	Reh
ACH-000968	PT-z7yLU0	COLO 792
ACH-000974	PT-cgXnS7	SNG-M
ACH-000975	PT-gNoIDb	HCC2450
ACH-000976	PT-z66Tka	HuCCT1
ACH-000977	PT-tY34fU	LNCaP clone FGC
ACH-000980	PT-DdDGB6	NCI-H1155
ACH-000984	PT-UZ2uk5	HEC-6
ACH-000995	PT-lj83Ht	JURKAT
ACH-001020	PT-WLHxY0	BT-16
ACH-001036	PT-XYdNvp	CMK-11-5
ACH-001038	PT-Wd5HrW	COG-E-352
ACH-001050	PT-30CR5P	CW9019
ACH-001054	PT-HMzBz8	D458
ACH-001061	PT-i0VYNQ	DLD-1
ACH-001129	PT-ej13Dz	MONO-MAC-1
ACH-001134	PT-YD7WB8	MYLA
ACH-001164	PT-VJQa5v	CCLF_PEDS_0003_T
ACH-001190	PT-IHNbDy	SK-MEL-2
ACH-001192	PT-MPUfgI	SK-NEP-1
ACH-001196	PT-9a1vbV	SMS-CTR
ACH-001197	PT-3YIeN9	SMZ-1
ACH-001228	PT-k3C7C0	UPCI-SCC-152
ACH-001229	PT-FRJzoR	UPCI-SCC-154
ACH-001232	PT-Qe9Gjx	UW228
ACH-001239	PT-JAyPtz	WM-266-4
ACH-001270	PT-isOde8	1273/99

ACH-001277	PT-yyLDZV	Yamato
ACH-001283	PT-yXtSGR	TC-106
ACH-001289	PT-773uN4	COG-AR-359
ACH-001303	PT-IFd9cu	NB-1643
ACH-001310	PT-1UiNjR	HA1E
ACH-001329	PT-tYbbCQ	ANGM-CSS
ACH-001338	PT-cvCz0R	CHP-134
ACH-001346	PT-VXDXrs	H103
ACH-001347	PT-C880aD	H157
ACH-001366	PT-jZHQTi	NGP
ACH-001385	PT-a3pn8l	RPMI 2650
ACH-001386	PT-hfsFIb	SCLC-22H
ACH-001407	PT-SuuJak	UM-UC-13
ACH-001412	PT-IRdqMO	UM-UC-10
ACH-001414	PT-8XYADU	UM-UC-6
ACH-001415	PT-gUUbZP	UM-UC7
ACH-001430	PT-uuajSv	TC138
ACH-001450	PT-wk0KRr	BLUE-1
ACH-001453	PT-pIyNqk	BPH-1
ACH-001454	PT-LAy4cf	C10
ACH-001494	PT-KZb32w	EGI-1
ACH-001496	PT-YHsN9r	ESO26
ACH-001509	PT-jrbPZG	H357
ACH-001520	PT-vloZI6	HG-3
ACH-001522	PT-wEoiUI	HMY-1
ACH-001523	PT-ae7zps	HSC-1
ACH-001524	PT-hQHCaO	HSC-5
ACH-001528	PT-1Qm9m0	IHH-4
ACH-001529	PT-RI1Xeu	JAR
ACH-001530	PT-hB4ARO	JEG-3
ACH-001532	PT-IYnIVo	JMU-RTK-2
ACH-001533	PT-04HLfu	KARPAS 1718
ACH-001549	PT-QtHHhA	Lu-135
ACH-001556	PT-go6neE	Mero-25
ACH-001557	PT-LIQ4kC	Mero-41
ACH-001558	PT-WxXGiC	Mero-48a
ACH-001560	PT-B0HUMd	Mero-83
ACH-001562	PT-9C9m7Z	Mero-95
ACH-001563	PT-uwdvUG	MM127
ACH-001566	PT-4UAKiS	MM370
ACH-001567	PT-fN0pV5	MM383
ACH-001568	PT-QuhZbF	MM386

ACH-001570	PT-bKFeuG	MM426
ACH-001574	PT-H3wdRq	MOLM-14
ACH-001609	PT-OT2kJe	NP 3
ACH-001610	PT-WoVaBP	NP 5
ACH-001619	PT-X8PfQy	OCUG-1
ACH-001622	PT-D5Ft7E	Onda 7
ACH-001624	PT-dDtvIC	Onda 9
ACH-001634	PT-cBta1E	PGA-1
ACH-001647	PT-8Jr4Fd	SHI-1
ACH-001648	PT-F8MgcH	Shmac 4
ACH-001649	PT-iy858F	Shmac 5
ACH-001669	PT-ffpEbF	TANOUE
ACH-001673	PT-oSlXkO	TFK-1
ACH-001685	PT-A1mKo8	U-HO1
ACH-001688	PT-tocbjR	UM-RC-7
ACH-001699	PT-uhmv08	UPCI-SCC-131
ACH-001701	PT-CvPqts	UPCI-SCC-200
ACH-001707	PT-XqTlID	WA-OSEL
ACH-001711	PT-lzKK9W	PFSK-1
ACH-001737	PT-qdQICQ	CTV-1-DM
ACH-001740	PT-vvfjiZ	RH28
ACH-001745	PT-s7RWi4	RhJT
ACH-001750	PT-Hk36HO	TTC442
ACH-001796	PT-7RM5sK	95T1000
ACH-001814	PT-2XpRTn	OS252
ACH-001841	PT-wNrZ5J	ICC15
ACH-001848	PT-PUXC1Q	ICC8
ACH-001863	PT-VWXKPj	TKKK
ACH-001959	PT-x2cqmS	CC-LP-1
ACH-001973	PT-oJTeSY	MM485
ACH-001977	PT-YF5RFe	NO36
ACH-001982	PT-6BEu4D	NZM3
ACH-001990	PT-PCXcZ8	NZM7
ACH-001992	PT-nrQ0Fm	ONE58
ACH-001997	PT-jmmNcQ	ECC2
ACH-001999	PT-pmGuZF	950-5-BIK
ACH-002014	PT-5vJu3k	Mel270
ACH-002018	PT-5vJu3k	Omm2.5
ACH-002043	PT-gB4Jfi	Ca9-22
ACH-002044	PT-v9ccBc	HSQ-89
ACH-002045	PT-a3mx1w	HO-1-u-1
ACH-002048	PT-oslMHT	RMS-YM

ACH-002077	PT-qVbV4Q	Lu-165
ACH-002080	PT-rlExpa	TN-2
ACH-002461	PT-Zy2EsL	RVH421 SKIN FV1
ACH-002485	PT-NJ3wbw	MAVER-1
ACH-002523	PT-0yqjae	SNU-739
ACH-002533	PT-wkGMuS	SNU-482
ACH-002659	PT-btmPL5	JVE-127
ACH-002800	PT-WTpRkW	NCC-MPNST2-C1
ACH-002925	PT-abxYPP	UPMM3

Table S2: List of non-Y bearing (ChrYNeg) cell lines

ModelID	PatientID	CellLineName
ACH-000029	PT-NdspH5	HCC-827-GR5
ACH-000093	PT-X8PfQy	Panc 05.04
ACH-000337	PT-0fXDWz	NCI-H3122
ACH-000556	PT-ahSjGm	SIHA
ACH-001029	PT-NX1XUV	CHLA-10
ACH-001098	PT-htpobI	KCI-MOH1
ACH-001145	PT-3doOpy	OC 316
ACH-001151	PT-u4FBpq	OVCAR-5
ACH-001163	PT-wOhyc6	CCLF_PEDS_0001_T
ACH-001172	PT-88IC1n	U-251 MG DM
ACH-001183	PT-ESM25t	RT112/84
ACH-001188	PT-ombRgU	SH-SY5Y
ACH-001301	PT-9ShVj5	COGN278
ACH-001334	PT-ERAmPK	C-4 I
ACH-001335	PT-ERAmPK	C-4 II
ACH-001367	PT-7QJIsM	NMB
ACH-001370	PT-rC8bwa	OCI-P5x
ACH-001388	PT-UklPiT	SUM-102PT
ACH-001389	PT-huyXeM	SUM-1315MO2
ACH-001392	PT-i9dYpA	SUM-185PE
ACH-001393	PT-Zd61pI	SUM-190PT
ACH-001396	PT-sYFvXw	SUM-52PE
ACH-001398	PT-Xr379n	SW 156
ACH-001400	PT-2KkY6l	SW 954
ACH-001403	PT-tuE0iI	TO14
ACH-001418	PT-JGzDYG	UWB1.289
ACH-001419	PT-vA9Pcv	VP229
ACH-001421	PT-WBS2Hf	WERI-Rb-1
ACH-001422	PT-EhPRzn	WPE1-NA22

ACH-001442	PT-QwG6Ej	A388
ACH-001443	PT-xji0Xg	ASH-3
ACH-001451	PT-gPKmS2	BOKU
ACH-001481	PT-GWiky5	CHLA-90
ACH-001495	PT-bHINin	EMTOKA
ACH-001498	PT-5d2l7D	Farage
ACH-001510	PT-8wgZXD	H376
ACH-001511	PT-L1Obji	H413
ACH-001513	PT-KwMOW6	HCA-1
ACH-001515	PT-4kA9Xl	HCS-2
ACH-001517	PT-YZF57N	HEC-1
ACH-001518	PT-emUGGo	HEC-116
ACH-001525	PT-GR4jOd	HT-3
ACH-001526	PT-JCLa8x	HuO9
ACH-001538	PT-LDOCPR	KKU-213
ACH-001539	PT-FzFmMI	KML-1
ACH-001543	PT-1EAB3W	KOSC-2
ACH-001547	PT-xjKkQm	LO68
ACH-001548	PT-TA4RrC	LS
ACH-001577	PT-wizE6v	MUTZ-8
ACH-001607	PT-yeY4QM	NOZ
ACH-001616	PT-oQqqCS	OCI-LY18
ACH-001618	PT-Oev2PO	OCI-M2
ACH-001623	PT-QBDrgb	Onda 8
ACH-001627	PT-a2ltr5	P4E6
ACH-001628	PT-i3tIXN	PEA1
ACH-001630	PT-FMp5RI	PEO1
ACH-001641	PT-4X1Phg	SAT
ACH-001651	PT-aKpEm3	SKG-I
ACH-001652	PT-IwYShD	SKG-II
ACH-001653	PT-ZJjbcp	SK-GT-2
ACH-001655	PT-yc0xLp	SKN
ACH-001670	PT-SJ98Vo	TASK1
ACH-001674	PT-o4jARg	TGW
ACH-001677	PT-PFlyLY	U-2904
ACH-001687	PT-V3AbhR	UM-RC-3
ACH-001690	PT-uLUnir	UPCI-SCC-026
ACH-001691	PT-km3C7x	UPCI-SCC-029A
ACH-001696	PT-YWwuRp	UPCI-SCC-111
ACH-001698	PT-sxiEGA	UPCI-SCC-116
ACH-001702	PT-vslXtO	VA-ES-BJ
ACH-001719	PT-l7kiMr	OCI-C4P

ACH-001786	PT-LbUj3S	SNU-1544
ACH-001791	PT-lRwItD	LPS6
ACH-001793	PT-TTxLCZ	LPS27
ACH-001795	PT-jDDO2a	94T778
ACH-001799	PT-VjYY7b	LPS141
ACH-001802	PT-JmLeEs	LPS853
ACH-001804	PT-0lPf2W	LPS510
ACH-001819	PT-FVLPZS	MFM-223
ACH-001820	PT-UXPdpL	COLO 824
ACH-001834	PT-EXxLVu	ICC10
ACH-001835	PT-EXxLVu	ICC10-6
ACH-001836	PT-EXxLVu	ICC10-8
ACH-001839	PT-oAAItB	ICC13-7
ACH-001843	PT-c6a9E7	ICC3
ACH-001849	PT-mD4L5a	ICC9
ACH-001850	PT-rx5EvX	G415
ACH-001853	PT-0MsFyj	KMCH-1
ACH-001856	PT-E0gpbj	RBE
ACH-001857	PT-Sv5Y9u	SG231
ACH-001858	PT-hoMjwu	SSP-25
ACH-001861	PT-5pDw3E	TGBC1TKB
ACH-001862	PT-6N8kTd	TGBC52TKB
ACH-001864	PT-mhrkCC	YSCCC
ACH-001960	PT-9dwZW4	CC-SW-1
ACH-001961	PT-v333Dc	GB2
ACH-001970	PT-75oSJn	MM253
ACH-001991	PT-WTNLuu	NZOV9
ACH-001993	PT-22pOAT	NALM-16
ACH-002001	PT-3FxmoJ	A375 SKIN CJ1
ACH-002002	PT-3FxmoJ	A375 SKIN CJ2
ACH-002003	PT-3FxmoJ	A375 SKIN CJ3
ACH-002005	PT-4QtR2m	SK-MEL-19
ACH-002016	PT-MucJf6	Mel290
ACH-002019	PT-AOzYCt	HOKUG
ACH-002020	PT-3SrUkP	SKG-IIIa
ACH-002021	PT-UGz23U	T3M-3
ACH-002023	PT-hlvUsv	TGBC18TKB
ACH-002024	PT-2Stxl0	ECC4
ACH-002025	PT-mIVrGc	TT1TKB
ACH-002026	PT-cgXnS7	HHUA
ACH-002027	PT-vIwQtl	HOUA-I
ACH-002029	PT-rJXazG	SAS

ACH-002035	PT-5NWbnb	LCAM1
ACH-002039	PT-mXNlfw	PK-8
ACH-002040	PT-YbtlK5	HMV-II
ACH-002041	PT-PqWEZm	HOTHC
ACH-002042	PT-vhf9cn	T3M-5
ACH-002046	PT-SKC9qY	HTMMT
ACH-002051	PT-K31XId	Lu-134-A
ACH-002059	PT-reOMOW	P30/OHK
ACH-002062	PT-2hETfh	SLVL
ACH-002066	PT-coZfvw	HS-Sch-2
ACH-002069	PT-3pqp8N	HS-Os-1
ACH-002070	PT-kM7sLu	HKBMM
ACH-002084	PT-Qsi22o	MMAc
ACH-002462	PT-ml8vcL	RPE1-ss48
ACH-002463	PT-ml8vcL	RPE1-ss77
ACH-002464	PT-ml8vcL	RPE1-ss6
ACH-002465	PT-ml8vcL	RPE1-ss119
ACH-002486	PT-pyZjZu	MES-OV
ACH-002510	PT-6g2PcW	M040416
ACH-002511	PT-iI63vt	M140325
ACH-002522	PT-7B82nW	SNU-2292
ACH-002524	PT-itoB60	SNU-251
ACH-002531	PT-GWa6kp	SNU-2535
ACH-002535	PT-W0h0s9	SNU-254
ACH-002647	PT-O1x5GT	CCC-5
ACH-002654	PT-anuBoi	JVE-015
ACH-002664	PT-FT4DA3	JVE-253
ACH-002669	PT-53ZOQS	KP-363T
ACH-002672	PT-yBlD98	MAPAC-HS-77
ACH-002680	PT-UACtvx	170-MG-BA
ACH-002687	PT-VBCF1O	WM3772F
ACH-002693	PT-DyxJsT	S462
ACH-002710	PT-nQk25T	MPNST-724
ACH-002785	PT-6sPicj	NCC-LMS1-C1
ACH-002799	PT-qqzgSc	NCC-MPNST1-C1
ACH-002834	PT-EcUHFc	OS384
ACH-002847	PT-AFnHpd	YUHOIN
ACH-002922	PT-LKZDpW	SK-N-MM
ACH-002926	PT-vu5jnE	UPMD1

Table S3: Valid Y chromosome gRNAs

guide	gene	geneid
GTATATATCTGACTCAGTAT	DDX3Y	8653
GCACCACCATAAACTACACA	DDX3Y	8653
TTTGGGTCTCGAGATTCTAG	DDX3Y	8653
ATTGGCTGTACAGATCTATG	DDX3Y	8653
CTGAACTCTGAAAAACAGAG	DDX3Y	8653
TCTTGGCAAGGTGTTCAGGA	ZFY	7404
GCATGAGCAGCAAATTGATG	ZFY	7404
CCCACACTCATCACATTCAA	ZFY	7404
AGAAATGGATCCTTGTAAAG	ZFY	7404
ACTCTGGTCAGAGCACCATG	UTY	7544
GTCTCTAATCGACAACCACA	UTY	7544
AATTCTTGCAGCAAGCGTAG	UTY	7544
CTATTGTGTCTTCTCCCACG	KDM5D	8284
CCCCTTCCTGAAATCCCCAG	KDM5D	8284
GTGAAGGATGAGCAAAGTGG	KDM5D	8284
GCTTATCATCTTCATCCCCA	KDM5D	8284
GCTGAATTCCAAGACCCGCT	KDM5D	8284
TAAAGATTCCCAATGTGGAG	KDM5D	8284
CCTCTCCTCAGAGTATGCTC	EIF1AY	1964
AGAGGTTATGCCATATCAGA	EIF1AY	1964
ACAGCAGTACCTTTATTCTT	EIF1AY	1964
GAGTTGGTGTTTAAAGAGGA	EIF1AY	1964
TGATGCGGTGAACAGCAAAA	RPS4Y1	6192
CCTTGGTGTCATAGACCAGG	RPS4Y1	6192
TGCTGTTCACCGCATCACAG	RPS4Y1	6192
GACAGGTGAACATTTCCGCC	RPS4Y1	6192
CGCCTGGTCTATGACACCAA	RPS4Y1	6192
GTCCATCTCGAAAAAAACGT	USP9Y	8287
CCAAGTTCTATACCTAACAG	USP9Y	8287
TGTTAGGTATAGAACTTGGG	USP9Y	8287
TGAACCATGTTGCGTCCCCA	NLGN4Y	22829
GTTTAACATGACACAGACAG	NLGN4Y	22829
AGTTATCCACAGAAGAACAT	NLGN4Y	22829
ACTGGACCCAAGATCTCACT	NLGN4Y	22829

Table S3: Y-chromosome gene dependencies in ChrYPos cell lines

CCLE_Index	DDX3Y effect scores	ModelID	Cell Line	Lineage	OncotreePrimaryDisease	OncotreeSubtype	Sex
1316	-1.9245298	ACH-001563	MM127	Skin	Melanoma	Melanoma	Male
762	-1.891060457	ACH-000766	NCIH1648	Lung	Non-Small Cell Lung Cancer	Lung Adenocarcinoma	Male

869 -1.303644931 ACH-000873 KYSE270 Esophagus/Stomach Esophageal Squamous Cell Carcinoma Esophageal Squamous Cell Carcinoma Male
650 -1.243418108 ACH-000654 RAJI Lymphoid Mature B-Cell Neoplasms Burkitt Lymphoma Male
363 -1.107296721 ACH-000365 SUDHL4 Lymphoid Mature B-Cell Neoplasms Diffuse Large B-Cell Lymphoma, NOS Male
806 -0.995114143 ACH-000810 SKMEL30 Skin Melanoma Cutaneous Melanoma Male
910 -0.993148677 ACH-000914 HT Lymphoid Mature B-Cell Neoplasms Diffuse Large B-Cell Lymphoma, NOS Male
400 -0.863814474 ACH-000402 BL70 Lymphoid Mature B-Cell Neoplasms Burkitt Lymphoma Male
1140 -0.436559666 ACH-001270 127399 Soft Tissue Synovial Sarcoma Synovial Sarcoma Male
4 -0.415852141 ACH-000005 HEL9217 Myeloid Acute Myeloid Leukemia Acute Myeloid Leukemia Male
1319 -0.396168725 ACH-001568 MM386 Skin Melanoma Melanoma Male
474 -0.287498603 ACH-000477 MALME3M Skin Melanoma Melanoma Male
691 -0.275762648 ACH-000695 CORL47 Lung Lung Neuroendocrine Tumor Small Cell Lung Cancer Male
34 -0.225116768 ACH-000036 U343 CNS/Brain Diffuse Glioma Glioblastoma Male
368 -0.223060067 ACH-000370 SNU626 CNS/Brain Diffuse Glioma Glioblastoma Male
495 -0.215058828 ACH-000499 EW8 Bone Ewing Sarcoma Ewing Sarcoma Male
1265 -0.207373514 ACH-001496 ESO26 Esophagus/Stomach Esophagogastric Adenocarcinoma Adenocarcinoma of the Gastroesophageal Junction Male
1317 -0.206723306 ACH-001566 MM370 Skin Melanoma Melanoma Male
512 -0.205608574 ACH-000516 CAL78 Bone Chondrosarcoma Dedifferentiated Chondrosarcoma Male
1501 -0.197882837 ACH-002045 HO1U1 Head and Neck Head and Neck Squamous Cell Carcinoma Oral Cavity Squamous Cell Carcinoma Male
339 -0.19580058 ACH-000341 SKNFI Peripheral Nervous System Neuroblastoma Neuroblastoma Male
72 -0.189346805 ACH-000074 KU812 Myeloid Myeloproliferative Neoplasms Chronic Myeloid Leukemia, BCR-ABL1+ Male
1289 -0.188660872 ACH-001530 JEG3 Uterus Gestational Trophoblastic Disease Choriocarcinoma Male
844 -0.179531622 ACH-000848 JHH7 Liver Hepatocellular Carcinoma Hepatocellular Carcinoma Male

835 -0.173052522 ACH-000839 SCABER Bladder/Urinary Tract Bladder Squamous Cell Carcinoma Bladder Squamous Cell Carcinoma Male

CCLE_Index	ZFY effect scores	ModelID	StrippedCellLineName	OncotreeLineage	OncotreePrimaryDisease	OncotreeSubtype	Sex
1225	-0.295880723	ACH-001407	UMUC13	Bladder/Urinary Tract	Bladder Urothelial Carcinoma	Bladder Urothelial Carcinoma	Male
360	-0.225082904	ACH-000362	MOLM13	Myeloid	Acute Myeloid Leukemia	Acute Myeloid Leukemia	Male
1323	-0.207099594	ACH-001574	MOLM14	Myeloid	Acute Myeloid Leukemia	Acute Myeloid Leukemia	Male
1394	-0.148030696	ACH-001707	WAOSEL	Lymphoid	Mature B-Cell Neoplasms	Chronic Lymphocytic Leukemia/Small Lymphocytic Lymphoma	Male
752	-0.031223809	ACH-000756	GI1	CNS/Brain	Diffuse Glioma	Gliosarcoma	Male
973	-0.020130962	ACH-000977	LNCAPCLONEFGC	Prostate	Prostate Adenocarcinoma	Prostate Adenocarcinoma	Male
357	-0.012260616	ACH-000359	MG63	Bone	Osteosarcoma	Osteosarcoma	Male
1408	0.000164366	ACH-001750	TTC442	Soft Tissue	Rhabdomyosarcoma	Embryonal Rhabdomyosarcoma	Male
1280	0.00494738	ACH-001520	HG3	Lymphoid	B-Lymphoblastic Leukemia/Lymphoma	B-Lymphoblastic Leukemia/Lymphoma	Male
385	0.017721334	ACH-000387	TF1	Myeloid	Acute Myeloid Leukemia	Acute Myeloid Leukemia	Male
934	0.020121109	ACH-000938	NALM6	Lymphoid	B-Lymphoblastic Leukemia/Lymphoma	B-Lymphoblastic Leukemia/Lymphoma	Male
90	0.022542487	ACH-000092	NCIH2452	Pleura	Pleural Mesothelioma	Pleural Mesothelioma, Biphasic Type	Male
434	0.023552218	ACH-000436	OCIMY7	Lymphoid	Mature B-Cell Neoplasms	Plasma Cell Myeloma	Male
863	0.030127469	ACH-000867	CHAGOK1	Lung	Non-Small Cell Lung Cancer	Non-Small Cell Lung Cancer	Male
399	0.036281167	ACH-000401	COLO800	Skin	Melanoma	Cutaneous Melanoma	Male
1318	0.038829275	ACH-001567	MM383	Skin	Melanoma	Melanoma	Male
1501	0.043414018	ACH-002045	HO1U1	Head and Neck	Head and Neck Squamous Cell Carcinoma	Oral Cavity Squamous Cell Carcinoma	Male

CCLE_Index	EIF1AY effect scores	ModelID	StrippedCellLineName	OncotreeLineage	OncotreePrimaryDisease	OncotreeSubtype	Sex
1316	-0.63632344	ACH-001563	MM127	Skin	Melanoma	Melanoma	Male

615 -0.533739363 ACH-000619 PECAPJ15 Head and Neck Head and Neck Squamous Cell Carcinoma Oral Cavity Squamous Cell Carcinoma Male
1318 -0.521818087 ACH-001567 MM383 Skin Melanoma Melanoma Male
1422 -0.349662329 ACH-001814 OS252 Bone Osteosarcoma Osteosarcoma Male
1478 -0.349542362 ACH-002014 MEL270 Eye Ocular Melanoma Uveal Melanoma Male
573 -0.286761298 ACH-000577 JHH2 Liver Hepatocellular Carcinoma Hepatocellular Carcinoma Male
204 -0.228850413 ACH-000206 C8166 Lymphoid T-Lymphoblastic Leukemia/Lymphoma T-Lymphoblastic Leukemia/Lymphoma Male
425 -0.211269003 ACH-000427 NCIN87 Esophagus/Stomach Esophagogastric Adenocarcinoma Tubular Stomach Adenocarcinoma Male
1144 -0.182266099 ACH-001277 YAMATO Soft Tissue Synovial Sarcoma Synovial Sarcoma Male
630 -0.175800096 ACH-000634 LN340 CNS/Brain Diffuse Glioma Glioblastoma Male
250 -0.173188138 ACH-000252 LS1034 Bowel Colorectal Adenocarcinoma Colon Adenocarcinoma Male
512 -0.099305429 ACH-000516 CAL78 Bone Chondrosarcoma Dedifferentiated Chondrosarcoma Male
1405 -0.094947218 ACH-001740 RH28 Soft Tissue Rhabdomyosarcoma Alveolar Rhabdomyosarcoma Male
514 -0.087108951 ACH-000518 CAL33 Head and Neck Head and Neck Squamous Cell Carcinoma Oral Cavity Squamous Cell Carcinoma Male
495 -0.080492495 ACH-000499 EW8 Bone Ewing Sarcoma Ewing Sarcoma Male

CCLE_Index RPS4Y1 effect scores ModelID StrippedCellLineName OncotreeLineage OncotreePrimaryDisease OncotreeSubtype Sex
1315 -1.330419862 ACH-001562 MERO95 Pleura Pleural Mesothelioma Pleural Mesothelioma, Epithelioid Type Male
1323 -0.842652147 ACH-001574 MOLM14 Myeloid Acute Myeloid Leukemia Acute Myeloid Leukemia Male
1240 -0.429620048 ACH-001430 TC138 Bone Ewing Sarcoma Ewing Sarcoma Male
434 -0.294429767 ACH-000436 OCIMY7 Lymphoid Mature B-Cell Neoplasms Plasma Cell Myeloma Male
1100 -0.289810405 ACH-001164 CCLFPEDS0003T Soft Tissue Undifferentiated Pleomorphic Sarcoma/Malignant Fibrous Histiocytoma/High-Grade Spindle Cell Sarcoma Undifferentiated Pleomorphic Sarcoma/Malignant Fibrous Histiocytoma/High-Grade Spindle Cell Sarcoma Male

CCLE_Index	NLGN4Y effect scores	ModelID	StrippedCellLineName	OncotreeLineage	OncotreePrimaryDisease	OncotreeSubtype	Sex
4	-0.251767436	ACH-000005	HEL9217	Myeloid	Acute Myeloid Leukemia	Acute Myeloid Leukemia	Male
630	-0.128681864	ACH-000634	LN340	CNS/Brain	Diffuse Glioma	Glioblastoma	Male
425	-0.107961732	ACH-000427	NCIN87	Esophagus/Stomach	Esophagogastric Adenocarcinoma	Tubular Stomach Adenocarcinoma	Male
514	-0.101342933	ACH-000518	CAL33	Head and Neck	Head and Neck Squamous Cell Carcinoma	Oral Cavity Squamous Cell Carcinoma	Male
400	-0.081574621	ACH-000402	BL70	Lymphoid	Mature B-Cell Neoplasms	Burkitt Lymphoma	Male
144	-0.063746023	ACH-000146	THP1	Myeloid	Acute Myeloid Leukemia	Acute Myeloid Leukemia	Male
75	-0.056642534	ACH-000077	MJ	Lymphoid	Non-Hodgkin Lymphoma	Mature T and NK Neoplasms	Male

CCLE_Index	KDM5D effect scores	ModelID	StrippedCellLineName	OncotreeLineage	OncotreePrimaryDisease	OncotreeSubtype	Sex
1396	-0.192954025	ACH-001711	PFSK1	CNS/Brain	Embryonal Tumor	Primitive Neuroectodermal Tumor	Male
1417	-0.102291418	ACH-001796	95T1000	Soft Tissue	Liposarcoma	Well-Differentiated Liposarcoma	Male
1817	-0.08593682	ACH-002461	RVH421SKINFV1	Skin	Melanoma	Melanoma	Male
1232	-0.030813076	ACH-001414	UMUC6	Bladder/Urinary Tract	Bladder Urothelial Carcinoma	Bladder Urothelial CarcinomaMale	
1311	0.011298005	ACH-001558	MERO48A	Pleura	Pleural Mesothelioma	Pleural Mesothelioma, Biphasic TypeMale	

CCLE_Index	UTY effect scores	ModelID	StrippedCellLineName	OncotreeLineage	OncotreePrimaryDisease	OncotreeSubtype	Sex
593	-0.59484115	ACH-000597	TTC709	Kidney	Rhabdoid Cancer	Rhabdoid CancerMale	
1170	-0.559197644	ACH-001338	CHP134	Peripheral Nervous System	Neuroblastoma	Neuroblastoma	Male
457	-0.496499104	ACH-000459	TUHR10TKB	Kidney	Renal Cell Carcinoma	Renal Clear Cell Carcinoma	Male
1478	-0.489816116	ACH-002014	MEL270	Eye	Ocular Melanoma	Uveal Melanoma	Male
1144	-0.464449045	ACH-001277	YAMATO	Soft Tissue	Synovial Sarcoma	Synovial Sarcoma	Male

CCLE_Index	USP9Y effect scores	ModelID	StrippedCellLineName	OncotreeLineage	OncotreePrimaryDisease	OncotreeSubtype	Sex
955	-0.338855911	ACH-000959	SNUC4	Bowel	Colorectal Adenocarcinoma	Colon Adenocarcinoma	Male
394	-0.234101926	ACH-000396	J82	Bladder/Urinary Tract	Bladder Urothelial Carcinoma	Bladder Urothelial Carcinoma	Male

Chapter 4:
Conclusions

Prior to this work, much of the scholarship about *DDX3X* and *DDX3Y* have focused on DDX3X function and its many roles in cellular processes. Despite its equally widespread expression and functional interchangeability in cells (Sekiguchi et al., 2004; Venkataramanan et al., 2021), there are no studies of DDX3Y function or of *DDX3X/DDX3Y* regulation. Using perturbations of *DDX3X* and *DDX3Y* in human cells, we have found a conserved auto- and cross-regulatory program that buffers the expression of these genes. This work represents the first study of human *DDX3X* and *DDX3Y* regulation. In this chapter I will briefly summarize the findings from Chapter 2 and Chapter 3 and their implications for human phenotypes caused by mutations of both homologs. I will conclude by describing several avenues for future work.

Conclusions:

In Chapter 2, we first establish *DDX3X* as a highly dosage-sensitive gene among the X-Y pair genes. Firstly, it is expressed from Xi in human females and has a protein-coding Y homolog in every therian species sequenced, demonstrating its haploinsufficiency. Human *DDX3X* also ranks highly in population metrics; it has highly conserved miRNA targeting sites and is depleted for loss-of-function variants. *DDX3X* and *DDX3Y* retain broad expression from their ancestral autosomal progenitors, as inferred by the expression breadth of chicken *DDX3X*. These findings imply that mechanisms must exist to tightly control *DDX3X* and *DDX3Y* dosage.

We show that human *DDX3X* or *DDX3Y* transcripts decrease linearly in cells with increasing Y and X chromosome copy number. We directly link this response to *DDX3X* and *DDX3Y* using natural deletions of the Y chromosome and CRISPRi knockdowns. *DDX3X* levels are elevated in cells with *DDX3Y* deletions, and both homologs increase following CRISPRi repression of their partner. Furthermore, this result holds in an independent dataset of cancer cell lines; *DDX3Y* transcripts are elevated in cells with *DDX3X* LOF mutations. In XY cells, *DDX3X* and *DDX3Y* cross-regulation buffers changes to total expression levels; upon *DDX3Y* knockdown, the upregulation of *DDX3X* fully maintains the summed expression of *DDX3X* and *DDX3Y* at control levels. However, the upregulation of *DDX3Y* is not sufficient to fully compensate for the larger impact of *DDX3X* knockdown. In XX cells, *DDX3X* transcripts are elevated in response to the inhibition of protein function, demonstrating that DDX3X can auto-regulate. Finally, we establish mRNA destabilization as the mechanism of the cross-regulation; *DDX3X* transcripts are destabilized in cells with many copies of *DDX3Y*.

In Chapter 3, we re-analyze functional genomics screens from the Cancer Dependency Map, incorporating Y-chromosome genes. We show that many Y-chromosome regulators are essential in Y-bearing (ChrYPos) cell lines, identifying 81 novel genetic dependencies across a wide range of cancer cell types. We do not identify these dependencies in cells without Y chromosomes (ChrYNeg), and do not see differences in the essentiality of autosomal genes between the ChrYPos and ChrYNeg subsets. *DDX3Y* emerges as a key regulator, with 25 ChrYPos lines showing a strong

dependency on *DDX3Y* expression. We find that cell lines with *DDX3Y* dependencies are enriched for *DDX3X* mutant cancers, implicating the negative cross-regulation we discovered in Chapter 2. As only cells with *DDX3X* mutations are vulnerable to *DDX3Y* loss, this finding highlights *DDX3Y* as a candidate drug target in male lymphomas, leukemias, melanomas and medulloblastomas.

Future Directions:

The work described in Chapters 2 and 3 give rise to many questions that can be addressed by future studies. There are two broad directions: 1. Characterizing the mechanism of *DDX3X* and *DDX3Y* regulation and 2. Characterizing the phenotypic consequences of this regulation in health and disease, particularly in relation to biological sex. I will address these directions and speculate more broadly about the evolution of the sex chromosomes and the future of X-and Y-genes in biomedical research.

Biochemical mechanisms of *DDX3X/DDX3Y* auto- and cross-regulation

We establish that *DDX3X* mRNA is destabilized to achieve *DDX3X-DDX3Y* cross regulation. But what is the mechanism of this regulation? Does it involve direct binding and helicase activity of *DDX3X* and *DDX3Y* on their own transcripts, or are there intermediate genes that are necessary for this regulation? In this thesis, we

demonstrate cross-regulation in LCLs, fibroblasts and several cancer cell lines. *DDX3X-DDX3Y* cross regulation is also seen in published data from mouse brains and macrophages (Patmore et al., 2020; Szappanos et al., 2018). While it is possible that a secondary regulator is expressed alongside *DDX3X* and *DDX3Y* in many species and tissue types, the universality of this regulation and its deep conservation argues for direct regulation. Furthermore, this response is induced within two hours of perturbation (Chapter 2 Supplementary Information), lending further credence to a direct effect. CLIP experiments could be performed to determine if DDX3X and DDX3Y bind their own mRNAs. Current studies of DDX3X binding have only been performed in XX cells. Further disruption of putative DDX3X/DDX3Y binding sites can reveal if binding is necessary for regulation.

Sex differences in human phenotypes

While Chapter 2 offers an explanation for the different consequences of *DDX3X* vs *DDX3Y* mutations in males, it does not explain why females and males with DDX3X mutations are different phenotypically. Females with *DDX3X* mutations have *de novo* mutations on one allele that completely ablate DDX3X helicase function and this causes a severe intellectual disability in these individuals (*DDX3X* syndrome) (Snijders Blok et al., 2015). No males with these mutations have been reported, suggesting embryonic lethality in 46,XY individuals. Most males with *DDX3X* syndrome inherit a hypomorphic *DDX3X* allele from an unaffected mother (Kellaris et al., 2018). This

suggests that both types of mutations are better compensated for by *DDX3X* auto-regulation in females than *DDX3Y* cross-regulation in males. One hypothesis to explain this observation comes from the cell-autonomous nature of X inactivation. As Xa expresses more *DDX3X* than Xi, the consequences of a deleterious *DDX3X* mutation can be offset if the X chromosome containing the mutant allele is preferentially inactivated in every cell, i.e. 'skewed' (Cotton et al., 2013). However, there is no skewing of X inactivation observed in girls with *DDX3X* syndrome (Snijders Blok et al., 2015) suggesting that the increase in *DDX3X* expression from Xa or Xi provides more robust compensation for *DDX3X* loss than an increase in *DDX3Y* expression. There is preliminary evidence from studies of allelic expression in other cell types; In XX LCLs, *DDX3X* is expressed from Xi at 55% of Xa levels, while in XY LCLs, *DDX3Y* is expressed at 30% of *DDX3X* levels (Godfrey et al., 2020; San Roman et al., 2023). Any extracellular functions of DDX3X in a heterozygous female brain could also potentially be rescued by upregulating *DDX3X* expression in cells with an intact copy on Xa. Studies of the developing brain will be needed to confirm this hypothesis.

DDX3X and *DDX3Y* regulation also has important implications for the phenotypes of sex chromosome aneuploidy. The summed levels of this pair increase less steeply with increasing sex chromosome copy number than that of similar gene pairs such as *ZFX-ZFY* and *KDM6A-UTY.* Additionally, the genes that change significantly upon *DDX3X* knockdown do not overlap with genes that respond to sex chromosome aneuploidy (Chapter 2 Supplementary Information). This is in contrast with

ZFX and *ZFY*, whose targets significantly overlap with sex chromosome responsive genes (Roman et al., 2024), implying that *DDX3X* and *DDX3Y* are not major contributors to gene expression changes in individuals with sex chromosome aneuploidies. This has important consequences for the study and treatment of individuals with Turner's syndrome and Klinefelter's syndrome, among others.

Inferring ancestral gene-regulatory mechanisms on the sex chromosomes

The presence of both *DDX3X* auto-regulation in XX cells and *DDX3X-DDX3Y* cross-regulation in XY cells suggests that this regulation predates the divergence of the sex chromosomes. Indeed, the yeast ortholog of *DDX3X, Ded1* is auto-regulated, suggesting that *DDX3X* regulation may be conserved over 1.3 billion years since the common ancestor of yeast and humans (Kumar et al., 2022; Ottoz, 2015). Studies of X-Y pair regulation may allow us to infer the ancestral state of gene regulatory mechanisms. The fossils of ancestral gene regulatory mechanisms on the sex chromosomes are seen in other studies of X-Y gene pairs. *ZFX* and *ZFY* dosage have similar genome-wide effects in LCLs and fibroblasts, suggesting that their transcriptional networks have been preserved during sex chromosome evolution (Roman et al., 2024). Similarly, miRNA sites on avian Z-W chromosomes have been preserved on human sex chromosomes (Naqvi et al., 2018). *EIF1AX*, a key component of translation initiation, has retained a miR-1 site that is disrupted in *EIF1AY*, leading to 2-fold up-regulation of the Y-homolog in heart tissues (Godfrey et al., 2020).

The role of X-Y pair genes in disease

The high dosage-sensitivity and conservation of X-Y gene pairs imply that they might play key roles in human diseases. However, sex chromosome genes, especially Y-chromosome genes, are frequently excluded from genomic studies, including genome-wide association studies, whole-exome sequencing and functional genomics screens. The study of these genes is crucial to identify sex differences in diseases, and their dosage-sensitivity and cellular functions merit their inclusion in future studies. As described in Chapter 3, inclusive studies can uncover new targets like *DDX3Y* in *DDX3X* mutant male cancers. Further study is also needed to investigate the structural differences between X- and Y-homologs so that protein-specific therapies can be developed, increasing our capacity for precision medicine.

References:

Cotton, A. M., Ge, B., Light, N., Adoue, V., Pastinen, T., & Brown, C. J. (2013). Analysis of expressed SNPs identifies variable extents of expression from the human inactive X chromosome. *Genome Biology*, *14*(11), R122. https://doi.org/10.1186/gb-2013-14-11-r122

Godfrey, A. K., Naqvi, S., Chmátal, L., Chick, J. M., Mitchell, R. N., Gygi, S. P., Skaletsky, H., & Page, D. C. (2020). Quantitative analysis of Y-Chromosome gene expression across 36 human tissues. *Genome Research*, *30*(6), 860–873. https://doi.org/10.1101/gr.261248.120

Kellaris, G., Khan, K., Baig, S. M., Tsai, I.-C., Zamora, F. M., Ruggieri, P., Natowicz, M. R., & Katsanis, N. (2018). A hypomorphic inherited pathogenic variant in DDX3X causes male intellectual disability with additional neurodevelopmental and neurodegenerative features. *Human Genomics*, *12*(1), 11. https://doi.org/10.1186/s40246-018-0141-y

Kumar, S., Suleski, M., Craig, J. M., Kasprowicz, A. E., Sanderford, M., Li, M., Stecher, G., & Hedges, S. B. (2022). TimeTree 5: An Expanded Resource for Species Divergence Times. *Molecular Biology and Evolution*, *39*(8), msac174. https://doi.org/10.1093/molbev/msac174

Naqvi, S., Bellott, D. W., Lin, K. S., & Page, D. C. (2018). Conserved microRNA targeting reveals preexisting gene dosage sensitivities that shaped amniote sex chromosome evolution. *Genome Research*. https://doi.org/10.1101/gr.230433.117

Ottoz, D. S. M. (2015). *A synthetic approach to study function and expression of the Saccharomyces cerevisiae RNA helicase Ded1* [Doctoral Thesis, ETH Zurich]. https://doi.org/10.3929/ethz-a-010603399

Patmore, D. M., Jassim, A., Nathan, E., Gilbertson, R. J., Tahan, D., Hoffmann, N., Tong, Y., Smith, K. S., Kanneganti, T.-D., Suzuki, H., Taylor, M. D., Northcott, P., & Gilbertson, R. J. (2020). DDX3X Suppresses the Susceptibility of Hindbrain Lineages to Medulloblastoma. *Developmental Cell*, *54*(4), 455-470.e5. https://doi.org/10.1016/j.devcel.2020.05.027

Roman, A. K. S., Skaletsky, H., Godfrey, A. K., Bokil, N. V., Teitz, L., Singh, I., Blanton, L. V., Bellott, D. W., Pyntikova, T., Lange, J., Koutseva, N., Hughes, J. F., Brown, L., Phou, S., Buscetta, A., Kruszka, P., Banks, N., Dutra, A., Pak, E., … Page, D. C. (2024). The human Y and inactive X chromosomes similarly modulate autosomal gene expression. *Cell Genomics*, *4*(1). https://doi.org/10.1016/j.xgen.2023.100462

San Roman, A. K., Godfrey, A. K., Skaletsky, H., Bellott, D. W., Groff, A. F., Harris, H. L., Blanton, L. V., Hughes, J. F., Brown, L., Phou, S., Buscetta, A., Kruszka, P., Banks, N., Dutra, A., Pak, E., Lasutschinkow, P. C., Keen, C., Davis, S. M., Tartaglia, N. R., … Page, D. C. (2023). The human inactive X chromosome modulates expression of the active X chromosome. *Cell Genomics*, *3*(2), 100259. https://doi.org/10.1016/j.xgen.2023.100259

Sekiguchi, T., Iida, H., Fukumura, J., & Nishimoto, T. (2004). Human DDX3Y, the Y-encoded isoform of RNA helicase DDX3, rescues a hamster temperature-sensitive ET24 mutant cell line with a DDX3X mutation. *Experimental Cell Research*, *300*(1), 213–222. https://doi.org/10.1016/j.yexcr.2004.07.005

Snijders Blok, L., Madsen, E., Juusola, J., Gilissen, C., Baralle, D., Reijnders, M. R. F., Venselaar, H., Helsmoortel, C., Cho, M. T., Hoischen, A., Vissers, L. E. L. M., Koemans, T. S., Wissink-Lindhout, W., Eichler, E. E., Romano, C., Van Esch, H., Stumpel, C., Vreeburg, M., Smeets, E., … Kleefstra, T. (2015). Mutations in DDX3X Are a Common

Cause of Unexplained Intellectual Disability with Gender-Specific Effects on Wnt Signaling. *American Journal of Human Genetics*, *97*(2), 343–352. https://doi.org/10.1016/j.ajhg.2015.07.004

Szappanos, D., Tschismarov, R., Perlot, T., Westermayer, S., Fischer, K., Platanitis, E., Kallinger, F., Novatchkova, M., Lassnig, C., Müller, M., Sexl, V., Bennett, K. L., Foong-Sobis, M., Penninger, J. M., & Decker, T. (2018). The RNA helicase DDX3X is an essential mediator of innate antimicrobial immunity. *PLoS Pathogens*, *14*(11), e1007397. https://doi.org/10.1371/journal.ppat.1007397

Venkataramanan, S., Gadek, M., Calviello, L., Wilkins, K., & Floor, S. N. (2021). DDX3X and DDX3Y are redundant in protein synthesis. *RNA (New York, N.Y.)*, *27*(12), 1577–1588. https://doi.org/10.1261/rna.078926.121